UiT The Arctic University of Norway

Faculty of Science and Technology
Department of Physics and Technology

Stochastic Modelling and Numerical Simulations of Radial Filament Motion and Average Profiles at the Boundary of Fusion Plasmas

Olga Paikina

FYS-3900 Master's thesis in physics - 60 ECTS
May 2022

Abstract

The boundary region of magnetically confined plasmas is well known to have inherently fluctuating parameters. Advances in experimental measurements and numerical computations have revealed that the fluctuation-driven transport of particles and heat across the magnetic field lines is mainly dominated by the radial motion of blob-like filament structures. These structures, which are localized in the drift plane perpendicular to the magnetic field and elongated along the field lines, can deposit intermittent loads on the first wall of the fusion reactor leading to destructive plasma-wall interactions. As such, an accurate description of all the statistical properties of the intermittent fluctuations is necessary for both understanding and predicting its causes and effects on the reactor and walls.

Recently, a stochastic model for intermittent fluctuations has been constructed based on a super-position of uncorrelated pulses moving in the radial direction with a random distribution of amplitudes, sizes and velocities. Numerical simulations of this model are utilized to investigate the implication of distribution and correlation between pulse sizes, velocities and amplitudes. The statistical analysis presented in this thesis includes lower-order statistical moments, probability density functions, auto-correlation functions and power spectral densities.

The results explain the mechanisms behind broad and flat time-average radial profiles of particle density in the scrape-off layer, the increase of the relative fluctuation amplitude as well as skewness and flatness in the far scrape-off layer. This proves valuable for describing intermittent fluctuations in the boundary region of magnetized plasmas.

Acknowledgements

First and foremost, I would like to thank Professor Odd Erik Garcia whose constant encouragement was vital in making this thesis a reality. He spent endless hours proofreading and giving me excellent suggestions which always resulted in improved versions of thesis. This thesis also would never have been finished without the endless support and guidance of my co-supervisors Juan M. Losada and Audun Theodorsen.

Finally, I would like to thank my fellow students, my family and friends for their support throughout the entire thesis process.

Contents

1 Introduction

For more than a half-century, there has been an attempt by the scientific community to develop controlled thermonuclear fusion as an unlimited and sustainable source of energy without emission of greenhouse gases or production of long-lived radioactive waste. The tokamak configuration maintained the most promising concept of magnetic confinement of the hot plasma. In its most primitive form, tokamak confinement relies upon the simultaneous action of three magnetic field components: a toroidal magnetic field created by external coils, a poloidal magnetic field created by a toroidal plasma current inductively driven by poloidal field coils, and a vertical magnetic field which is used to maintain confinement.

Many phenomena that determine the behavior of plasma in a tokamak critically depend on edge effects. Therefore, an understanding of the processes occurring in the boundary region of a magnetically confined plasma is necessary to create an efficient fusion power reactor.

In the vicinity of the first wall, the plasma is divided by the last closed magnetic flux surface (separatrix) into two fundamentally different regions. Inside the separatrix, the magnetic surfaces are closed upon themselves. Particles are held on them and move across the magnetic field lines due to collisions and anomalous transport from turbulence. In the outer region, scrape-off layer (SOL), the magnetic field lines intersect material surfaces: limiters or divertor plates. In a divertor tokamak, the main load is carried by the divertor plates to remove escaping particles and energy from the system. Despite divertor configuration, research has shown that there is substantial transport of heat and particles across the magnetic field lines, determining the high level of interaction between the plasma and the material surfaces.

1.1 Cross-field transport in the scrape-off layer

Confinement in tokamaks is limited by cross-field transport and "traditionally" make its appearance as particle diffusion. The basic mechanism involved in classical transport is binary collisions causing the particle guiding centers to jump from one orbit to another neighboring orbit. The transport coefficients for a fully ionized plasma in a magnetic field were given in the review by Braginskii [1]. He suggested that electrons diffuse due to a random walk with electron gyroradius ρ_e as the "step length" and calculated the coefficient as the ratio of the squared thermal gyroradius to the elecron–ion collision time,

$$D_{\text{class}} = \rho_e^2 \nu_{ei}. \tag{1.1}$$

However, for the tokamak configurations, the particle and energy fluxes turned out to be considerably higher than the classical theory predicted. Therefore, Galeev and Sagdeev proposed a "neoclassical" theory [2], which takes into account the shift of the banana orbits associated with the complication of the magnetic field configuration and leading to an increase in transport coefficients,

$$D_{\text{neo}} \sim \nu_{ei} \rho_e^2 q^2 \sim D_{\text{class}} q^2, \tag{1.2}$$

where q is a safety factor, which describes the pitch of the magnetic field lines. However, calculations from the neoclassical transport theory have shown that the results of this model give higher electron temperature, T_e, and energy confinement time, τ_e, than those observed experimentally [3]. This evidence indicates the existence of additional transport mechanisms that are not taken into account by neoclassical theory and is usually refereed to anomalous.

Presently, the work on cross-field transport in the SOL has attempted to characterize it in terms of an effective diffusivity, D_{eff} [4]. The most common approach to predict impact of anomalous transport is based on mixing length estimates [5]. The anomalous transport coefficient, D_{eff}, is given by the expression

$$D_{\text{eff}} = \frac{\gamma}{k_\perp^2}, \tag{1.3}$$

where γ and $k_\perp$ are the growth rate and cross-field wave number of the linear instability underlying the turbulence, respectively. By considering the condition for the boundary region [6], the cross-field particle flux in the SOL can be expressed by Fick's law,

$$\Gamma_\perp = -D_{\text{eff}} \frac{\partial n}{\partial x} \tag{1.4}$$

With this simplified SOL description, the radial density variation/profile can be characterized. Further, if one assumes that an effective diffusion coefficients is approximately radially constant,

then one expects the density profile to be

$$n(x) = n_0 \exp\left(-\frac{x}{L_n}\right), \tag{1.5}$$

with decay length $L_n = (D_{\text{eff}} L_{\parallel}/C_{\text{s}})^{1/2}$, where $L_{\parallel}/Cs$ is a constant rate describe parallel losses of particles along field lines.

However, it was found that the behavior of transport is radically different than the constant particle diffusion coefficient that is often assumed. In fact experiments have shown that, D_{eff} increases rapidly with distance from the separatrix [7]. The SOL fluctuations "change" transport from relatively slow diffusive to very fast convective. Moreover, a broad set of experimental data and simulation results supporting the idea that the coherent structures with excess energy and particle density, referred to as filaments, are responsible for the anomalous cross-field transport. As a consequence, the theoretical limitation of the diffusion approach invalidates its predictive ability towards future fusion reactors. A different approach is needed to understand SOL turbulence and describe the role of fluctuations on the plasma parameters. In order to address such an approach, it is necessary to review the current understanding of fluctuations in the SOL.

1.2 SOL profiles and intermittent fluctuations

The plasma in the SOL is typically very turbulent due to the presence of nearly flat profiles and a variety of instabilities. A comparative study of turbulence fundamental properties at the boundary shows the universality of their basic statistical characteristics [7, 8, 9]. These works present an analysis of probe measurements from the outboard mid-plane region of discharges with varying line-averaged particle density, $\overline{n}_{\text{e}}$. $\overline{n}_{\text{e}}$ is an experimental control parameter, since the high plasma density is advantageous for the fusion process. However, each machine has its own empirical discharge density limit, $n_G \equiv I_p/(\pi a^2)$, which is expressed by the ratio of plasma current, I_{p}, to minor radius, a and when operating near its density limit often terminate with disruptions [10].

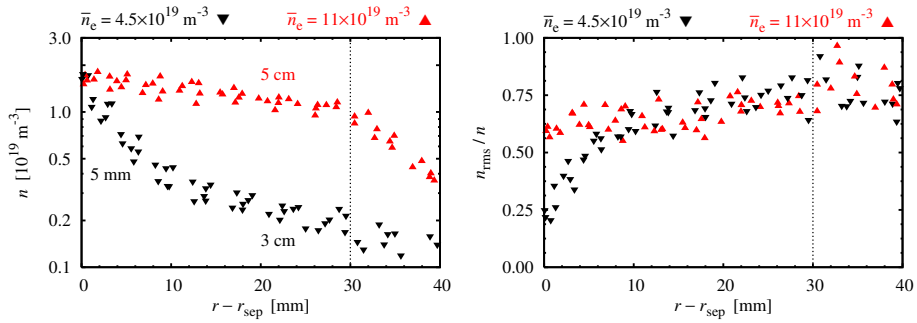

Figure 1: Radial profile of (left panel) the average particle density normalized to the separatrix value and (right panel) the relative fluctuation level on TCV. Image courtesy of O. E. Garcia.

Measurements on the TCV tokamak of average profiles and relative particle density fluctuation levels as a function of minor radius in the SOL are shown in figure 1. For low $\overline{n}_{\text{e}}/n_G$, the mid-plane profile close to the separatrix is characterized by a strong gradient region with a moderate fluctuations level, the so-called near SOL, which extends roughly one e-folding length into the SOL. Here the decay length is observed to be approximately 5 mm. Close to the first wall, the profile has a much longer decay length ~ 3 cm, the far SOL region with shallow gradients and large fluctuation levels [7]. The amplitude and character of fluctuations is markedly different across the SOL. Universally across machines as the density is raised, the profile tends to flatten and develop a "shoulder" at a certain distance from the separatrix. This nature of the profiles, which is called flattening in the literature, led to the distinction between the near and the far SOL. Increasing line average density strongly affects the radial variation of the decay length by factor of two in both the near and far SOL regions [7, 11]. Close to discharge density limit, the density shoulder moves to the separatrix which results in significant fluctuation levels and weak gradients dominating the entire SOL region (broadening) [12]. This leads to stronger plasma interactions with the main chamber walls.

1.3 Radial filament motion and scaling

A large body of theoretical modelling and numerical simulations suggests that an interchange motion due to the non-uniform magnetic field is the plausible mechanism underlying the radial filament motion. The basic mechanism by which filaments move radially outwards was first proposed by Krasheninnikov [13]. Assuming that filaments are generated in the SOL by turbulent processes around the separatrix, he suggested that gradient and curvature drifts lead to a polarisation of charge and thus the formation of an electric field within a filament. Through $\mathbf{E} \times \mathbf{B}$ motion, the filament acquires a radial velocity $\mathbf{V}_E$ by which it is advected radially outwards towards the first wall (see figure 2).

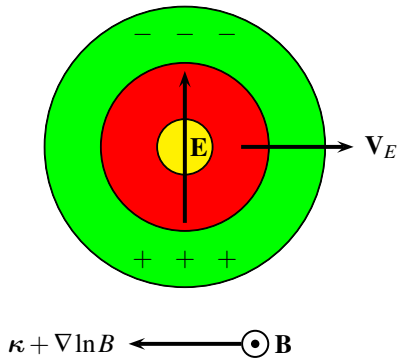

Figure 2: Sketch of a patch of excess pressure compared to background (plasma blob) showing the charge polarization mechanism responsible for the radial transport. Here $\boldsymbol{\kappa} = (\boldsymbol{b} \cdot \nabla)\boldsymbol{b}$ is the magnetic filed curvature vector, where $\boldsymbol{b}$ denote a unit vector in the direction of magnetic field and $\nabla \ln B$ is the gradient vector arise from non-uniformity of magnetic field. Image courtesy of O. E. Garcia.

Figure 3 shows the propagation of a single filament from the core plasma and its radial motion in the SOL in the NSTX device. The filament is visualized in the plane perpendicular to the field lines. Due to their appearance in the two-dimensional plane, filaments are often referred to as blobs in this context. Blob seen in figure 3 propagating radially outwards with steep front and trailing wake. This is in an agreement with the numerical simulations of the interchange model, which shows that the blob structure develops a steep front and a trailing wake and its amplitude decay with time as the blob propagate radially outwards [14, 15].

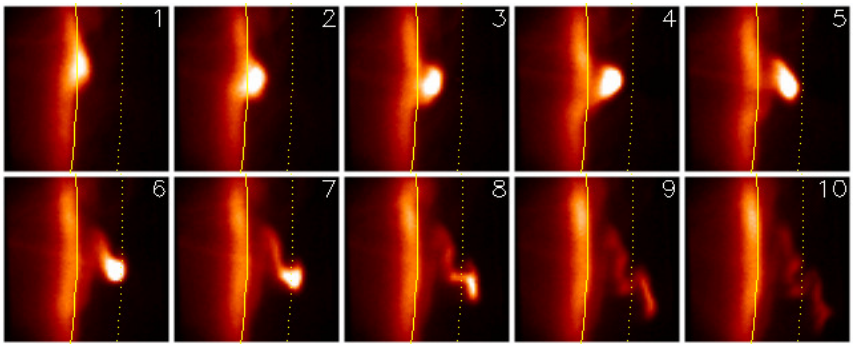

Figure 3: Blob-like structure moving through the SOL in NSTX. Structure is localized in the plane perpendicular to magnetic field. The solid line is the separatrix and the dotted line is the limiter shadow. Figure taken from [16].

A simple model describing the dynamics of these plasma blobs consists of a vorticity equation and a particle density continuity equation derived from the laws of conservation of charge and particle density, respectively [17]. From the theoretical point of view, this model is able to predict the radial velocity scaling with the blob cross-field size, depending on what closure is dominant for the parallel dynamics. In the regime, often referred as ideal, when high plasma collisionality impending parallel electron motion to the divertor region, the radial velocity scales as the square root of blob size $v \sim \ell^{1/2}$ [14, 18]. If the blob is subject to dissipation by electric currents to the sheaths, the radial velocity scales inversely with the square of blob size $v \sim \ell^{-2}$. This is commonly

referred to as the sheath dissipative regime [13]. These analutical scaling predictions have been confirmed by 2D numerical simulations [19]. However, this empirical scalings of blob size versus blob radial speed has shown a fairly wide range scatter among different devices [20]. Recently more general scaling estimates shows that the maximal radial blob velocity depends as a power law on the its amplitude relative to background $v \sim (\Delta n/N)^{\alpha}$, with two prompt scalings $\alpha = \{0.5, 1\}$ [14, 21, 22, 23, 24, 25, 19]. There are several other important aspects of blob dynamics, such as finite ion temperature effects, blobs interaction with neutral particles, effects of parallel electron dynamics such as resistive drift waves and blob spinning. These aspects are beyond the scope of this thesis and comprehensive reviews can be found in [17, 20].

1.4 Single-point measurement analysis as support for stochastic modelling

This section begins with a motivation of the stochastic model based on the properties of filament motion in the SOL as recorded by single-point measurements. Single-point measurements in the SOL are characterized by frequent large amplitude events. The Gas Puff Imaging (GPI) measurements in the Alcator C-Mod device (figure 4) illustrate such behaviour. At the separatrix ($R = 89.54$ cm) there are small-amplitude and symmetric fluctuations, while there are intermittent and large-amplitude bursts in the far SOL ($R = 91.08$ cm). Standard analyses of single-point time series include estimates of statistical moments, as the mean, variance, skewness and kurtosis, frequency spectrum, probability distribution functions and auto-correlation functions to describe the character of fluctuations in a turbulent field. Some of these methods require exceptionally long time series since they can be sensitive to infrequent events. The PDFs are found to be unimodal as well as positively skewed and flattened, and to have an exponential tail towards positive values [7, 26, 27].

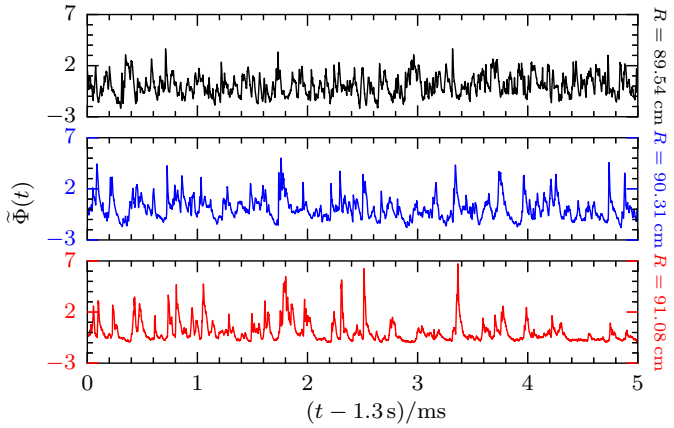

Figure 4: Single point data time series recorded at different radial distances on Alcator C-Mod. Figure taken from [28].

Large-amplitude fluctuations in single-point measurement in the SOL are observed to have the following properties:

- Conditional average shape of large-amplitude fluctuations are sharply peaked with a faster rise than decay, well described by a two-sided exponential function [7, 29, 27, 30, 31].
- The peak amplitudes of the conditional events are exponentially distributed [29, 32, 33, 34].
- The waiting times between the maxima of subsequent conditional events are exponentially distributed [32, 33, 34].
- The event duration is independent of the burst amplitude and the plasma parameters [7, 28, 29, 34, 35].

In the stochastic model to be described in the following section, these quantities pertain to filaments arriving at the probe view position as for an isolated events [26]. The conditionally averaged shape and amplitude distribution describe the shape and amplitude of the filaments. The waiting time distribution and duration times represents how filaments are separated in time and space.

2 Stochastic Modelling

This section begins with highlighting previous work on stochastic modelling of the fluctuations in the SOL based on a super-position of uncorrelated pulses. This is will be followed by presenting a stochastic model describing a super-position of one-sided exponential pulses moving in the radial direction with a random distribution of and correlation between amplitudes, sizes and velocities. The properties and predictions will be derived and discussed (some aspects closely follows [36]).

2.1 The filtered Poisson process

A process formed by super-posing independent random events is commonly called a shot noise process or a filtered Poisson process (FPP) [37, 38]. Each such event labelled k appears in a pulse function $\varphi(\theta)$ arriving at time t_k and is characterized by an amplitude A_k and duration time τ_k. A shot noise process consists of K identical events on a time interval of duration T. The resulting super-position of pulses is given by

$$\Phi_K(t) = \sum_{k=1}^{K(T)} A_k \, \varphi\left(\frac{t - t_k}{\tau_k}\right). \tag{2.1}$$

For the process defined by equation (2.1) the distribution of all random variables must be specified. For uncorrelated events, the arrival times t_k are assumed to be uniformly distributed and independent of all other pulse parameters, namely,

$$P_t(t_k) = \frac{1}{T} \quad \text{for} \quad t_k \in [0, T]. \tag{2.2}$$

Moreover, the number of events K in a fixed time interval T is given by the Poisson distribution

$$P_K(K|T) = \frac{1}{K!}\left(\frac{T}{\tau_\mathrm{w}}\right)^K \exp\left(-\frac{T}{\tau_\mathrm{w}}\right), \tag{2.3}$$

where $1/\tau_\mathrm{w}$ is the average rate of pulse arrivals. From this it follows that the waiting times between two consecutive events are exponentially distributed. The average number of events in a realization of duration T is

$$\langle K \rangle = \sum_{K=0}^{\infty} K P_K(K|T) = \frac{T}{\tau_\mathrm{w}}, \tag{2.4}$$

where here and in the following, angular brackets denote an average over all random variables. This justifies referring to the model as a Poisson process. For a general distribution of pulse duration times P_τ, their average is given by

$$\tau_\mathrm{d} = \int_0^\infty \mathrm{d}\tau \, \tau P_\tau(\tau). \tag{2.5}$$

The ratio of the average pulse duration time to the average pulse waiting time is referred to as the intermittency parameter

$$\gamma = \frac{\tau_\mathrm{d}}{\tau_\mathrm{w}}. \tag{2.6}$$

This determines the degree of pulse overlap and the intermittency of the process. In the regime $\gamma \ll 1$, individual pulses appear isolated, whereas $\gamma \gg 1$ describes the case of significant pulse overlap. Thus, γ serve as an indication of the intermittency of the process.

The pulse function $\varphi(\theta)$, where θ is a dimensionless variable, is assumed to be identical for all pulses in (2.1) and satisfy normalization constraint

$$\int_{-\infty}^{\infty} \mathrm{d}\theta \, |\varphi(\theta)| = 1. \tag{2.7}$$

In order to calculate the moments of the process, an integral of the n-th power of the pulse function is defined as

$$I_n = \int_{-\infty}^{\infty} \mathrm{d}\theta \, [\varphi(\theta)]^n. \tag{2.8}$$

The pulse function integral is assumed to converge for all positive integers n. For an exponential pulse function, this integral gives the well known result

$$I_n = \frac{1}{n}. \tag{2.9}$$

In particular, $I_1 = 1$, as should be the case for a non-negative $\varphi(\theta)$. The two lowest order moments of the FPP process can be calculated in a straight forward manner by averaging over all random variables. The mean value is given by

$$\begin{aligned}\langle \Phi_K \rangle = &\int_{-\infty}^{\infty} \mathrm{d}A_1 \, P_A(A_1) \int_0^{\infty} \mathrm{d}\tau_1 \, P_\tau(\tau_1) \int_0^T \frac{\mathrm{d}t_1}{T} \ldots \\ &\int_{-\infty}^{\infty} \mathrm{d}A_K \, P_A(A_K) \int_0^{\infty} \mathrm{d}\tau_K \, P_\tau(\tau_K) \int_0^T \frac{\mathrm{d}t_K}{T} \sum_{k=1}^{K(T)} A_k \varphi\left(\frac{t - t_k}{\tau_k}\right)\end{aligned} \tag{2.10}$$

Neglecting end effects by taking the integration limits for t_k to infinity and make a change of integration variable defined by $\theta = (t - t_k)/\tau_k$ and $\mathrm{d}\theta = -\mathrm{d}t_k/\tau_k$, gives the conditional mean

$$\langle \Phi_K \rangle = \tau_\mathrm{d} I_1 \langle A \rangle \frac{K}{T}. \tag{2.11}$$

Averaging over the number of pulses K gives the mean of the stationary FPP

$$\langle \Phi \rangle = \frac{\tau_\mathrm{d}}{\tau_\mathrm{w}} I_1 \langle A \rangle. \tag{2.12}$$

This gives large mean value for significant overlap of pulses, $\gamma \gg 1$. In a similar fashion, the variance can be calculated by averaging the square of the random variable Φ_K. For finite mean the relative fluctuation level of the stationary process is given by

$$\frac{\Phi_\mathrm{rms}}{\langle \Phi \rangle} = \left(\frac{\tau_\mathrm{w}}{\tau_\mathrm{d}}\right)^{1/2} \frac{I_2^{1/2}}{I_1} \frac{\langle A^2 \rangle^{1/2}}{\langle A \rangle}, \tag{2.13}$$

which is large when the pulses appear isolated, $\gamma \ll 1$. More generally, all moments follow from the characteristic function of the process defined as the Fourier transform of the probability density function. The cumulants of the process are given by the coefficients in the expansion of the logarithm of the characteristic function. A closed form expression for the cumulants has been given in [39],

$$\kappa_n = \gamma I_n \langle A^n \rangle. \tag{2.14}$$

From this, the skewness and flatness moments are readily obtained and are given by

$$S_\Phi = \frac{1}{\gamma^{1/2}} \frac{I_3}{I_2^{3/2}} \frac{\langle A^3 \rangle}{\langle A^2 \rangle^{3/2}}, \quad F_\Phi = \frac{1}{\gamma} \frac{I_4}{I_2^2} \frac{\langle A^4 \rangle}{\langle A^2 \rangle^2}. \tag{2.15}$$

It is evident that skewness and flatness moments increase with decreasing γ and vanish in the limit $\gamma \to \infty$. It should be emphasised that here and in the following flatness denotes excess kurtosis. It is a useful to define excess kurtosis, since it compares the kurtosis of a distribution against the kurtosis of a normal distribution.

Constant duration and exponentially distributed amplitudes

A particularly interesting case is that of the pulse amplitudes A_k being exponential distributed

$$P_A(A) = \frac{1}{\langle A \rangle} \exp\left(-\frac{A}{\langle A \rangle}\right), \quad A > 0, \tag{2.16}$$

and the pulse duration times τ_k are assumed to be constant

$$P_\tau(\tau) = \delta(\tau - \tau_\mathrm{d}). \tag{2.17}$$

Here, $\langle A \rangle$ and $\tau_\mathrm{d} = \langle \tau_k \rangle$ are the statistical average of the amplitudes and duration times, respectively, and δ denotes the Dirac delta function (see Appendix A). Under these assumptions and also

assume exponential function, the mean, the relative fluctuation level, the coefficient of skewness and flatness are given by

$$\langle \Phi \rangle = \langle A \rangle \frac{\tau_\mathrm{d}}{\tau_\mathrm{w}}, \qquad \frac{\Phi_\mathrm{rms}}{\langle \Phi \rangle} = \left(\frac{\tau_\mathrm{d}}{\tau_\mathrm{w}} \right)^{1/2}, \tag{2.18}$$

$$S_\Phi = 2 \left(\frac{\tau_\mathrm{d}}{\tau_\mathrm{w}} \right)^{1/2}, \qquad F_\Phi = 6 \frac{\tau_\mathrm{d}}{\tau_\mathrm{w}}. \tag{2.19}$$

It results that the model parameters of the FPP process are the average pulse amplitude $\langle A \rangle$, the pulse duration τ_d and the average waiting time τ_w.

When the pulse amplitudes are exponentially distributed, the probability density function for the FPP process is a Gamma distribution with scale parameter $\langle A \rangle$ and shape parameter γ

$$P_\Phi(\Phi) = \frac{1}{\langle A \rangle \Gamma(\gamma)} \left(\frac{\Phi}{\langle A \rangle} \right)^{\gamma - 1} \exp\left(- \frac{\Phi}{\langle A \rangle} \right), \ \Phi > 0. \tag{2.20}$$

The auto-correlation function of the normalized process is a two-sided decaying exponential function with an e-folding time given by the pulse duration

$$R_{\widetilde{\Phi}}(r) = \exp\left(- \frac{|\tau|}{\tau_\mathrm{d}} \right), \tag{2.21}$$

while the power spectral density has a Lorentzian shape

$$\Omega_{\widetilde{\Phi}} = \frac{2\tau_\mathrm{d}}{1 + \tau_\mathrm{d}^2 \omega^2}. \tag{2.22}$$

Detailed derivations and discussion of what have been presented here can be found in [39].

The FPP model, however, only describes single-point measurements. Recently, the FPP model have been generalized to include radial filament motion due to advection of a single pulse [39, 36]. In idealized case when the filament assumed to move with constant size and velocity, the radial scale length is given by the product of the radial filament velocity and parallel transit time. Equivalent result were also found in [40, 41], where model is formulate based on a Lagrangian approach to filament dynamics. While, this result can not explain experimental observations associated with the flattening and broadening of the profiles and with the radially changing statistics, its reveals how the variation in a average profile depends on the filament statistics. The results presented in [36] extend previous work [39] by including predictions for statistical moments and auto-correlation functions for joint probability distribution between amplitudes, sizes and velocities and were presented.

2.2 Super-position of filament structures

The thermodynamic variable, Φ, can be described as a super-position of uncorrelated pulses (filaments), ϕ_k,

$$\Phi_K(x,t) = \sum_{k=1}^{K} \phi_k(x,t) \tag{2.23}$$

By neglecting interaction between pulse structures, the evolution of each pulse k is in general governed by advection-dissipation equation

$$\frac{\partial \phi_k}{\partial t} + v_k \frac{\partial \phi_k}{\partial x} + \frac{\phi_k}{\tau_{\shortparallel}} = 0, \tag{2.24}$$

where v_k is the radial velocity for pulse k and the third term is the parallel drainage due to acoustic streaming along magnetic field lines. In the SOL, the parallel transient time $\tau_{\shortparallel}$ is estimated through the ratio of the magnetic connection length from the outboard mid-plane to the divertor target, $L_\parallel$, to the acoustic speed C_s. The pulse labeled k with amplitude a_k is assumed to arrive at the reference position $x = 0$ at the reference time t_k,

$$\phi_k(x, t_k) = a_k \, \varphi\left(\frac{x}{\ell_k} \right). \tag{2.25}$$

The pulse function consist of an exponential rise and an exponential decay. This particular shape is common for the conditionally averaged probe data. Thus, the pulse function is taken to be an asymmetric, two-sided exponential function

$$\varphi(\theta,\lambda) = \begin{cases} \exp\left(\dfrac{\theta}{1-\lambda}\right), & \theta \leqslant 0 \\ \exp\left(-\frac{\theta}{\lambda}\right), & \theta > 0, \end{cases} \tag{2.26}$$

where θ is a dimensionless space variable and the asymmetry parameter λ is in the range $0 < \lambda < 1$. For $\lambda < 1/2$, the pulse has a faster rise than decay. In the following, setting $\lambda = 0$ indicates a one-sided exponential pulse function

$$\varphi(\theta) = \begin{cases} \exp(\theta), & \theta \leqslant 0, \\ 0, & \theta > 0. \end{cases} \tag{2.27}$$

For the exponential pulse function, $I_n = 1/n$, and therefore, independent of the asymmetry parameter λ. It follows that the distribution and moments of Φ are independent of λ.

If the pulse velocities v_k are time-independent, the general solution in an infinite domain of the 1D advection equation has the form

$$\phi_k(x,t) = A_k(t)\,\varphi\left(\frac{x - X_k(t)}{\ell_k}\right), \tag{2.28}$$

where φ is the function that specifies by the initial condition and $X_k(t) = v_k(t - t_k)$ is the pulse trajectory. This shows that the initial pulse is simply swept along by the velocity v_k without changing its shape.

Equation (2.28) is a solution to the advection-dissipation equation, if the amplitude $A_k(t)$ satisfy

$$\frac{dA_k}{dt} = -\frac{A_k}{\tau_{\text{II}}}. \tag{2.29}$$

The solution of the amplitude equation can be written as

$$A_k(t) = a_k \exp\left(-\frac{t - t_k}{\tau_{\text{II}}}\right), \tag{2.30}$$

where a_k is the pulse amplitude at the reference time t_k. The process can be written as

$$\Phi_K(x,t) = \sum_{k=1}^{K} a_k \exp\left(-\frac{t - t_k}{\tau_{\text{II}}}\right) \varphi\left(\frac{x - X_k(t)}{\ell_k}\right). \tag{2.31}$$

This special case can be generalized to pulse velocities $V_k(t)$ which are taken to be a function of time. Noteworthy is that the velocity field will not enter the model as an input field since it will be constrained by the amplitude evolution. Applying the method of characteristics for the differential equation (2.24) leads to the general solution

$$\phi_k(x,t) = a_k \exp\left(-\frac{t - t_k}{\tau_{\text{II}}}\right) \varphi\left(\frac{x}{\ell_k} - \frac{1}{\ell_k}\int_{t_k}^{t} \mathrm{d}t' V_k(t')\right). \tag{2.32}$$

The details of the derivation can be found in Appendix B. The pulse velocity is assumed to be given by a function of the instantaneous amplitude $A_k(t)$ and possibly other pulse parameters

$$V_k(t) = f(A_k(t), v_k, \ell_k). \tag{2.33}$$

In the following, the notation is employed in a way that the capital $V_k(t)$ and $A_k(t)$ denote the time dependence of these quantities, while lowercase v_k and a_k denote random variables representing the pulse amplitude and velocity at reference time t_k. It is also worth to note that all time dependency in the velocity is due to the exponential decay of the amplitude.

2.2.1 Process for time-independent pulse velocities at reference position ξ

Consider the process given by equation (2.31) at some reference position ξ

$$\Phi_K(\xi,t) = \sum_{k=1}^{K} a_k \exp\left(-\frac{t-t_k}{\tau_{\shortparallel}}\right)\varphi\left(\frac{\xi - x_k - v_k t}{\ell_k}\right). \tag{2.34}$$

Let us then introduce the reference time $t_{\xi,k}$ by

$$t_{\xi,k} = \frac{(\xi - x_k)}{v_k}. \tag{2.35}$$

Then, the contribution of the filament at the reference position ξ is

$$\phi_k(\xi,t) = a_k \exp\left(-\frac{\xi}{v_k\tau_{\shortparallel}}\right)\exp\left(-\frac{t-t_{\xi,k}}{\tau_{\shortparallel}}\right)\varphi\left(-\frac{t-t_{\xi,k}}{\ell_k/v_k}\right) \tag{2.36}$$

Essentially, the process is translated from the spatial domain to the temporal domain. The pulse function in the radial direction is translated (flipped) to the temporal domain, as its get recorded at position ξ.

Consider an one-side exponential pulse function given by equation (2.27). The linear damping term can be included in the pulse function and the pulse at $x = \xi$ can be written as

$$\phi_k(\xi,t) = a_{\xi,k}\varphi\left(-\frac{t-t_{\xi,k}}{\tau_k}\right) \tag{2.37}$$

where the pulse amplitude and duration time are

$$a_{\xi,k} = a_k \exp\left(-\frac{\xi}{v_k\tau_{\shortparallel}}\right), \tag{2.38}$$

$$\tau_k = \frac{\tau_{\shortparallel}\ell_k}{v_k\tau_{\shortparallel} + \ell_k}. \tag{2.39}$$

At the radial position $\xi = 0$ the process can be written as

$$\Phi_K(\xi = 0,t) = \sum_{k=1}^{K(T)} a_k\varphi\left(-\frac{t-t_k}{\tau_k}\right). \tag{2.40}$$

This is just the filtered Poisson process which was addressed in previous section. At any radial position $\xi \neq 0$ the process is given by

$$\Phi_K(\xi,t) = \sum_{k=1}^{K(T)} a_{\xi,k}\varphi\left(-\frac{t-t_{\xi,k}}{\tau_k}\right). \tag{2.41}$$

In the stationary limit $T \to \infty$, the arrival times $t_{\xi,k}$ are uniformly distributed and equation (2.41) is a filtered Poisson process where the pulse amplitudes are modified by a factor $\exp(-\xi/(v_k\tau_{\shortparallel}))$. Clearly, when the pulse velocities are randomly distributed, the amplitude distribution will be different from one specified at the reference position $\xi = 0$.

2.3 Statistical analysis

In this subsection, the derivations of the lowest order statistical moments, the characteristic function, probability density function, correlation functions and power spectral densities for a sum of uncorrelated pulses will be presented for the case of time-independent pulse velocities.

Average radial profile

The first lowest order moment of the stochastic process defined by Eq. (2.31) can be calculated by averaging over all random variables by virtue of Campbell's theorem [42]. In the following it will

be assumed that the random variables are independent and identically distributed, such that the conditional mean is given by

$$\begin{aligned}\langle \Phi_K \rangle = &\int_{-\infty}^{\infty} \mathrm{d}a_1 \, P_a(a_1) \int_{-\infty}^{\infty} \mathrm{d}\ell_1 \, P_\ell(\ell_1) \int_{-\infty}^{\infty} \mathrm{d}v_1 \, P_v(v_1) \int_0^T \frac{\mathrm{d}t_1}{T} \ldots \\ &\int_{-\infty}^{\infty} \mathrm{d}a_K \, P_a(a_K) \int_{-\infty}^{\infty} \mathrm{d}\ell_K \, P_\ell(\ell_K) \int_{-\infty}^{\infty} \mathrm{d}v_K \, P_v(v_K) \int_0^T \frac{\mathrm{d}t_K}{T} \sum_{k=1}^{K(T)} \phi_k(x,t) \\ &= \sum_{k=1}^{K} \langle \phi_k(x,t) \rangle = K \langle \phi_k(x,t) \rangle, \end{aligned} \tag{2.42}$$

using that the pulse arrival times are uniformly distributed and $\langle \cdot \rangle$ indicates the average over all random variables. The process Φ_K is conditional in the sense that exactly K structures appear in the interval of duration T. Using that K is Poisson distributed as defined by equation (2.3), averaging over the number of structures K gives the mean of the process

$$\langle \Phi \rangle(x) = \sum_{K=0}^{\infty} \langle \Phi_K \rangle P_K(K|T) = \frac{T}{\tau_\mathrm{w}} \langle \phi_k(x,t) \rangle. \tag{2.43}$$

Neglecting end effects by taking the integration limits over t_k to infinity and making a change of integration variable defined by

$$\begin{aligned} \theta &= \frac{x - v(t - t_k)}{\ell}, \\ \mathrm{d}\theta &= \frac{\mathrm{d}t_k}{\ell / v}, \end{aligned}$$

the mean value follows directly

$$\langle \Phi \rangle(x) = \frac{1}{\tau_\mathrm{w}} \left\langle \frac{a\ell}{v} \exp\left(-\frac{x}{v\tau_{\shortparallel}}\right) \int_{-\infty}^{\infty} \mathrm{d}\theta \, \exp\left(\frac{\theta \ell}{v\tau_{\shortparallel}}\right) \varphi(\theta) \right\rangle. \tag{2.44}$$

In the case of the one-sided exponential pulse function given by equation (2.27) and any joint distribution between pulse amplitudes, sizes and velocities, the average profile result,

$$\langle \Phi \rangle(x) = \frac{1}{\tau_\mathrm{w}} \left\langle a\tau \exp\left(-\frac{x}{v\tau_{\shortparallel}}\right) \right\rangle, \tag{2.45}$$

where the duration time τ of individual pulse is given by the harmonic mean of radial and parallel transit times,

$$\tau = \frac{\tau_{\shortparallel} \tau_\perp}{\tau_{\shortparallel} + \tau_\perp}, \tag{2.46}$$

with the radial transit time defined by $\tau_\perp = \ell / v$.

In the case of a degenerate distribution of pulse velocities and sizes, the average radial profile takes form

$$\langle \Phi \rangle(x) = \frac{\tau_\mathrm{d}}{\tau_\mathrm{w}} \langle a \rangle \exp\left(-\frac{x}{\langle v \rangle \tau_{\shortparallel}}\right), \tag{2.47}$$

where τ_d is the pulse duration and is the same for all pulses with the assumptions given,

$$\tau_\mathrm{d} = \frac{\langle \ell \rangle \tau_{\shortparallel}}{\langle v \rangle \tau_{\shortparallel} + \langle \ell \rangle}. \tag{2.48}$$

The average profile is proportional to the pulse duration and mean amplitude and inversely proportional to the average waiting time. The ratio $\gamma = \tau_\mathrm{d} / \tau_\mathrm{w}$ determines the degree of pulse overlap in the process and is referred as the intermittency parameter. Moreover, how fast the profile radially decay is only determined by the velocity of the pulse and the strength of the parallel transit time (under the assumption that these variables independent and the velocity and size is the same for all pulses).

Cumulants and moments

In the following, the characteristic function and the PDF of the process in the case when structures arrive in accordance with a Poisson process will be determined. The characteristic function of the random variable Φ_K at the radial position x is given by the Fourier transform of the PDF $P_{\Phi_K}(\Phi|K)$,

$$C_\Phi(u,x) = \langle \exp(iu\Phi)\rangle = \int_{-\infty}^{\infty} \mathrm{d}\Phi\, P_\Phi(\Phi)\exp(iu\Phi). \tag{2.49}$$

The characteristic function of the sum of the independent random variables, $\phi_k(x,t)$, is the product of their characteristic functions. Applying the inverse Fourier transform to the characteristic functions, the conditional distribution for Φ_K is

$$P_{\Phi_K}(\Phi|K) = \frac{1}{2\pi}\int_{-\infty}^{\infty} \mathrm{d}u\, \exp(-iu\Phi_K)\langle \exp(iu\Phi_K)\rangle, \tag{2.50}$$

where

$$\langle \exp(iu\Phi_K)\rangle = \prod_{k=1}^{K} \langle \exp(iu\phi_k)\rangle.$$

This expression gives a conditional probability of the number of pulses K in a time interval T to be given. By averaging over all K, the probability density function of the stationary process can be obtained, namely

$$P_\Phi(\Phi) = \sum_{K=0}^{\infty} P_K(K|T) P_{\Phi_K}(\Phi|K). \tag{2.51}$$

Using that K is assumed to be Poisson distributed and performing the summation by use of $e^z = \sum_{n=0}^{\infty} z^n/n!$, the PDF of the stationary process can be written as

$$P_\Phi(\Phi) = \frac{1}{2\pi}\int_{-\infty}^{\infty} \mathrm{d}u\, \exp(-iu\Phi)\exp\left(\frac{T}{\tau_\mathrm{w}}[\langle \exp(iu\phi_k)\rangle - 1]\right), \tag{2.52}$$

where the characteristic function of $P_\Phi(\Phi)$ is

$$\langle \exp(iu\Phi)\rangle = \exp\left(\frac{T}{\tau_\mathrm{w}}[\langle \exp(iu\phi_k)\rangle - 1]\right). \tag{2.53}$$

It follows that the logarithm of the characteristic function $C_\Phi(u,x)$ is

$$\ln C_\Phi = \frac{T}{\tau_\mathrm{w}}(\langle \exp(iu\phi_k)\rangle - 1). \tag{2.54}$$

If all the moments of Φ exist and are finite, then the characteristic function can be obtained by expanding the complex exponential function in its power series. By extending the integral over t_k to infinity, the expansion of $\ln C_\Phi$ gives

$$\ln C_\Phi = \frac{1}{\tau_\mathrm{w}}\left\langle \int_{-\infty}^{\infty} \mathrm{d}t_k \sum_{n=1}^{\infty} \frac{(iu\phi_k)^n}{n!}\right\rangle. \tag{2.55}$$

The cumulants κ_n are the coefficients in the expansion of $\ln C_\Phi$ such that

$$\ln C_\Phi = \sum_{n=1}^{\infty} \kappa_n \frac{(iu)^n}{n!}. \tag{2.56}$$

A comparison with equation (2.55) gives the cumulants

$$\kappa_n(x) = \frac{1}{\tau_\mathrm{w}}\left\langle \int_{-\infty}^{\infty} \mathrm{d}t_k \sum_{n=1}^{\infty} [iu\phi_k]^n\right\rangle. \tag{2.57}$$

Following a similar procedure as for calculating the average radial profile, the general expression for the cumulants is

$$\kappa_n(x) = \frac{1}{\tau_\mathrm{w}}\left\langle \frac{a^n\ell}{v}\exp\left(-\frac{nx}{v\tau_{\shortparallel}}\right)\int_{-\infty}^{\infty}\mathrm{d}\theta\, \exp\left(\frac{n\theta\ell}{v\tau_{\shortparallel}}\right)[\varphi(\theta)]^n\right\rangle, \tag{2.58}$$

In the case of a one-sided exponential pulse shape function and any joint probability distribution between pulse amplitudes, sizes and velocities, this gives

$$\kappa_n(x) = \frac{1}{n\tau_{\mathrm{w}}}\left\langle a^n \tau \exp\left(-\frac{nx}{v\tau_{\shortparallel}}\right)\right\rangle, \tag{2.59}$$

with τ defined by equation (2.46). In the case when pulse velocities are constant, it is clear that the cumulants decrease exponentially with radial position x. Moreover, this exponential profile can be only modified by a random distribution of the pulse velocities or the parallel transit time $\tau_{\shortparallel}$. In general, the parallel transit time can be treated as a random variable, motivated by the fact that the filaments are ballooned along magnetic field lines and that their initial elongation likely slightly changes. Nevertheless, all pulses were assumed to have the same linear damping, and the role of a random velocity distribution on profiles is to be investigated.

A power series expansion shows that the characteristic function is related to the raw moments of P_Φ, defined by $\mu'_n = \langle \Phi^n \rangle$ as

$$\langle \exp(iu\Phi) \rangle = 1 + \sum_{n=1}^{\infty} \frac{\langle iu\Phi \rangle^n}{n!} = 1 + \sum_{n=1}^{\infty} \mu'_n \frac{(iu)^n}{n!}. \tag{2.60}$$

The lowest order centered moments $\mu_n = \langle (\Phi - \langle \Phi \rangle)^n \rangle$ are related to the cumulants by the relations,

$$\begin{aligned} \mu_2 &= \kappa_2, \\ \mu_3 &= \kappa_3, \\ \mu_4 &= \kappa_4 + 3\kappa_2^2. \end{aligned}$$

Gives that all moments follow from the characteristic function and cumulants. Thus, the variance, skewness and flatness coefficients are given by

$$\Phi_{\mathrm{rms}}^2 = \left\langle (\Phi - \langle \Phi \rangle)^2 \right\rangle = \kappa_2, \tag{2.61}$$

$$S_\Phi = \frac{\left\langle (\Phi - \langle \Phi \rangle)^3 \right\rangle}{\Phi_{\mathrm{rms}}^3} = \frac{\kappa_3}{\kappa_2^{3/2}}, \tag{2.62}$$

$$F_\Phi = \frac{\left\langle (\Phi - \langle \Phi \rangle)^4 \right\rangle}{\Phi_{\mathrm{rms}}^4} - 3 = \frac{\kappa_4}{\kappa_2^2}. \tag{2.63}$$

In the case of exponentially distributed pulse amplitudes and a degenerate distribution of pulse velocities and sizes, the relative fluctuation level, skewness and flatness moments become

$$\frac{\Phi_{\mathrm{rms}}}{\langle \Phi \rangle} = \left(\frac{\tau_{\mathrm{w}}}{\tau_{\mathrm{d}}}\right)^{1/2}, \quad S_\Phi = 2\left(\frac{\tau_{\mathrm{w}}}{\tau_{\mathrm{d}}}\right)^{1/2}, \quad F_\Phi = 6\frac{\tau_{\mathrm{w}}}{\tau_{\mathrm{d}}}. \tag{2.64}$$

The ratio $\tau_{\mathrm{d}}/\tau_{\mathrm{w}}$ have been previously defined as intermittency parameter γ. Clearly, the relative fluctuation level, skewness and flatness do not depend on the radial position.

Existence of cumulants

For one-sided exponential pulse function, the cumulants are given by equation (2.59),

$$\kappa_n(x) = \frac{1}{n\tau_{\mathrm{w}}}\left\langle a^n \frac{\tau_{\shortparallel}}{\frac{v}{\ell}\tau_{\shortparallel} + 1} \exp\left(-\frac{nx}{v\tau_{\shortparallel}}\right)\right\rangle,$$

where a, v and ℓ are random variables with known distributions defined on $\mathbb{R}^+$ and satisfies

- $P_Y(y) \geqslant 0 \quad \forall y \geqslant 0$
- $\int_{\mathbb{R}^+} \mathrm{d}y\, y P_Y(y) < \infty$ i.e. Y is integrable

At first glance the expected value may not pose any formal problem. However, the average may not admit the expectation for $x < 0$ and the requirement for cumulants existence is needed.

As a relevant example, consider the case when pulse amplitudes are exponentially distributed, pulse sizes are degenerate distributed, and velocities distributed according to $P_v(v)$. Then, the existence of the n-th cumulant depends on the convergence of the integral

$$\kappa_n(x) = \frac{\tau_{\shortparallel}\langle a\rangle^n}{\tau_{\mathrm{w}}}(n-1)!\int_0^\infty \mathrm{d}v\, \frac{P_v(v)}{\frac{v}{\ell}\tau_{\shortparallel}+1}\exp\left(-\frac{nx}{v\tau_{\shortparallel}}\right). \tag{2.65}$$

It can be noted that the fraction term $1/(\frac{v}{\ell}+1)$ takes values in the interval $(0,1)$. Therefore, it does not affect the integral convergence and can be dropped. Under this consideration, let us study the integral behaviour for $x<0$

$$I = \int_0^\infty \mathrm{d}v\, P_v(v)\exp\left(\frac{n|x|}{v\tau_{\shortparallel}}\right), \tag{2.66}$$

where absolute value emphasize that $x<0$. Changing to new variable of integration $u=1/v$ and using the relation $P_u(u) = P_v(1/u)/u^2$ (see Appendix C) integral takes the form

$$I = \int_0^\infty \mathrm{d}u\, P_u(u)\exp\left(\frac{nu|x|}{\tau_{\shortparallel}}\right). \tag{2.67}$$

It should be emphasized that if the intregrand does not decay to zero for large u, then it is guaranteed that the integral will diverge. Consequently, the above integral converge for any radial position x and any cumulant order n, when $P_u(u)$ decays faster than exponential for large u. Additionally, assuming $P_u(u)\sim\exp(-cu)$ than

$$\lim_{u\to\infty}\exp(-cu)\exp\left(\frac{n|x|u}{\tau_{\shortparallel}}\right) = \begin{cases} 0, & \text{if} \quad \frac{n|x|}{\tau_{\shortparallel}} < c \\ 1, & \text{if} \quad \frac{n|x|}{\tau_{\shortparallel}} = c \\ \infty, & \text{if} \quad \frac{n|x|}{\tau_{\shortparallel}} > c \end{cases}$$

which implies that the integral may diverge for sufficiently large $|x|$ or n. Therefore, it is required at least a stretched exponential behavior $P_u(u)\sim\exp\left(-cu^\beta\right)$ for large u, such that

$$\lim_{u\to\infty}\exp\left(-cu^\beta\right)\exp\left(\frac{n|x|u}{\tau_{\shortparallel}}\right) = 0, \quad \text{if } \beta>1.$$

Consequently, $P_v(v)\sim\exp\left(-c/v^\beta\right)$ for $v\to 0^+$ and $\beta>1$. This result can be formulated in a more convenient form. The support of the velocity's distribution $P_v(v)$ is bounded below by a minimum velocity $v_{\min}$ such that $P_v(v)=0$ if $v<v_{\min}$.

In summary, the reason for the possible divergence of cumulants and moments of the process is the dominant contribution of slow pulses at negative radial positions. And the arbitrarily small velocities should be arrested to provide well-defined model.

Uniform arrival times distribution

A pulse with amplitude a_k moving with constant velocity v_k will arrive at the position ξ at time $t_{\xi,k}$ given by

$$t_{\xi,k} = t_k + \frac{\xi}{v_k}.$$

The arrivals t_k at $x=0$ are assumed to be uniformly distributed on the interval $[0,T]$. Note that $t_{\xi,k}$ is given by the sum of two random variables. In the case of a random distribution of pulse velocities v_k, the distribution of arrivals $t_{\xi,k}$ at $x=\xi$ are thus given by the convolution

$$P_{t_\xi}(t) = \int_{-\infty}^{\infty}\mathrm{d}r P_{\xi/v}(r)P_t(t-r) = \frac{1}{T}\int_t^{T+t}\mathrm{d}r P_{\xi/v}(r), \tag{2.68}$$

where $P_{\xi/v}$ is the distribution of the radial transit times $r=\xi/v$. It follows that the pulse arrivals at $x=\xi$ are in general not uniformly distributed. The presence of arbitrarily small pulse velocities result in long transit times and end effects that influence the arrival time distribution at $x>0$. This is solely an effect of the radial motion and is independent of the parallel drainage and amplitude decay in the case of time-independent velocities.

In order to determine the arrival time distribution, consider the case of a velocity distribution $P_v(v)$ that is bounded by a minimum velocity $v_{\min}$ and maximum velocity $v_{\max}$, which result in a maximum transit time $r_{\max} = \xi/v_{\min}$ and a minimum transit time $r_{\min} = \xi/v_{\max}$, respectively. The probability distribution $P_{\xi/v}(r)$ then vanishes for $r < r_{\min}$ as well as for $r > r_{\max}$, and the integral in equation (2.68) can be rewritten as

$$P_{t_\xi}(t) = \frac{1}{T} \int_{\max(t,r_{\min})}^{\min(T+t,r_{\max})} \mathrm{d}r \, P_{\xi/v}(r). \tag{2.69}$$

Thus, for arrivals times t such that $r_{\max} < t < T$,

$$P_{t_\xi}(t) = \frac{1}{T} \int_{r_{\min}}^{r_{\max}} \mathrm{d}r \, P_{\xi/v}(r) = \frac{1}{T}. \tag{2.70}$$

That is, a broad velocity distribution leading to transit times in the interval $(r_{\max}, r_{\min})$, will result in a distribution of arrival times t_ξ at the radial position ξ that is uniform in the interval $[r_{\min}, r_{\max}]$. Equivalently, the arrival times at the radial position ξ constitute a Poisson process in this interval. Note that this assumption $T > r_{\max}$. In the case that the velocity distribution is degenerate $r_{\min} = r_{\max} = \xi/v$ and the arrival times at $x = \xi$ preserve a Poisson process in the translated interval $[\xi/v, T + \xi/v]$.

These end effects are clearly demonstrated with the example of a uniform distribution of pulse velocities, $P_v(v) = 1/(v_{\max} - v_{\min})$ for $v_{\min} \leqslant v \leqslant v_{\max}$. The inverse distribution for the transit times $r = \xi/v$ is then given by

$$P_{\xi/v}(r) = \begin{cases} 0, & r < r_{\min}, \\ \dfrac{r_{\min} r_{\max}}{r_{\max} - r_{\min}} \dfrac{1}{r^2}, & r_{\min} < r < r_{\max}, \\ 0, & r_{\max} < r, \end{cases} \tag{2.71}$$

and the distribution of pulse arrival times at position ξ follows from,

$$P_{t_\xi}(t) = \frac{1}{T} \frac{r_{\min} r_{\max}}{r_{\max} - r_{\min}} \left(\frac{1}{\max(r_{\min}, t)} - \frac{1}{\min(r_{\max}, t+T)} \right). \tag{2.72}$$

Assuming $T > r_{\max} - r_{\min}$ leads to the desired result for the arrival time distribution,

$$TP_{t_\xi}(t) = \begin{cases} 0, & t < r_{\min}, \\ \dfrac{r_{\min} r_{\max}}{r_{\max} - r_{\min}} \left(\dfrac{1}{r_{\min}} - \dfrac{1}{t+T} \right), & r_{\min} < t < r_{\max}, \\ 1, & r_{\max} < t < T + r_{\min}, \\ \dfrac{r_{\min} r_{\max}}{r_{\max} - r_{\min}} \left(\dfrac{1}{t} - \dfrac{1}{r_{\max}} \right), & T + r_{\min} < t < T + r_{\max}, \\ 0 & t > T + r_{\max}. \end{cases} \tag{2.73}$$

Similarly to the above case, the arrival distribution can be also calculated analytically for a case of a discrete uniform velocity distribution. Consider velocities that can take two different values with equal probability

$$P_v(v) = \frac{1}{2} \left[\delta(v - v_{\min}) + \delta(v - v_{\max}) \right] \tag{2.74}$$

where δ denotes Dirac's delta distribution. In the case of discrete random variable, the convolution is simply given by a sum of two translated uniform distributions. Again, assuming $T > r_{\max} - r_{\min}$ gives the arrival time distribution,

$$TP_{t_\xi}(t) = \begin{cases} 0, & t < r_{\min}, \\ \frac{1}{2}, & r_{\min} < t < r_{\max}, \\ 1, & r_{\max} < t < T + r_{\min}, \\ \frac{1}{2}, & T + r_{\min} < t < T + r_{\max}, \\ 0 & t > T + r_{\max}. \end{cases} \tag{2.75}$$

In the figure 5, these distributions are presented. As stated above, the distribution of arrivals times is $1/T$ in the range $r_{\max} < t < T + r_{\min}$.

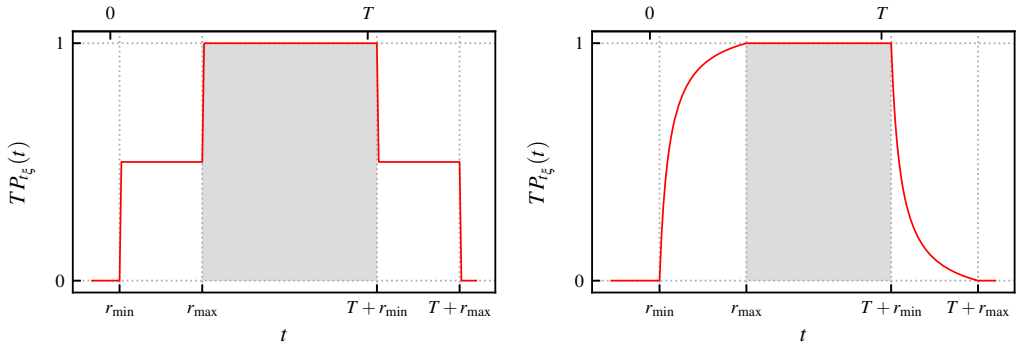

Figure 5: Distribution of pulse arrival times t_ξ at the radial position $x = \xi$ for a discrete (left panel) and continuous (right panel) uniform distribution of pulse velocities. Here $r_{\min}$ is the minimum radial transit time and $r_{\max}$ is the maximum transit time.

End effects in realizations of the process can be neglected by taking $T \gg r_{\max} - r_{\min}$, then the pulse arrivals are uniformly distributed at radial positions limited by the results above and the process retain its Poisson property. It is to be noted that the interval of uniform arrivals diminishes as $v_{\min}$ becomes arbitrarily small, again revealing issues with pulse velocities which are close to zero.

The auto-correlation function

The two-point correlation of the process $\Phi_K(x,t)$ for a spatial lag Δx and temporal lag Δt is given by a double sum

$$\begin{aligned} R_{\Phi_K}(x,t;\Delta x,\Delta t) &= \langle \Phi_K(x,t)\, \Phi_K(x+\Delta x, t+\Delta t)\rangle \\ &= \left\langle \sum_{k=1}^{K}\sum_{k'=1}^{K} \phi_k(x,t)\, \phi_{k'}(x+\Delta x, t+\Delta t)\right\rangle. \end{aligned} \tag{2.76}$$

This double sum contains two types of contributions. There are K terms for which $k = k'$, and then $K(K-1)$ for which $k \neq k'$. For the $k \neq k'$ case, t_k and $t_{k'}$ are independent and the average of the product becomes a product of averages. Again, neglecting end effects by taking the integration limits for t_k and $t_{k'}$ to infinity, changing integration variables and averaging over the number of pulses occurring in the interval of duration T, the auto-correlation function for the stationary process becomes

$$\begin{aligned} R_\Phi(x,\Delta x,\Delta t) &= \langle\Phi\rangle(x)\langle\Phi\rangle(x+\Delta x) + \\ &\frac{1}{\tau_{\mathrm{w}}}\left\langle \frac{a^2\ell}{v}\exp\left(-\frac{2x+v\Delta t}{v\tau_{\shortparallel}}\right)\int_{-\infty}^{\infty}\mathrm{d}\theta\,\exp\left(\frac{2\theta\ell}{v\tau_{\shortparallel}}\right)\varphi(\theta)\varphi\left(\theta+\frac{\Delta x - v\Delta t}{\ell}\right)\right\rangle. \end{aligned} \tag{2.77}$$

In the case of an one-sided exponential pulse function, the auto-correlation function is readily obtained

$$R_\Phi(x,\Delta x,\Delta t) = \langle\Phi\rangle(x)\langle\Phi\rangle(x+\Delta x) + \frac{1}{2\tau_{\mathrm{w}}}\left\langle a^2\tau\,\exp\left(-\frac{2x+\Delta x}{v\tau_{\shortparallel}} - \frac{|\Delta x/v - \Delta t|}{\tau}\right)\right\rangle, \tag{2.78}$$

where the pulse duration τ is given by equation (2.46). Defining the centered and scaled random variable

$$\widetilde{\Phi}(x,t) = \frac{\Phi(x,t) - \langle\Phi\rangle(x)}{\Phi_{\mathrm{rms}}(x)}, \tag{2.79}$$

the correlation function for the normalized process is

$$R_{\widetilde{\Phi}}(x,\Delta x,\Delta t) = \frac{\left\langle a^2\tau\,\exp\left(-\frac{2x+\Delta x}{v\tau_{\shortparallel}} - \frac{|\Delta x/v-\Delta t|}{\tau}\right)\right\rangle}{\sqrt{\left\langle a^2\tau\,\exp\left(-\frac{2x}{v\tau_{\shortparallel}}\right)\right\rangle}\sqrt{\left\langle a^2\tau\,\exp\left(-\frac{2(x+\Delta x)}{v\tau_{\shortparallel}}\right)\right\rangle}}. \tag{2.80}$$

For vanishing spatial lag $\Delta x = 0$ the temporal auto-correlation function is given by

$$R_{\widetilde{\Phi}}(x, \Delta x = 0, \Delta t) = \frac{\left\langle a^2 \tau \, \exp\left(-\frac{2x}{v\tau_{\shortparallel}} - \frac{|\Delta t|}{\tau}\right)\right\rangle}{\left\langle a^2 \tau \, \exp\left(-\frac{2x}{v\tau_{\shortparallel}}\right)\right\rangle}. \tag{2.81}$$

Here the correlation time is given by the harmonic mean of the radial transit time and the linear damping time, $1/\tau = v/\ell + 1/\tau_{\shortparallel}$. The overall factor $\exp[-2x/(v\tau_{\shortparallel})]$ is due to the parallel drainage that a pulse subjected to while it advects radially outwards. Similarly, for vanishing temporal lag, the spatial auto-correlation function is

$$R_{\widetilde{\Phi}}(x, \Delta x, \Delta t = 0) = \frac{\left\langle a^2 \tau \, \exp\left(-\frac{2x+\Delta x}{v\tau_{\shortparallel}} - \frac{|\Delta x|}{v\tau}\right)\right\rangle}{\sqrt{\left\langle a^2 \tau \, \exp\left(-\frac{2x}{v\tau_{\shortparallel}}\right)\right\rangle}\sqrt{\left\langle a^2 \tau \, \exp\left(-\frac{2(x+\Delta x)}{v\tau_{\shortparallel}}\right)\right\rangle}}. \tag{2.82}$$

Here the correlation length is given by the harmonic mean of pulse size and the radial distance traveled during the linear damping time, $1/v\tau = 1/\ell + 1/v\tau_{\shortparallel}$. In the reference case when all pulses have the same size and velocity the auto-correlation function can be written as

$$R_{\widetilde{\Phi}}(\Delta x, \Delta t) = \exp\left(-\frac{|\Delta x/v - \Delta t|}{\tau_{\mathrm{d}}}\right). \tag{2.83}$$

It follows that the correlation function decreases exponentially with both spatial and temporal lag. It also should be noted that this is independent of the radial position x.

Spectral decomposition

According to the Wiener-Khinchin theorem, the auto-correlation function is related to the wavenumber-frequency composition of the stationary process. By Fourier transforming the correlation function the frequency spectrum can be obtained by

$$E_{\widetilde{\Phi}}(k, \omega) = \mathcal{F}\left[R_{\widetilde{\Phi}}(\Delta x, \Delta t)\right] = \int_{-\infty}^{\infty}\int_{-\infty}^{\infty} \mathrm{d}\Delta x \, \mathrm{d}\Delta t \, R_{\widetilde{\Phi}}(\Delta x, \Delta t) \exp\{-i(\omega \Delta t - k\Delta x)\}. \tag{2.84}$$

where the wavenumber k dual to x and the angular frequency ω to t.

In the reference case for the degenerate velocities and sizes and exponentially distributed amplitudes at the reference position, the wavenumber-frequency spectrum is

$$E_{\widetilde{\Phi}}(k, \omega) = \frac{2\tau_{\mathrm{d}}}{1 + \tau_{\mathrm{d}}^2 \omega^2} \delta\Big(k - \frac{\omega}{v}\Big). \tag{2.85}$$

Obviously, this spectrum is defined on a line in wavenumber-frequency space, implying that the process has a specific direction of propagation. This is accounted by the model where pulses move radially in the same direction. The wavenumber transform is

$$S_{\widetilde{\Phi}}(k, \Delta t) = \frac{2v\tau_{\mathrm{d}} \exp\left(ikv\Delta t\right)}{1 + v^2 \tau_{\mathrm{d}}^2 k^2}. \tag{2.86}$$

For vanishing temporal lag Δt, the wavenumber power spectral density is

$$S_{\widetilde{\Phi}}(k) = \frac{2v\tau_{\mathrm{d}}}{1 + v^2 \tau_{\mathrm{d}}^2 k^2}. \tag{2.87}$$

The frequency transform is

$$\Omega_{\widetilde{\Phi}}(\Delta x, \omega) = \frac{2\tau_{\mathrm{d}} \exp\left(-i\frac{\omega}{v}\Delta x\right)}{1 + \tau_{\mathrm{d}}^2 \omega^2}. \tag{2.88}$$

Similarly, for vanishing spatial lag Δx, the frequency power spectral density is

$$\Omega_{\widetilde{\Phi}}(\omega) = \frac{2\tau_{\mathrm{d}}}{1 + \tau_{\mathrm{d}}^2 \omega^2}. \tag{2.89}$$

Both spectra are a Lorentzian function which are flat for small wavenumbers/frequencies and has a power-law scaling for high wavenumbers/frequencies proportional to ω^{-2}. It also should be emphasized that the wavenumber and frequency spectra of the process given by equations (2.87) and (2.89), are determined by both the one-sided exponential pulse shape and pulse duration time. Further, the attention will be focused only on the temporal behavior of the process for a random distribution of pulse velocities.

The probability density function

Consider the reference case of an exponential pulse-shape, degenerate distribution of pulse velocities and sizes and exponentially distributed pulse amplitudes. The raw amplitude moments are $\langle a^n \rangle = n!\langle a \rangle$ and thus cumulants are given by

$$\kappa_n(x) = \frac{\tau_\mathrm{d}}{\tau_\mathrm{w}}(n-1)!\langle a \rangle^n \exp\left(-\frac{nx}{\langle v \rangle \tau_{\shortparallel}}\right). \tag{2.90}$$

This gives the logarithm of the characteristic function as

$$\ln C_\Phi(u,x) = \frac{\tau_\mathrm{d}}{\tau_\mathrm{w}} \sum_{n=1}^{\infty} \frac{1}{n}\left[iu\langle a \rangle \exp\left(-\frac{x}{\langle v \rangle \tau_{\shortparallel}}\right)\right]^n = -\frac{\tau_\mathrm{d}}{\tau_\mathrm{w}} \ln\left[1 - iu\langle a \rangle \exp\left(-\frac{x}{\langle v \rangle \tau_{\shortparallel}}\right)\right], \tag{2.91}$$

here the power series expansion of logarithmic function has been used (see Appendix A). The inverse transform of the characteristic function gives

$$C_\Phi(u,x) = \left[1 - iu\langle a \rangle \exp\left(-\frac{x}{\langle v \rangle \tau_{\shortparallel}}\right)\right]^{-\gamma}. \tag{2.92}$$

This is the characteristic function of a Gamma distribution with scale parameter $\langle a \rangle \exp(-x/\langle v \rangle \tau_{\shortparallel})$ and shape parameter $\gamma = \tau_\mathrm{d}/\tau_\mathrm{w}$. Note that the scale parameter can be written as $\langle a \rangle \exp(-x/\langle v \rangle \tau_{\shortparallel}) = \langle \Phi \rangle / \gamma$, thus the PDF of the process in term of its average value is given by

$$\langle \Phi \rangle P_\Phi(\Phi) = \frac{\gamma}{\Gamma(\gamma)}\left(\frac{\gamma\Phi}{\langle \Phi \rangle}\right)^{\gamma-1} \exp\left(-\frac{\gamma\Phi}{\langle \Phi \rangle}\right), \ \Phi > 0, \tag{2.93}$$

where Γ here is the Gamma function (see Appendix A). Using the normalization defined by equation (2.79), the distribution of the normalized process is

$$P_{\widetilde{\Phi}}(\widetilde{\Phi};\gamma) = \frac{\gamma^{\gamma/2}}{\Gamma(\gamma)}\left(\widetilde{\Phi} + \gamma^{1/2}\right)^{\gamma-1} \exp\left(-\gamma^{1/2}\widetilde{\Phi} - \gamma\right), \ \widetilde{\Phi} > -\gamma^{1/2}. \tag{2.94}$$

Note that the PDF of $\widetilde{\Phi}$ only depends on the intermittency parameter γ. Moreover, it can be evident that the cumulants of the process for a random distribution of pulse velocities (i.e. time-independent) and exponential amplitude distribution at reference position $x = 0$ are given by

$$\kappa_n(x) = \frac{1}{\tau_\mathrm{w}}(n-1)!\langle a_0 \rangle^n \left\langle \frac{\tau_{\shortparallel}\ell}{v\tau_{\shortparallel} + \ell} \right\rangle, \tag{2.95}$$

where amplitudes with a zero in the subscript emphasized the exponential distribution of the pulse amplitudes at reference position. Correspondingly, the process at reference position is also a Gamma distribution given by equation (2.94). As will be seen later, no closed form expression of the probability distribution function for $x > 0$ can be obtained, since distribution of pulse velocities causes a radial change in the amplitude distribution.

3 Numerical implementation of stochastic process

Consider a layer of SOL plasma bounded radially between $x = 0$ and $x = L$, where L represents the width of the SOL. A reference position $x = 0$ is defined as the beginning of a simulation domain and gives any reference position which is reasonable, i.e. the position of the separatrix or the position of the break point between near and far SOL/shoulder. Figure 6 illustrates how filament motion would look like if projected on this layer. Consider a filament/pulse ϕ_k of size ℓ_k moving along the radial coordinate x with prescribed constant velocity v_k. During its radial propagation, the filament retain the same shape at all times, which represented here by an one-sided exponential pulse function given by Eq. (2.27). At reference time t_k the pulse arrives at the reference position $x = 0$ with specified initial amplitude a_k. As the pulse advects radially, its amplitude will be modified due to linear damping with time-scale $\tau_{\shortparallel}$.

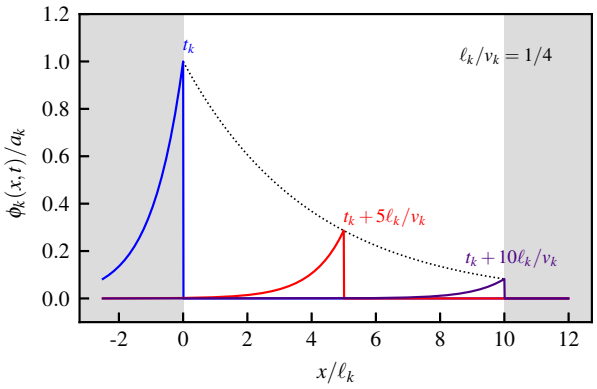

Figure 6: Radial variation of a one-sided exponential pulse with constant velocity v_k and size ℓ_k. The white region represents the simulation domain. The dotted line display the exponential damping of the pulse amplitude in the presence of parallel drainage time.

Simulation domain and evolution equation

The simulation domain is taken to be uniformly discretised with spatial resolution $\Delta_x = L/N_x$ as $x_j = j \cdot \Delta_x$ where $j = 0, 1 \ldots N_x$. The temporal domain of the length T is also discretised into small intervals of uniform duration $\Delta_t = T/N_t$ such that $t_i = i \cdot \Delta_t$ where $i = 0, 1 \ldots N_t$. In this space-time domain each pulse $\phi_k(x,t)$ can be discretized, such that the pulse at x_j and at time t_i is $\phi(x_j, t_n)$. Here, and in the following, subscripts i and j refers to these discrete sampling times and positions. In numerical study there are K pulses in a time interval T and the propagation of the $k-$th pulse from reference position occurs at the time $t_i = t_k$. When this pulse has been initialized, its evolution will be governed by in accordance with equation (2.32),

$$\phi_k(x_j, t_i) = a_k \exp\left(-\frac{t_i - t_k}{\tau_{\shortparallel}}\right)\varphi\left(\frac{x_i - X_k(t_i)}{\ell_k}\right). \tag{3.1}$$

Here random variables t_k, a_k and ℓ_k defined by a value, associated with given probability distribution. As one have seen in the previous section, the radial position of the pulse is given by the integral

$$X_k(t) = \int_{t_k}^{t} \mathrm{d}t'\, V_k(t').$$

By defining X_k in this way, the observed position of the pulse is dependent on the integral values. Given that the pulse velocity is a function of a pulse parameters and instantaneous amplitude, this integral can be calculated explicitly and its numerical evaluation can be avoided. In present work, two case have been considered for which integration gives

- **Time-independent velocities**

$$X_k(t) = v_k(t - t_k) \tag{3.2}$$

  Here the values v_k are associated with considered probability distribution.

- **Time-dependent velocities**

$$X_k(t) = \frac{v_0 \tau_{\shortparallel} a_{0,k}^{\zeta}}{\zeta \langle a_0 \rangle^{\zeta}} \left[1 - \exp\left(-\frac{\zeta (t - t_k)}{\tau_{\shortparallel}} \right) \right]. \tag{3.3}$$

  Equation (3.3) relies on a very specific relation between v_0 and $a_{0,k}$. This relation between velocities and amplitudes and resulting radial position has been introduced in section 5.

The next step is to build a synthetic realization of the process by summing K pulses for each radial position, namely

$$\Phi(x_j, t_i) = \sum_{k=1}^{K} \phi_k(x_j, t_i). \tag{3.4}$$

Numerical setup

To produce a synthetic 1D realization of the process with duration T, the pulse waiting time $\tau_{\mathrm{w}}(0)$ at $x = 0$, the parallel transit time $\tau_{\shortparallel}$, the sampling time Δ_t and the spatial resolution Δ_x should be specified. With Δ_x, an array holds a $N_x = L/\Delta_x$ number of a time series evaluated at x_j. At a constant sampling rate $1/\Delta_t$, a total of $N_t = T/\Delta_t$ samples are obtained. The pulse arrivals t_k are uniformly distributed and consider to arrive over time interval $0 \leqslant t_k \leqslant T_k$.

To make analysis more general, the model may be normalized. The final goal of normalization process is to make all random variables involved in process to be comparable. For the computations the pulse parameters are normalized by their average value, all times by $\tau_0 = \langle l \rangle / \langle v \rangle$, and radial coordinate by $\langle \ell \rangle$, such that

$$\bar{x} = \frac{x}{\langle \ell \rangle}, \quad \bar{a} = \frac{a}{\langle a_0 \rangle}, \quad \bar{\ell} = \frac{\ell}{\langle \ell \rangle}, \quad \bar{v} = \frac{v}{\langle v \rangle}, \quad \overline{T} = \frac{T}{\tau_0}, \quad \bar{\Delta}_t = \frac{\Delta_t}{\tau_0}, \quad \bar{\tau}_{\shortparallel} = \frac{\tau_{\shortparallel}}{\tau_0}, \quad \bar{\tau}_{\mathrm{w}} = \frac{\tau_{\mathrm{w}}}{\tau_0}. \tag{3.5}$$

In general, the dimensional parameters at the boundary of fusion plasmas widely vary from one plasma discharge to another. Therefore, an order of magnitude estimate will be considered. In a medium size tokamak, the width of the SOL is typically estimated to be a few centimetres, $L_{\perp} < 0.1$ m, the parallel connection length $L_{\parallel} \approx 10$ m and acoustic speed $C_{\mathrm{s}} \approx 10$ km/s. These give reasonable estimate for the parallel transient time $\tau_{\shortparallel} = L_{\parallel}/C_{\mathrm{s}} \approx 10^{-4}$ s. A filament has cross-field size typically $\langle \ell \rangle \sim 1 - 3$ cm, moves radially outwards with typical velocity $\langle v \rangle \sim 0.5 - 1$ km/s [20]. With these considerations $\tau_{\shortparallel} = 10\,\tau_0$ and $L = 10\langle \ell \rangle$ in the following.

For the succeeding analysis, the realisation for $\bar{\tau}_w = 0.1$ are produced with $\bar{\Delta}_t = 0.01$ and $\bar{\Delta}_x = 1$ for time-independent velocities and $\bar{\Delta}_x = 0.5$ for time-dependent velocities. Quantities given by equation (3.5) normalised such that $\langle \ell \rangle = \langle v \rangle = \langle a_0 \rangle = 1$ and thus $\tau_0 = 1$. Therefore, each time series at x_j is generated with $T = 10^6$ and $\Delta_t = 0.01$ and have $N_t = 10^8$ samples. While the spatial resolution may be chosen in accordance how well the radial profiles will be resolved, the requirement on sampling time and duration of time series in order to accurately compute lower order statistical moments need to be given and will be addressed in preceding subsection. It is also worth to note, that the generation of single realization is a quite memory and time demanding computations, thus the spatial sampling rate has been taken to be low. An example of a synthetic realization is given in figure 7. Note that initially time series at $\bar{x} = 0$ is non-stationary. This is due to the transient building up at small times and where only few pulses contribute to statistics of the process. Therefore the time series will be examined after the initial transient. Moreover, the end effects can be accounted for in a realization of the process at $x > 0$ by considering results obtained previously for uniform distribution of arrival time. However, this results only holds for time-independent velocities, and the time series should be analyze manually in the case of time-dependent velocities.

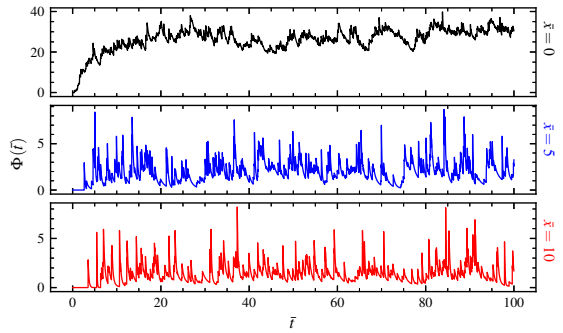

Figure 7: A short part of the times series of the normalized synthetic process for a degenerate pulse sizes, a truncated exponentially distributed pulse amplitudes and velocities that have a linear dependence on the initial amplitudes at different normalized radial positions.

3.1 Moment Estimators and Convergence

In order to estimate the moments of the synthetic time series underlying a set of N_t samples at some position x_j, the method of moments can be used. The estimators of mean, variance, skewness and flatness are defined respectively by

$$\hat{\mu} = \frac{1}{N_t}\sum_{i=1}^{N_t} y_i, \tag{3.6a}$$

$$\hat{\sigma}^2 = \frac{1}{N_t - 1}\sum_{i=1}^{N_t}(y_i - \hat{\mu})^2, \tag{3.6b}$$

$$\hat{S} = \frac{\sum_{i=1}^{N_t}(y_i - \hat{\mu})^3}{\left(\sum_{i=1}^{N_t}(y_i - \hat{\mu})^2\right)^{3/2}}, \tag{3.6c}$$

$$\hat{F} = \frac{\sum_{i=1}^{N_t}(y_i - \hat{\mu})^4}{\left(\sum_{i=1}^{N_t}(y_i - \hat{\mu})^2\right)^{2}} - 3. \tag{3.6d}$$

here y_i refer to values of the time series at given x_j at some time instant t_i. In general, these estimators are the functions of random variable y_i and therefore a random variable itself. Under the condition that large outliers are unlikely, the law of large numbers states that with increasing sample size N_t its value converges to the true value that one wishes to estimate. Namely, the estimators given by equation (3.6) as N_t grows would result in a random path that, as stated by the law of large numbers, show a tendency to approach the true value of moments. Additionally, it has previously been found that for a FPP process with one-sided exponential pulse shapes and exponentially distributed pulse amplitudes, the mean square error of all estimators are inversely proportional to the number of samples N_t for $N\Delta_t/\tau_{\mathrm{d}} \gg 1$ [43]. Meaning that the time series of duration $T = N\Delta_t$ is well resolved on the time scale of a single pulse. Also, it was found that the relative mean squared error is inversely proportional to γ. Consequently, a strongly intermittent process (that is $\gamma \ll 1$) has a much larger relative error on mean estimator than a process with significant pulse overlap (that is $\gamma \gg 1$). Thus, in order to obtain predictions from synthetic realizations with high accuracy, long time series with high sampling frequency are required as well as relatively large intermittency parameter, i.e. $\bar{\tau}_{\mathrm{w}}$ is small, are required. As an example, the estimators of the mean and variance of the process for degenerate distribution of pulse velocities as function of sample size N_t are illustrated in figure 8. Showing that the model parameters defined in previous section (i.e. $\bar{T} = 10^6, \bar{\Delta}_t = 0.01, \bar{\tau}_{\mathrm{w}} = 0.1$) are sufficient to produce accurate predictions.

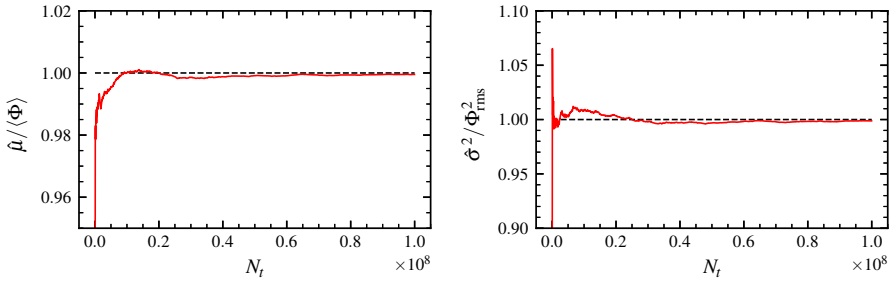

Figure 8: Estimators normalized to their true values obtained from synthetic time series at $\bar{x} = 5$ of the process for degenerate distribution of pulse velocities and sizes and exponentially distributed amplitudes.

4 Time-independent pulse velocities

In the following, the case of the time-independent pulse velocities will be considered. All pulses are one-sided exponential and assumed to have the same, fixed size $\langle \ell \rangle$. Also, pulse amplitudes are exponentially distributed at the reference position $x = 0$ with mean amplitude $\langle a_0 \rangle$.

In this contribution, three qualitatively different velocity distributions will be considered; a uniform distribution, a unimodal distribution and an exponential distribution. The velocity distribution will be parameterized such that it is only defined by mean velocity $\langle v \rangle$ and either a width or a shape parameter. The parameterization can be performed, by taking account of the two inherent properties of the probability distribution,

$$\int_0^\infty \mathrm{d}v \, P_v(v) = 1, \tag{4.1a}$$

$$\langle v \rangle = \int_0^\infty \mathrm{d}v \, v P_v(v). \tag{4.1b}$$

For example, traditionally, the Gamma distribution with a shape parameter $k > 0$ and a scale parameter $\theta > 0$ and its mean value are given by

$$P_v(v; s, \theta) = \frac{v^{s-1}}{\theta^s \Gamma(s)} \exp\left(-\frac{v}{\theta}\right), \tag{4.2a}$$

$$\langle v \rangle = \theta s. \tag{4.2b}$$

Equation (4.2b) yields in an expression for the scale in terms of the mean and the shape parameter, $\theta = \langle v \rangle / s$. Substituting this in (4.2a), results in the distribution which is defined only by $\langle v \rangle$ and s,

$$P_v(v; \langle v \rangle, s) = \frac{s}{\langle v \rangle \Gamma(s)} \left(\frac{sv}{\langle v \rangle}\right)^{s-1} \exp\left(-\frac{sv}{\langle v \rangle}\right), \tag{4.3}$$

and for which the requirement (4.1a) satisfied.

For a particularly relevant case, the power-law relation between pulse amplitudes and velocities will also be considered. The effect of a random distribution of pulse velocities on the lowest order statistical moments, auto-correlation function and frequency spectrum will be investigated and compared to the reference case for the degenerate distribution of pulse velocities. In all cases, the realizations have been normalized to have unit mean of pulse sizes, amplitudes and velocities.

4.1 Discrete uniform pulse velocity distribution

Consider pulse velocities v_k that can take two different values $v_1 = \langle v\rangle(1-w)$ and $v_2 = \langle v\rangle(1+w)$ and each of them having the same probability. Then, the velocity distribution can be described by the discrete uniform distribution

$$P_v(v;\langle v\rangle, w) = \frac{1}{2}\left[\delta(v-v_1) + \delta(v-v_2)\right], \tag{4.4}$$

where w in the range $0 < w < 1$ is the width parameter of the velocity distribution. Figure 9 (left panel) illustrates this velocity distribution for different values of the width parameter w.

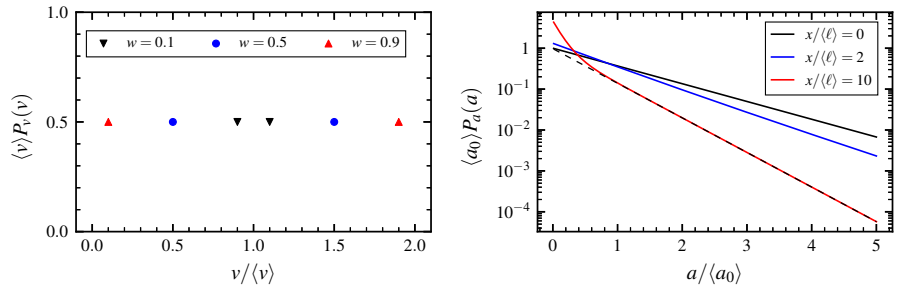

Figure 9: (left panel) Discrete uniform pulse velocity distribution for various values of the width parameter w. (right panel) Probability distribution function of the pulse amplitude with width parameter $w = 0.5$ and $\langle v\rangle\tau_{\shortparallel}/\langle\ell\rangle = 10$ at different radial positions. The black dashed lines corresponds to second term in equation (4.11).

The cumulants for a discrete uniform pulse velocity distribution are readily obtained as

$$\kappa_n(x) = \frac{\langle a_0\rangle^n (n-1)!}{2\tau_{\mathrm{w}}}\left[\tau_1 \exp\left(-\frac{nx}{v_1\tau_{\shortparallel}}\right) + \tau_2 \exp\left(-\frac{nx}{v_2\tau_{\shortparallel}}\right)\right], \tag{4.5}$$

where $\langle a_0\rangle$ is the average of the amplitudes which are specified at reference position $x = 0$ and $\tau_{1,2}$ is the pulse duration dependent on the corresponding pulse velocity, which takes the form

$$\tau_{1,2} = \frac{\tau_{\shortparallel}\langle\ell\rangle}{\tau_{\shortparallel}v_{1,2} + \langle\ell\rangle}. \tag{4.6}$$

For simplicity of notation, hereafter, quantities denoted by a subscript will be associated with the corresponding subscripts of the pulse velocity. The average pulse duration is given by integrating equation (2.46) over the discrete velocity distribution

$$\tau_{\mathrm{d}} = \frac{1}{2}\left(\frac{\tau_{\shortparallel}\langle\ell\rangle}{v_1\tau_{\shortparallel} + \langle\ell\rangle} + \frac{\tau_{\shortparallel}\langle\ell\rangle}{v_2\tau_{\shortparallel} + \langle\ell\rangle}\right). \tag{4.7}$$

In the absence of linear damping, the average duration is

$$\lim_{\langle v\rangle\tau_{\shortparallel}/\langle\ell\rangle\to\infty} \tau_{\mathrm{d}} = \frac{1}{2}\left(\frac{\langle\ell\rangle}{\langle v\rangle(1-w)} + \frac{\langle\ell\rangle}{\langle v\rangle(1+w)}\right) \tag{4.8}$$

As $w \to 0$, the pulse duration is just the radial transit time $\langle\ell\rangle/\langle v\rangle$. As $w \to 1$, there is a divergence due to arbitrarily slow pulses ($v_1 \to 0$) leading to excessively long pulse durations. The average pulse duration both with $\langle v\rangle\tau_{\shortparallel}/\langle\ell\rangle = 10$ and $\langle v\rangle\tau_{\shortparallel}/\langle\ell\rangle \to \infty$ as function of the width parameter w is presented in figure 10 (left panel). From equation (4.5) it follows that the average radial profile for the process is given by

$$\langle\Phi\rangle(x) = \frac{\langle a_0\rangle}{2\tau_{\mathrm{w}}}\left[\tau_1 \exp\left(-\frac{x}{v_1\tau_{\shortparallel}}\right) + \tau_2 \exp\left(-\frac{x}{v_2\tau_{\shortparallel}}\right)\right]. \tag{4.9}$$

In figure 11 the radial profiles of the average, relative fluctuation level, skewness and flatness moments of the process are presented for different values of width parameter w and $\langle v\rangle\tau_{\mathrm{w}}/\langle\ell\rangle = 0.1$. In this figure, markers depict moments which are obtained from the realizations of the process, while curves are analytical results based on equation (4.5). The excellent agreement allows to claim the ability of numerically implemented model to correctly predict the statistical properties of the process.

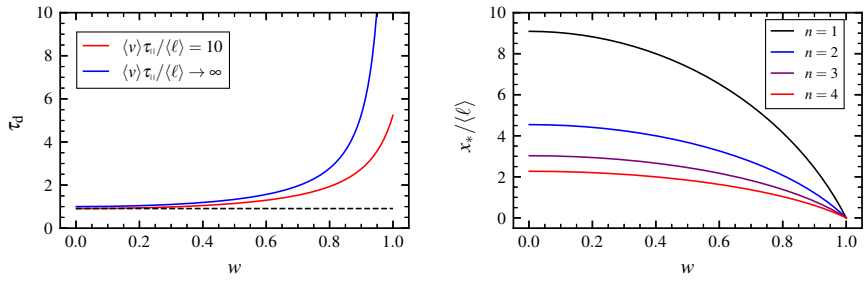

Figure 10: (left panel) Average pulse duration $\tau_{\rm d}$ for a discrete uniform distribution of pulse velocities as function of the width parameter w. (right panel) Break point location as a function of the width parameter w for $\langle v\rangle\tau_{\shortparallel}/\langle\ell\rangle = 10$ and $\langle v\rangle\tau_{\shortparallel}/\langle\ell\rangle \to \infty$ and the first four orders of cumulants n.

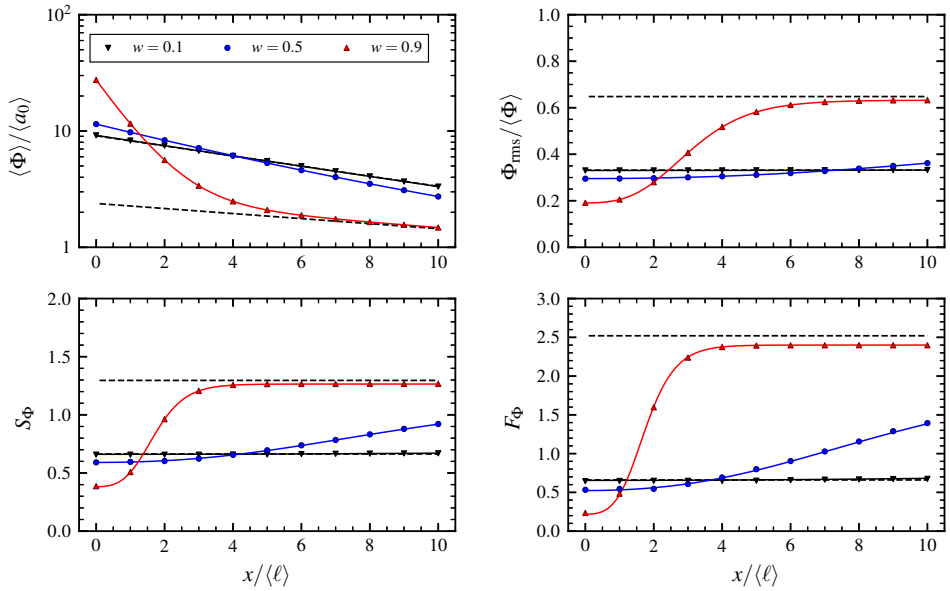

Figure 11: Radial profiles of the average value (top left), relative fluctuation level (top right), skewness (bottom left) and flatness (bottom right) for a discrete uniform distribution of pulse velocities with different values of the width parameter w. Markers indicate simulation results and curves indicate moments obtained from equation (4.5). The black dashed lines gives the radial profiles in the limits $w \to 0$ and $w \to 1$.

The results shown in figure 11 highlight several key features. It is notable that the case $w = 0.1$ is practically indistinguishable from the case of a degenerate distribution of pulse velocities (that is, in the limit $w \to 0$). Namely, for small w the average profile is exponential and the relative fluctuation level, skewness and flatness moments have only weak variation with radial position. As w increases, the average profile exhibits a bi-exponential behaviour. It is steep for small x and has a longer scale length for large x, where it is dominated by the fast pulses. This variation relates to reduced relative fluctuation level, skewness and flatness for small x, while these quantities increase substantially radially outwards until they saturate at the values associated with the process dominated by the fast pulses. This is attributed to the fact that slow pulses have long pulse duration time and short pulse amplitude e-folding length, while fast pulses have short duration time and long e-folding length. Due to such the intrinsic link between pulse amplitudes and durations the profiles show up in the form of short and long exponential decays. As one ensure later, such intimate connection between pulse amplitudes and durations plays an important role on the radial variation of the process statistics, since amplitudes will be modified and get correlated with durations by a distribution of pulse velocities for positive x. As discussed in section 2, the pulse amplitudes change radially according to

$$a(x) = a_0\left(-\frac{x}{v\tau_{\shortparallel}}\right). \tag{4.10}$$

Since the pulse velocities v_1 and v_2 have equal probability to occur, it follows that the conditional

probability distribution of pulse amplitudes, which are exponentially distributed at the reference position $x = 0$, at considered radial position is given by

$$P_a(a; \langle a_0 \rangle, s, x) = \frac{1}{2}\left(\frac{1}{\lambda_1}\exp\left(-\frac{a}{\lambda_1}\right) + \frac{1}{\lambda_2}\exp\left(-\frac{a}{\lambda_2}\right)\right), \tag{4.11}$$

with $\lambda_1 = \langle a_0 \rangle \exp[-x/(v_1\tau_{\shortparallel})]$ and $\lambda_2 = \langle a_0 \rangle \exp[-x/(v_1\tau_{\shortparallel})]$. Since the expected value of a sum is the sum of the expected values, the radial profile of the average pulse amplitude at any radial position x is

$$\langle a \rangle(x) = \frac{\langle a_0 \rangle}{2}\left[\exp\left(-\frac{x}{v_1\tau_{\shortparallel}}\right) + \exp\left(-\frac{x}{v_2\tau_{\shortparallel}}\right)\right]. \tag{4.12}$$

where $\langle a_0 \rangle$ is an average pulse amplitude at reference position $x = 0$. Figure 9 (right panel) shows how the distribution of pulse amplitudes in the case $w = 0.5$ changes at different radial positions. This can be interpreted as follows: at $x > 0$, there is a significant amplitudes reduction of slow pulses. Therefore, at large x, the process will be dominated by the fast pulses which have larger amplitudes due to their short duration. This is indicated by dashed black line in figure 9, corresponding to the second term in equation (4.11). This leads to a radially increasing relative fluctuation level, skewness and flatness moments since the amplitude of pulses contributing significantly to the moments decreases radially. The increase in relative fluctuation level, skewness and flatness is evident from figure 11. Additionally, as stated above, a distribution of pulse velocities leads to a correlation between pulse amplitudes and duration times. The general expression for the cumulants for one-sided exponential pulses is given by

$$\kappa_n(x) = \frac{1}{n\tau_{\mathrm{w}}}\left\langle a^n \tau \exp\left(-\frac{nx}{v\tau_{\shortparallel}}\right)\right\rangle.$$

Clearly, at the reference position $x = 0$ the pulse amplitudes and durations are specified to be independent, and thus are uncorrelated, however at $x > 0$ amplitudes will be modified by velocities which are included in an exponential term. Recall that pulse durations are also dependent on velocity distribution, gives that durations and amplitudes get correlated. In order to quantify this, introduce a linear correlation coefficient which is defined as the covariance of the amplitudes and durations divided by the product of their standard deviations,

$$\rho = \frac{\langle a\tau \rangle - \langle a \rangle \tau_{\mathrm{d}}}{\sqrt{\langle a^2 \rangle - \langle a \rangle^2}\sqrt{\langle \tau^2 \rangle - \tau_{\mathrm{d}}^2}}. \tag{4.13}$$

In figure 13 (right panel) the radial variation of the correlation coefficient for a discrete uniform distribution of pulse velocities is presented for various w. Clearly, a broad distribution of pulse velocities, leads to a strong anti-correlation between pulse durations and amplitudes. Again emphasize that pulses with small (large) velocity will have smaller (larger) amplitudes and large (small) duration times. In much the same way for the n-th order of the cumulants $\kappa_n \sim \langle a^n \tau \rangle$, the build-up correlation between durations and amplitudes is also present, but the correlation will weakness with increasing n, this is illustrated in figure 13 for the width parameter $w = 0.9$ and $n = 1, 2, 3$ and 4. This negative correlation will subsequently enhance the intermittency of the process for large radial positions.

The ratio between two exponential decays in equation (4.5) provides a measure of the slow-fast pulse contribution. Thus, the break point at which fast pulses start to take over is given by the equal contribution of these decays,

$$\frac{x_*}{\langle \ell \rangle} = \frac{\langle v \rangle \tau_{\shortparallel}}{n\langle \ell \rangle}\frac{1 - w^2}{2w}\ln\left(\frac{\langle v \rangle(1 + w)\tau_{\shortparallel} + \langle \ell \rangle}{\langle v \rangle(1 - w)\tau_{\shortparallel} + \langle \ell \rangle}\right), \tag{4.14}$$

and depend on the width of the velocity distribution, linear damping and order of cumulants. It is worth to note that as the order of cumulants and width parameter w increase, the break point moves closer to reference position $x = 0$ as illustrated in figure 10 (right panel). Indeed, in the limit $w \to 1$ or in the limit $n \to \infty$, the break point approaches the reference position $x = 0$. This is consistent with the profiles presented in figure 11. In addition, the radial location of the break point increases with the linear damping, $\langle v \rangle \tau_{\shortparallel}/\langle \ell \rangle$. This is attributed to the fact that in the

absence of linear damping, the pulse propagates without change in amplitude and with a duration given by ℓ/v and the general expression for the cumulants in this case becomes

$$\kappa_n(x) = \frac{1}{n\tau_w}\left\langle \frac{a^n}{v/\ell} \right\rangle. \tag{4.15}$$

It is clear that there is no variation in the radial direction x. Therefore, the profiles are radially constant and there is no break point present.

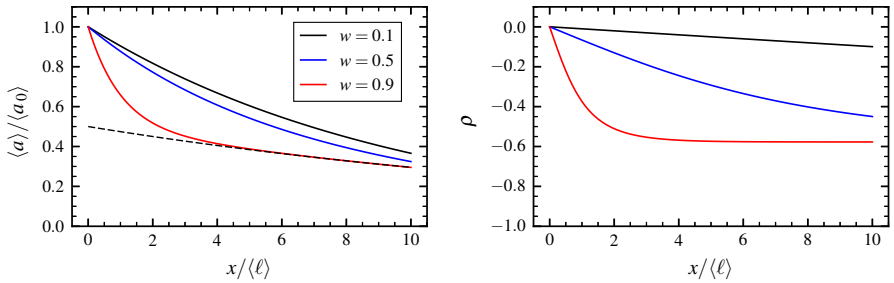

Figure 12: (left panel) Average pulse amplitude as function of radial position for a discrete uniform distribution of pulse velocities for various values of shape parameter w. The black dashed line corresponds to the second term in equation (4.12). (right panel) Linear correlation coefficient as function of radial position for a discrete uniform distribution of pulse velocities for various values of shape parameter w.

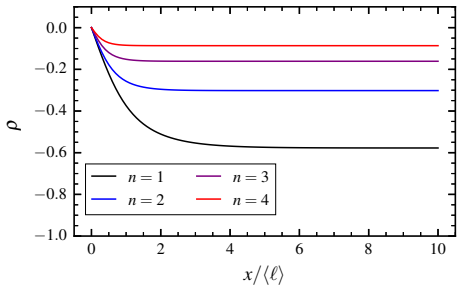

Figure 13: Linear correlation coefficient as function of radial position for a discrete uniform distribution of pulse velocities for the shape parameter $w = 0.9$.

One can find the PDF in closed form for the discrete uniform distribution of pulse velocities. Evidently, the process can be written as the sum of two sub-processes corresponding to small(large) velocity and half number of pulses. The distribution of the process for the case of exponentially distributed amplitudes and degenerate sizes and velocities is a Gamma distribution. Therefore, if two sub-processes Φ_1 and Φ_2 are independent gamma-distributed random variables with parameters (γ_1, θ_1) and (γ_2, θ_2), then the PDF of their sum $\Phi = \Phi_1 + \Phi_2$ is given by convolution and can be written as

$$P_\Phi(\Phi) = \frac{\mathcal{M}(\gamma_1, \gamma_1+\gamma_2, \Phi/\theta_2 - \Phi/\theta_1)}{\Gamma(\gamma_1+\gamma_2)\theta_1^{\gamma_1}\theta_2^{\gamma_2}} \Phi^{\gamma_1+\gamma_2-1} \exp\left(-\frac{\Phi}{\theta_2}\right), \quad \Phi > 0, \tag{4.16}$$

where $\gamma_1 = \tau_1/2\tau_w$ is the shape parameter associated with slow pulses, $\gamma_2 = \tau_2/2\tau_w$ is the shape parameter associated with fast pulses and $\mathcal{M}$ is the confluent hypergeometric function of the first kind. The scale parameters $\theta_{1,2}$ are the same as $\lambda_{1,2}$, which are corresponding components of the average amplitude given by equation 4.12. This closed form expression of the distribution of a sum of two gamma distributed variables is based on the more general result given in [44]. Using the mean and root mean square values given by equation (4.5), the distribution of the normalized

process is given by

$$P_{\widetilde{\Phi}}(\widetilde{\Phi}) = \frac{\mathcal{M}\left(\gamma_1, \gamma_1+\gamma_2, \sqrt{\gamma_1\theta_1^2+\gamma_2\theta_2^2}\,(\theta_1-\theta_2)\,\widetilde{\Phi}/\theta_1\theta_2 + \gamma_2\left(1-\frac{\theta_2}{\theta_1}\right) - \gamma_1\left(1-\frac{\theta_1}{\theta_2}\right)\right)}{\Gamma(\gamma_1+\gamma_2)\theta_1^{\gamma_1}\theta_2^{\gamma_2}}$$
$$\times \left(\sqrt{\gamma_1\theta_1^2+\gamma_2\theta_2^2}\right)^{\gamma_1+\gamma_2}\left(\widetilde{\Phi}+\frac{\gamma_1\theta_1+\gamma_2\theta_2}{\sqrt{\gamma_1\theta_1^2+\gamma_2\theta_2^2}}\right)^{\gamma_1+\gamma_2-1}\exp\left(-\frac{\sqrt{\gamma_1\theta_1^2+\gamma_2\theta_2^2}\,\widetilde{\Phi}}{\theta_2}-\gamma_2-\gamma_1\frac{\theta_1}{\theta_2}\right),$$
$$\widetilde{\Phi} > -\frac{\gamma_1\theta_1+\gamma_2\theta_2}{\sqrt{\gamma_1\theta_1^2+\gamma_2\theta_2^2}}. \tag{4.17}$$

In figure 14, the probability distribution of the normalized realization of the process for the discrete uniform distribution of the pulse velocities for different values of the width parameter w compared to the analytical PDF given by equation (4.17) shown with the dashed black line is presented is presented at different radial positions x.

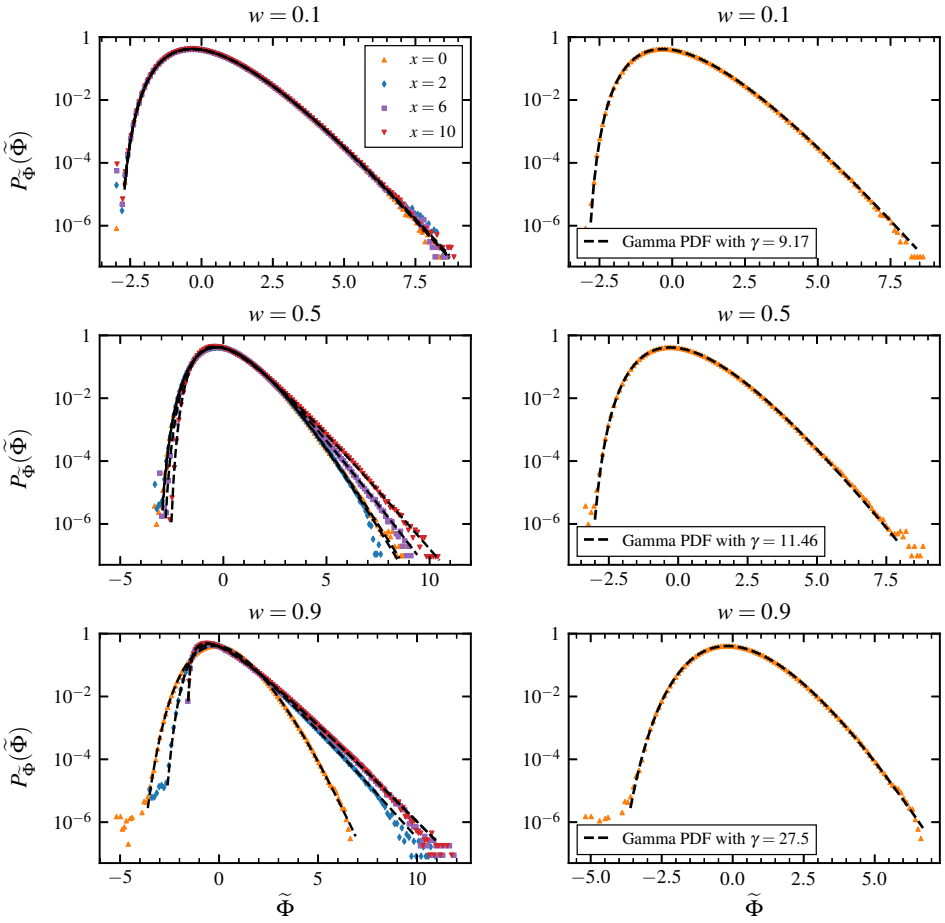

Figure 14: (left panel) Probability density functions of the normalized process at different radial positions and various values of the shape parameter w. The dashed black lines give the true distributions. The values of x and their corresponding color are shown in the inset. (right panel) Probability distribution function of the normalized process at $x = 0$ with various values of w compared to a normalized gamma distribution with shape parameter $\gamma = \gamma_1 + \gamma_2$ shown with the dashed black line.

At the reference position $x = 0$ the scale parameter θ for two sub-processes are the same, and the sum of the two gamma distributed variables is also a gamma distribution but with shape parameter $\gamma_1 + \gamma_2$. Contribution of the slow pulses is negligible at large radial positions and the PDF approaches a Gamma distribution with shape parameter γ_2. In figure 14, the consequence of enhanced intermittency with increased radial position is seen. The tail of the distribution get heavier, which is expected from increasing skewness and kurtosis coefficients (see figure 11). This is clearest for the case $w = 0.9$, where the intermittency change rapidly from $\gamma = \gamma_1 + \gamma_2$ at $x = 0$ to $\gamma = \gamma_2$ at $x = 10$.

The auto-correlation function for one-sided exponential pulses is readily obtained as

$$R_\Phi(x,\Delta x,\Delta t) = \langle\Phi\rangle(x)\langle\Phi\rangle(x+\Delta x) + \frac{\langle a_0\rangle^2}{2\tau_\mathrm{w}}\left[\tau_1 \exp\left(-\frac{2x+\Delta x}{v_1\tau_{\shortparallel}} - \frac{|\Delta x/v_1 - \Delta t|}{\tau_1}\right)\right.$$
$$\left.+\tau_2 \exp\left(-\frac{2x+\Delta x}{v_2\tau_{\shortparallel}} - \frac{|\Delta x/v_2 - \Delta t|}{\tau_2}\right)\right] \tag{4.18}$$

A temporal correlation function at arbitrary position x can be realized by the equation (4.18), by choosing the $\Delta x = 0$. In that case, the normalized auto-correlation function is given by

$$R_{\widetilde{\Phi}}(x,\Delta x=0,\Delta t) = \frac{\tau_1 \exp\left(-\frac{2x}{v_1\tau_{\shortparallel}} - \frac{|\Delta t|}{\tau_1}\right) + \tau_2 \exp\left(-\frac{2x}{v_2\tau_{\shortparallel}} - \frac{|\Delta t|}{\tau_2}\right)}{\tau_1 \exp\left(-\frac{2x}{v_1\tau_{\shortparallel}}\right) + \tau_2 \exp\left(-\frac{2x}{v_2\tau_{\shortparallel}}\right)}, \tag{4.19}$$

and appears in the form of two-exponential decay. The corresponding frequency spectrum becomes

$$\Omega_{\widetilde{\Phi}}(x,\omega) = \frac{2}{\tau_1 \exp\left(\frac{2x}{\tau_{\shortparallel}v_2}\right) + \tau_2 \exp\left(\frac{2x}{\tau_{\shortparallel}v_1}\right)}\left(\frac{\tau_1^2 \exp\left(\frac{2x}{\tau_{\shortparallel}v_2}\right)}{1+\tau_1^2\,\omega^2} + \frac{\tau_2^2 \exp\left(\frac{2x}{\tau_{\shortparallel}v_1}\right)}{1+\tau_2^2\,\omega^2}\right), \tag{4.20}$$

where ω is the angular frequency. The choice of angular frequencies stemmed from greatly simplified Fourier transforms. The linear frequency f is related to the angular frequency by $\omega = 2\pi f$. The power spectral density has the double Lorentzian form. For large radial positions,

$$\lim_{x\to\infty} R_{\widetilde{\Phi}}(x,\Delta t) = \exp\left(-\frac{|\Delta t|}{\tau_2}\right), \tag{4.21a}$$

$$\lim_{x\to\infty} \Omega_{\widetilde{\Phi}}(x,\omega) = \frac{2\tau_2}{1+\tau_2^2\,\omega^2}. \tag{4.21b}$$

In this limit, the ACF and PSD are the same as for the case with constant pulse velocity at v_2. The correlation functions and corresponding power spectra with linear frequencies of normalized realizations of the process are presented in figure 15. As w increase, they both reveal the presence of two distinct characteristic time scales. This is particularly clear in the case $w = 0.9$, when the auto-correlation function is presented with semi-logarithmic plot (figure 16: left panel), in which a fast decay of short e-folding time τ_2 is followed by a slow one of longer e-folding time τ_1. With increasing radial position, the correlation function dominated by short decay times of fast pulses for small and further larger time lags. Also, it is worth noting that the auto-correlation function decay have a significant impact on break point frequencies. In fact, a pair of characteristic decay times corresponds to a pair of break point angular frequencies in the Lorentzian function. From equation (4.19), it is evident that the pair of e-folding times of $R_{\widetilde{\Phi}}$, is the pair of pulse duration times τ_1 and τ_2. Moreover, break point linear frequencies $f_{1,2} = 1/(2\pi\tau_{1,2})$ in figure 16 (right panel), giving the approximate pair of frequencies where the PSD changes from a flat spectrum to a power law behavior. For $w \leqslant 0.1$, only a small gap between break point frequencies is observable. Alternatively, the spectrum amplitude before the term $2\tau_1/(1+\tau_1^2\,\omega^2)$ may be negligible at large radial positions (see equation (4.20) and equation (4.21b)). All these cases lead to a specific limit of the single Lorentzian spectum.

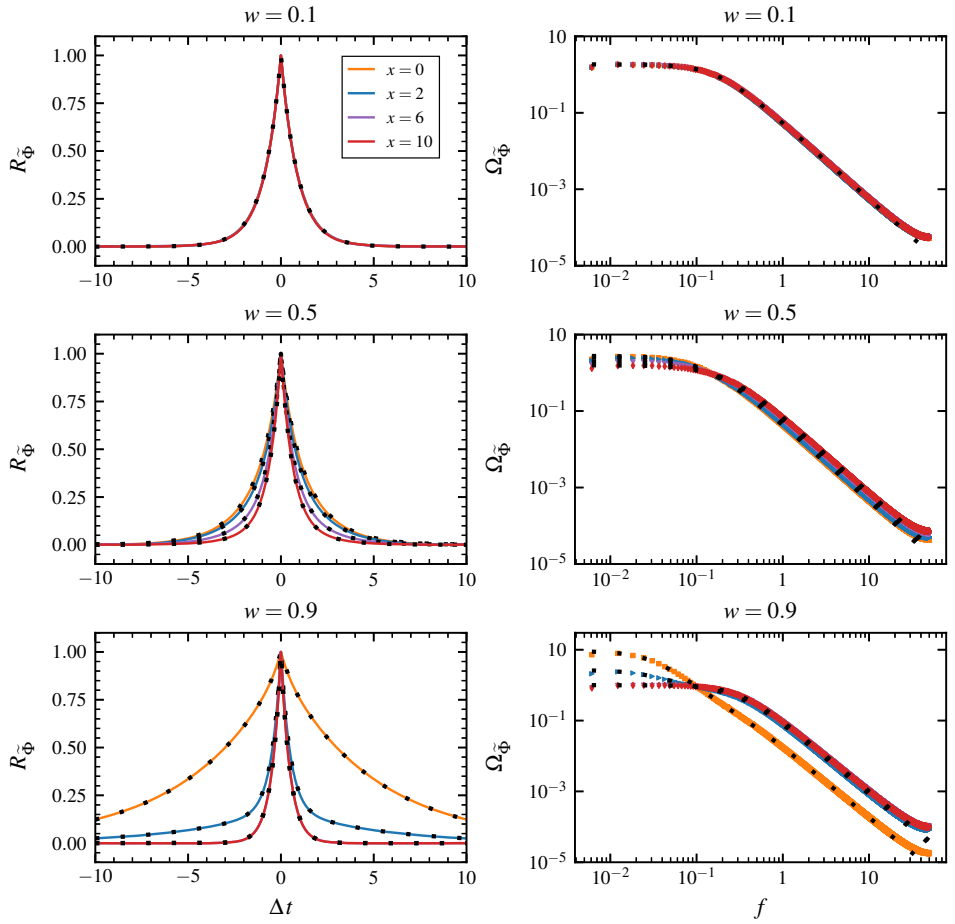

Figure 15: Auto-correlation function and power spectral density for various radial positions x of the normalized process for various values of the width parameter w. The colored lines denote estimates from realizations of a discrete uniform distribution of pulse velocities and black dotted lines denote analytical expressions given by (4.19) and (4.20). The values of x and their corresponding color are shown in the inset.

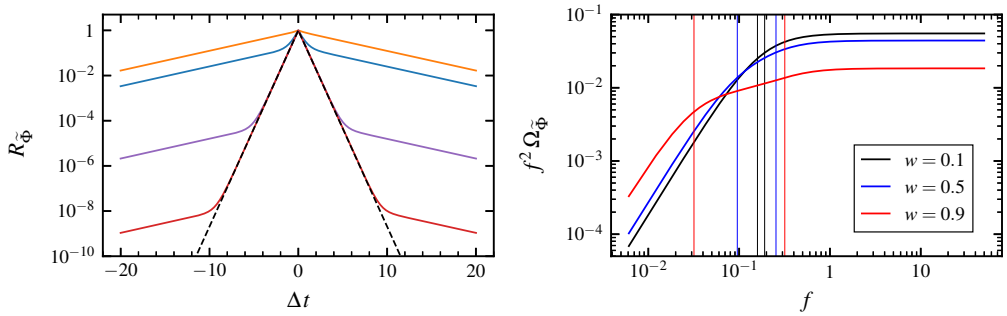

Figure 16: (left panel) Log-linear plot of the analytic auto-correlation function with the width parameter $w = 0.9$ for various radial positions. The values of x and their corresponding color are the same as for Figure 15. The dashed black line correspond to the limit $x \to \infty$ given by equation (4.21a). (right panel) Analytic compensated power spectral density at $x = 0$ for different width parameter w of the discrete uniform velocity distribution. The vertical lines give a pair of break point linear frequencies of the corresponding case, $f_{1,2}$.

4.2 Continuous uniform pulse velocity distribution

In contrast to the discrete case studied in the previous subsection, consider the continuous uniform velocity distribution given by

$$P_v(v;\langle v\rangle,w)=\begin{cases}\dfrac{1}{2\langle v\rangle w}, & \text{if } v\in[v_{\min},v_{\max}],\\ 0, & \text{otherwise,}\end{cases} \tag{4.22}$$

where the minimum and maximum pulse velocities are given by $v_{\min}=\langle v\rangle(1-w)$ and $v_{\max}=\langle v\rangle(1+w)$, respectively, and w in the range $0<w<1$ is the width parameter of the distribution. The limit $w\to 0$ corresponds to the case of a degenerate distribution of pulse velocities.

When the pulse duration times are given by equation (2.46) and velocities have a continuous uniform distribution, the pulse duration's distribution becomes

$$P_\tau(\tau;s)=\begin{cases}\dfrac{\langle\ell\rangle}{2\langle v\rangle w}\dfrac{1}{\tau^2}, & \text{if } \tau\in[\tau_{\min},\tau_{\max}],\\ 0, & \text{otherwise,}\end{cases} \tag{4.23}$$

where $\tau_{\min}=\tau_{\shortparallel}\langle\ell\rangle/(\langle v\rangle(1+w)\tau_{\shortparallel}+\langle\ell\rangle)$ is the minimum pulse duration and $\tau_{\max}=\tau_{\shortparallel}\langle\ell\rangle/(\langle v\rangle(1-w)\tau_{\shortparallel}+\langle\ell\rangle)$ is the maximum duration. The continuous uniform velocity distribution and corresponding duration time distribution are presented in figure 17 for various values of the width parameters w.

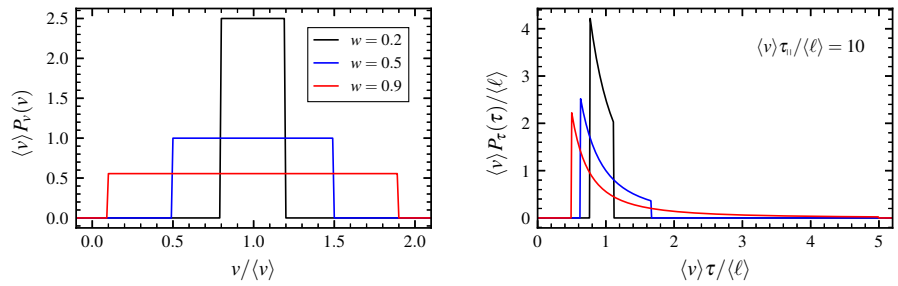

Figure 17: Marginal velocity and duration time distribution functions given by equations (4.22) and (4.23), respectively, for different values of the width parameter w of the continuous uniform distribution of pulse velocities.

The average pulse duration is

$$\tau_{\mathrm{d}}=\frac{\langle\ell\rangle}{2w\langle v\rangle}\ln\left(\frac{\langle v\rangle(1+w)\tau_{\shortparallel}+\langle\ell\rangle}{\langle v\rangle(1-w)\tau_{\shortparallel}+\langle\ell\rangle}\right). \tag{4.24}$$

As expected, in the limit $w\to 0$ the average pulse duration is the same as for the case of a degenerate distribution of pulse velocities. For a broad velocity distribution, the average pulse duration reaches its maximum value given by limit

$$\lim_{w\to 1}\tau_{\mathrm{d}}=\frac{\langle\ell\rangle}{2\langle v\rangle}\ln\left(2\frac{\langle v\rangle}{\langle\ell\rangle}\tau_{\shortparallel}+1\right). \tag{4.25}$$

In figure 18 (left panel), the average pulse duration both with $\langle v\rangle\tau_{\shortparallel}/\langle\ell\rangle=10$ and $\langle v\rangle\tau_{\shortparallel}/\langle\ell\rangle\to\infty$ is presented for different width parameter w. It should be noted that in the absence of parallel drainage (that is, in the limit $\langle v\rangle\tau_{\shortparallel}/\langle\ell\rangle\to\infty$), equation (4.25) logarithmically diverge since the maximum pulse duration becomes infinitely large when the minimum pulse velocity vanishes.

As the preceding subsection pointed out, a radial change of the amplitude distribution leads to radial changes of the statistical properties of the process. In general, the probability distribution function of pulse amplitudes for a continuous distribution of pulse velocities is not possible to find in closed form. An integral representation can be found by noting that the amplitudes in equation (2.38) include the product of two independent random variables; exponentially distributed amplitudes a_0 at the reference position, $x=0$, and a random variable obtained as a result of the transformation of the pulse velocities, $y=\exp(-x/(v\tau_{\shortparallel}))$.

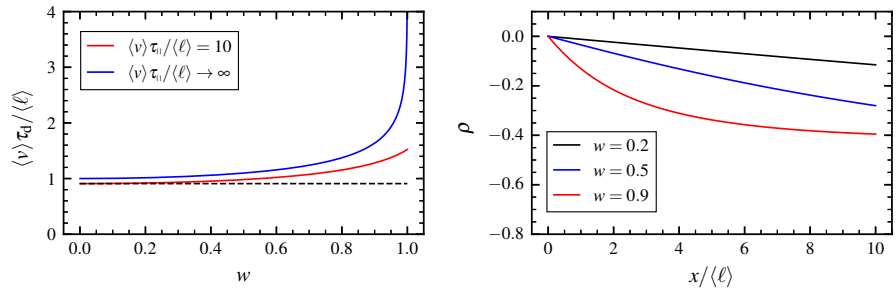

Figure 18: (left panel) Average pulse duration for a continuous uniform distribution of pulse velocities as function of the width parameter w. The dashed black line indicate the average pulse duration for a degenerate distribution of pulse velocities. (right panel) Radial profile of the linear correlation coefficient between pulse durations and amplitudes for a continuous uniform distribution of pulse velocities for different values of the width parameter w.

Thus, the PDF of the pulse amplitudes at position $x/\langle\ell\rangle$ is accessible as a product convolution (see Appendix D)

$$\langle a_0\rangle P_a(a) = \frac{x/\langle\ell\rangle}{2\langle v\rangle w\tau_{\shortparallel}\, a}\int_{a\exp[(x/\langle\ell\rangle)/(v_{\min}\tau_{\shortparallel})]}^{a\exp[(x/\langle\ell\rangle)/(v_{\max}\tau_{\shortparallel})]} \mathrm{d}a_0\, \exp\left(-\frac{a_0}{\langle a_0\rangle}\right)\ln^{-2}\left(\frac{a}{a_0}\right). \tag{4.26}$$

The average pulse amplitude is given by the product of the individual averages of the random variables a_0 and y,

$$\langle a\rangle(x) = \frac{x/\langle\ell\rangle\langle a_0\rangle}{2\langle v\rangle s\tau_{\shortparallel}}\left[\frac{v_{\max}\tau_{\shortparallel}}{x/\langle\ell\rangle}\exp\left(-\frac{x/\langle\ell\rangle}{v_{\max}\tau_{\shortparallel}}\right) - \frac{v_{\min}\tau_{\shortparallel}}{x/\langle\ell\rangle}\exp\left(-\frac{x/\langle\ell\rangle}{v_{\min}\tau_{\shortparallel}}\right) + \mathrm{Ei}\left(-\frac{x/\langle\ell\rangle}{v_{\max}\tau_{\shortparallel}}\right) - \mathrm{Ei}\left(-\frac{x/\langle\ell\rangle}{v_{\min}\tau_{\shortparallel}}\right)\right], \tag{4.27}$$

where Ei is an exponential integral function (see Appendix A). In figure 19 (left panel), the radial profile of the average pulse amplitude given by equation (4.27) is presented for various values of the width parameter w. For $w = 0.2$, the average amplitude decay nearly exponentially with radial position x and e-folding length $\langle v\rangle\tau_{\shortparallel}$, similar to the base case. While the integral (4.26) can not be expressed in closed-form the numerical estimate can be found. Normalizing the amplitude distribution by (4.27) and estimating the normalized integral (4.26) numerically gives the PDFs as presented in figure 19 (right panel). Here the width parameter is $w = 0.9$ and the radial position x varies. This result shows a radial change in the shape of the amplitude distribution and high probability for small pulse amplitudes at large x. As one will ensure later, this is a universal feature of the model and will be investigated in more detail later on.

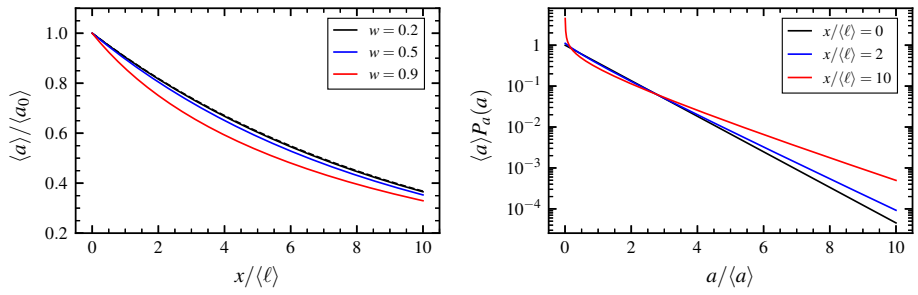

Figure 19: (left panel) Average pulse amplitude as function of radial position for a continuous uniform distribution of pulse velocities with different values of the width parameter w. (right panel) Probability distribution function of the pulse amplitudes for a continuous uniform distribution of pulse velocities with width parameter $w = 0.9$ at different radial positions. The full black line corresponds to the exponential amplitude distribution at the reference position $x = 0$.

The radial profiles of the average value, relative fluctuation level, skewness and flatness moments for the continuous uniform distribution of pulse velocities are shown in figure 20 for three different values of the width parameter w. As w increases, the average value of the process at the reference position $x = 0$ increases since the average duration time also increases. For $w = 0.2$, that is the case of a narrow distribution of pulse velocities, the average profile is nearly exponential and relative fluctuation level is approximately constant, as for the base case with a degenerate distribution of pulse velocities. The skewness and flatness moments only have weak radial variation for large x. For a broad distribution of pulse velocities, the radial profiles are qualitatively similar to those for the discrete uniform distribution of pulse velocities but the length scale change is smoother since there is a continuum of pulse velocities. In order to quantify the change in scale length associated with the average profile for a random distribution of pulse velocities in practical way, introduce

$$L_\Phi = -\tau_{\shortparallel}\langle v\rangle \frac{\mathrm{d}\ln\langle\Phi\rangle}{\mathrm{dx}} \tag{4.28}$$

where its definition follows straightly from average profile with constant velocities. A comparison between radial profiles of the scale length for the discrete and continuous case is presented in figure 21 for width parameter $w = 0.9$.

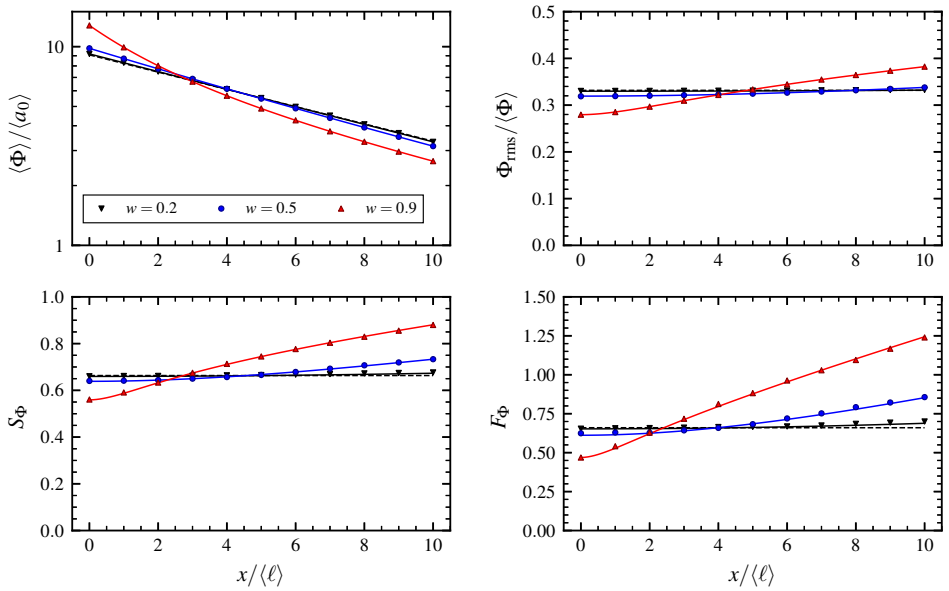

Figure 20: Radial profiles of the average value (top left), relative fluctuation level (top right), skewness (bottom left) and flatness (bottom right) for a continuous uniform distribution of pulse velocities with various values of the width parameter w. Markers correspond to simulation results while curves corresponds to numerically evaluated cumulants given by equation (2.59). The black dashed line indicates the radial profiles for a degenerate distribution of pulse velocities.

The probability distribution function of the normalized process with uniformly distributed velocities at different radial positions is presented in figure 22. At the reference position $x = 0$, this is again a Gamma distribution with shape parameter $\gamma = \tau_{\mathrm{d}}/\tau_{\mathrm{w}}$. For all cases, the shape parameter γ estimated by the maximum likelihood method is in a good agreement with what one will expect based on the average pulse duration (see figure 18). As expected, the distribution of the process with the width parameter $w = 0.2$ practically does not change. For $w = 0.9$, the radial increase of intermittency level is apparent but not so drastic as for the discrete case with the same width parameter. This results are consistent with the radial profiles of the lowest order statistical moments presented in figure 20.

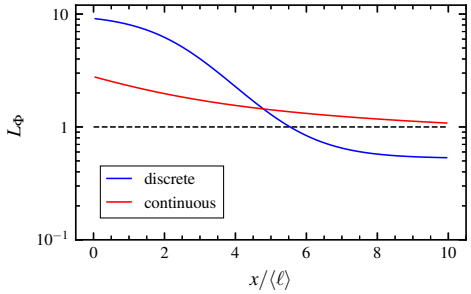

Figure 21: Comparison of the scale length profiles for a discrete and continuous uniform distribution of the pulse velocities with the width parameter $w = 0.9$. The dashed black line indicate profile constant e-folding length for a degenerate distribution of pulse velocities.

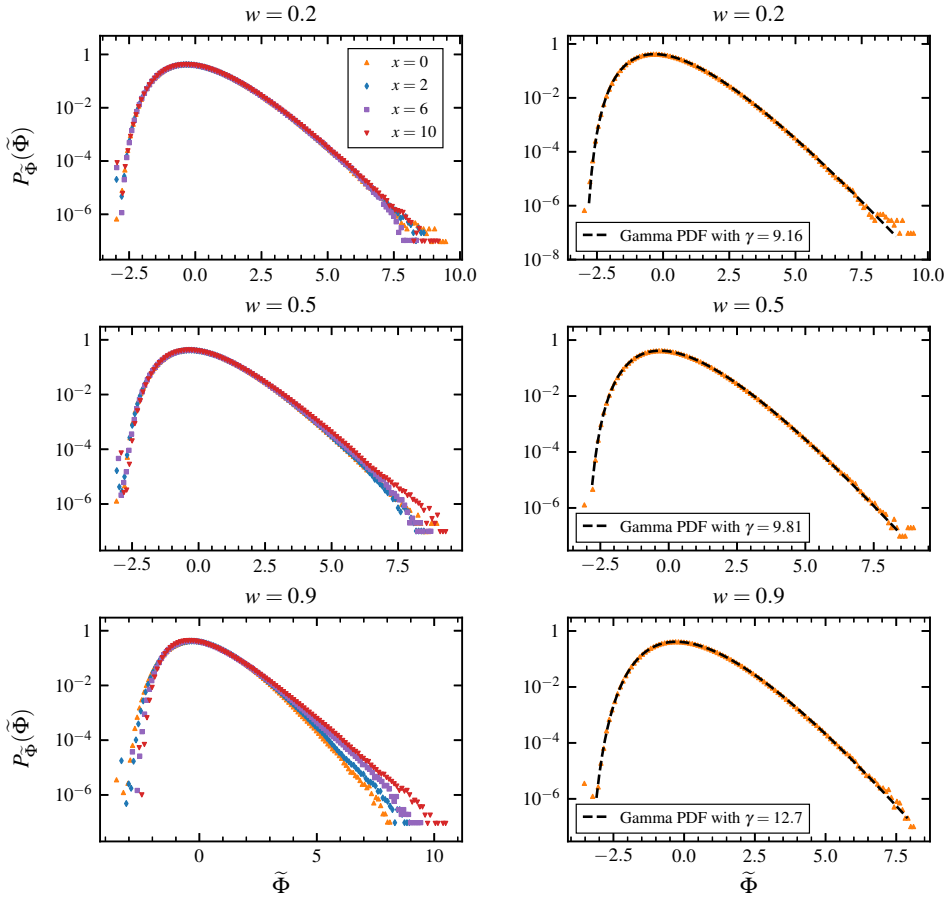

Figure 22: Probability distribution function of the normalized process for a continuous uniform distribution of pulse velocities for various values of width parameter w at different radial positions. The values of the radial position and their corresponding colors are shown in the inset. The distribution of the normalized process at reference position $x = 0$ is compared to a Gamma distribution with estimated parameter γ shown with the dashed black lines.

The auto-correlation function and power spectral density at different radial positions for the normalized process are presented in figure 23 for various values of the width parameter w. This clearly shows that the energy in the low-frequency part of the spectrum is large for large values of the width parameter w, while the power law tail for high frequencies is the same as for the case with constant pulse velocity. For $w = 0.9$, the change of the characteristic decay time in the auto-correlation function is smoother compared to discrete case due to the continuum of allowed velocities.

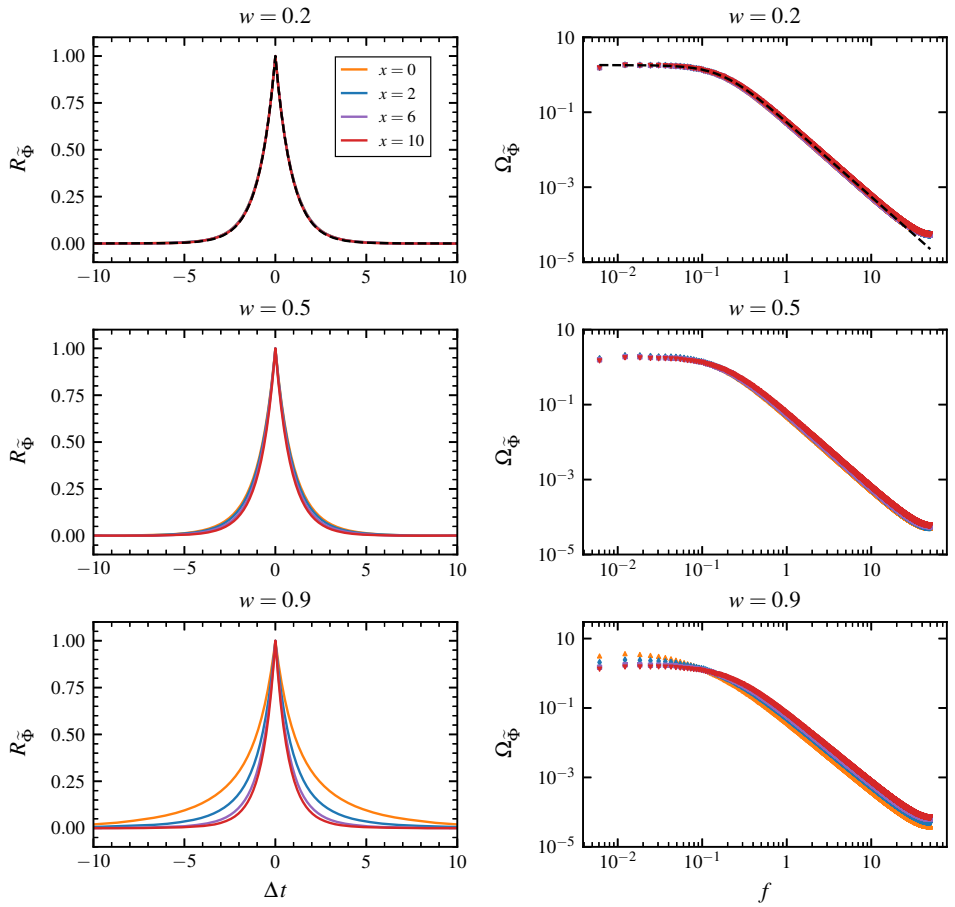

Figure 23: Auto-correlation function and power spectral density of the normalized process for different radial positions with uniformly distributed pulse velocities with different values of the width parameter w. The case $w = 0.2$ is compared to the case for a degenerate distribution of pulse velocities shown with the dashed black lines.

4.3 Gamma distributed pulse velocities

So far, the cases with the pulse velocities that are equally likely to occur have been addressed. Consider now a unimodal distribution which is based on a Gamma distribution. The Gamma distribution for the pulse velocities with scale parameter $\langle v\rangle/s$ and shape parameter s is given by

$$\langle v\rangle P_v(v;\langle v\rangle,s) = \frac{s}{\Gamma(s)}\left(\frac{sv}{\langle v\rangle}\right)^{s-1}\exp\left(-\frac{sv}{\langle v\rangle}\right), \quad v>0. \tag{4.29}$$

For small values of s, there is a high probability for small pulse velocities. For $s=1$, this is equivalent to the exponential distribution with scale parameter $\langle v\rangle$. The Gamma distribution with shape parameter $s>1$ is unimodal and has an exponential tail for large pulse velocities and tends to 0 as $v\to 0$. For large values of s, the distribution more closely resembling a normal distribution and the limit $s\to\infty$ corresponds to the reference case with constant pulse velocities. Taking into consideration the above notions, the restriction imposed on the shape parameter to be $s>1$ due to large number of very slow pulses for $s<1$ which are posing several issues, as indicated in the section 2.3.

For Gamma distributed velocities, the pulse durations are distributed according to

$$\frac{\langle v\rangle}{\langle\ell\rangle}P_\tau(\tau;\langle v\rangle,\langle\ell\rangle,\tau_{\shortparallel},s) = \frac{s}{\Gamma(s)}\left(\frac{\langle\ell\rangle s(\tau_{\shortparallel}-\tau)}{\tau_{\shortparallel}\langle v\rangle\tau}\right)^{s-1}\frac{1}{\tau^2}\exp\left(-\frac{s\langle\ell\rangle(\tau_{\shortparallel}-\tau)}{\tau_{\shortparallel}\langle v\rangle\tau}\right), \tag{4.30}$$

for durations in range $0<\tau\leqslant\tau_{\shortparallel}$. The Gamma velocity distribution and the corresponding duration time distribution are presented in figure 24 for two different values of the shape parameter s.

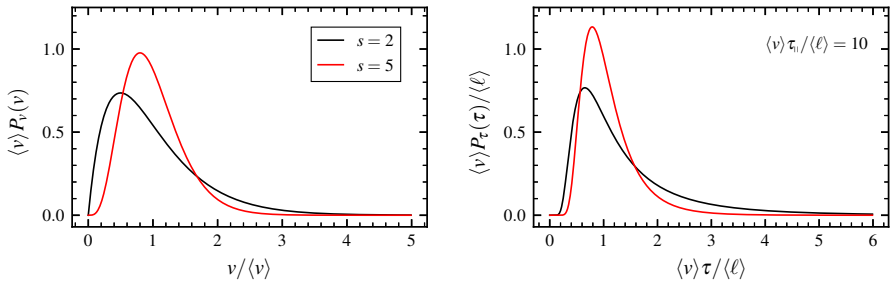

Figure 24: Marginal velocity and duration distribution functions given by equations (4.29) and (4.30), respectively, for different shape parameter s for a Gamma distribution of pulse velocities.

The average pulse duration is given by integrating over the duration distribution in equation (4.30),

$$\tau_{\mathrm{d}} = \frac{\langle\ell\rangle s}{\langle v\rangle}\exp\left(\frac{\langle\ell\rangle s}{\langle v\rangle\tau_{\shortparallel}}\right)\mathrm{E}_s\left(\frac{\langle\ell\rangle s}{\langle v\rangle\tau_{\shortparallel}}\right), \tag{4.31}$$

where E_n gives an exponential integral generalized to $n=s$ (see Appendix A). In the limit $s\to 0$, the average pulse duration approaches the maximum duration $\tau_{\shortparallel}$. For large s, the average pulse duration is the same as for the case of degenerate distributed velocities. In the absence of linear damping, equation (4.31) takes form

$$\lim_{\langle v\rangle\tau_{\shortparallel}/\langle\ell\rangle\to\infty}\tau_{\mathrm{d}} = \frac{\langle\ell\rangle}{\langle v\rangle}\frac{s}{s-1}. \tag{4.32}$$

In the limit $s\to\infty$, this is simply the radial transit time, $\langle\ell\rangle/\langle v\rangle$, as expected. The average pulse duration as function of the shape parameter s is presented for $\langle v\rangle\tau_{\shortparallel}/\langle\ell\rangle=10$ and $\langle v\rangle\tau_{\shortparallel}/\langle\ell\rangle\to\infty$ in figures 25 and 26.

The distribution of pulse amplitudes at some normalized radial position x is given by product convolution of the random variables a_0 and one obtained by transformation of the pulse velocities which a Gamma distributed, $y=\exp(-x/(v\tau_{\shortparallel}))$, (see Appendix D),

$$\langle a_0\rangle P_a(a) = \frac{\left(\frac{(x/\langle\ell\rangle)s}{\langle v\rangle\tau_{\shortparallel}}\right)^s}{\Gamma(s)\,a}\int_a^\infty \mathrm{d}a_0\,\exp\left(\frac{(x/\langle\ell\rangle)s}{\langle v\rangle\tau_{\shortparallel}\ln\left(\frac{a}{a_0}\right)}-\frac{a_0}{\langle a_0\rangle}\right)\left(-\frac{1}{\ln\left(\frac{a}{a_0}\right)}\right)^{s+1}, \tag{4.33}$$

where amplitudes a_0 and their mean $\langle a_0 \rangle$ are specified at reference position. The average pulse amplitude at radial position $x > 0$ is

$$\langle a \rangle(x) = \frac{2\langle a_0 \rangle}{\Gamma(s)} \left(\frac{sx}{\langle v \rangle \tau_{\text{ll}}} \right)^{s/2} \mathcal{K}_s \left(2\sqrt{\frac{sx}{\langle v \rangle \tau_{\text{ll}}}} \right),$$

where $\mathcal{K}$ here denote modified Bessel function of the second kind (see Appendix A). Figure 25 shows how the shape parameter s affects the average pulse durations and amplitudes at some radial position x while holding the linear damping to be $\langle v \rangle \tau_{\text{ll}} / \langle \ell \rangle = 10$ and in the absence of linear damping. Figure 26 emphasize that the statistical averages are nearly the same as for the base case when s is large. Moreover, in the the absence of linear damping the average pulse duration goes to infinity for $s < 1$, which is consistent with what have been stated above.

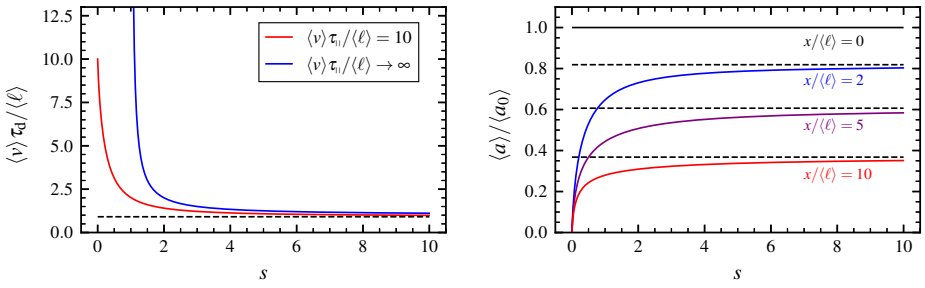

Figure 25: Average pulse duration presented with semi-logarithmic plot and average amplitude at normalized radial position $x/\langle \ell \rangle$ given by equations (4.31) and (4.3), respectively, as a function of the shape parameter s for a Gamma distribution of pulse velocities. The black dashed line indicate the base case with fixed pulse velocities.

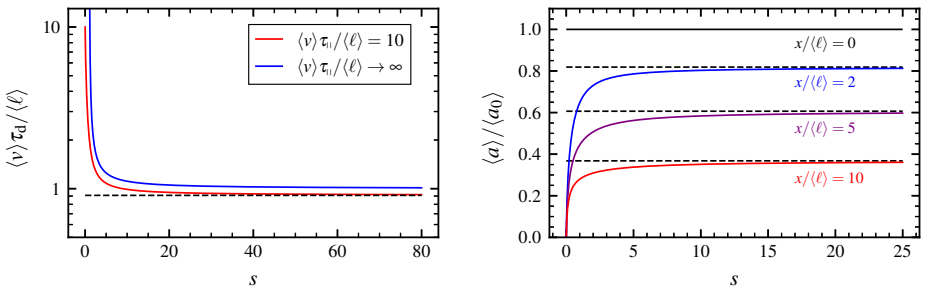

Figure 26: Average pulse duration and average amplitude at normalized radial position $x/\langle \ell \rangle$ given by equations (4.31) and (4.3), respectively, as a function of the shape parameter s for a Gamma distribution of pulse velocities. The black dashed line indicate the base case with fixed pulse velocities.

In figure 27, the numerical calculation of the amplitude distribution given by equation (4.33) normalized by average pulse amplitude given by equation (4.3) at different radial positions is presented both for $s = 2$ (left panel) and $s = 5$ (right panel). All the main features of amplitude distribution discussed in previous subsection are naturally accounted for. Noteworthy is that for $s = 2$ the small amplitudes have a higher probability at large x when compared to the the case $s = 5$. This is of course agreeing with a change in the shape of pulse velocity distribution, where the smaller values of s gives a large number of slower pulses.

In figure 28 the average pulse and linear correlation coefficient between pulse durations and amplitudes as function of radial position are presented for two different values of the shape parameter s. The dashed black line corresponds to radial profiles in the case of a continuous uniform distribution of pulse velocities with $w = 0.9$. Noteworthy is that the average amplitude decay sharply and the linear correlation profile is steeper for small x for the case $s = 2$ when compared to a broad uniform distribution of pulse velocities.

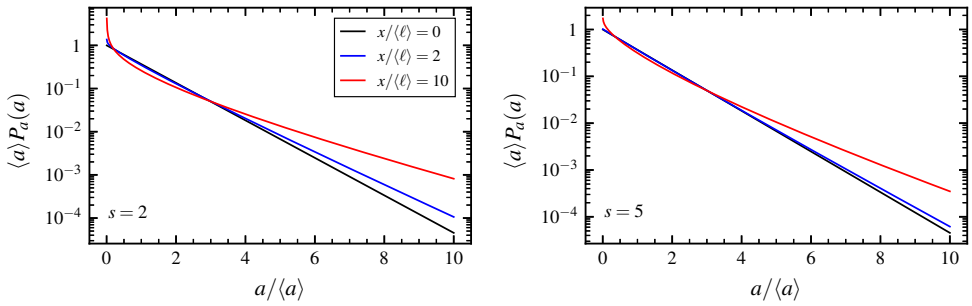

Figure 27: Probability distribution function of the pulse amplitudes for a Gamma distribution of pulse velocities at different radial positions for two different values of the shape parameter s. The full black line indicates exponentially distributed amplitudes at the reference position $x = 0$.

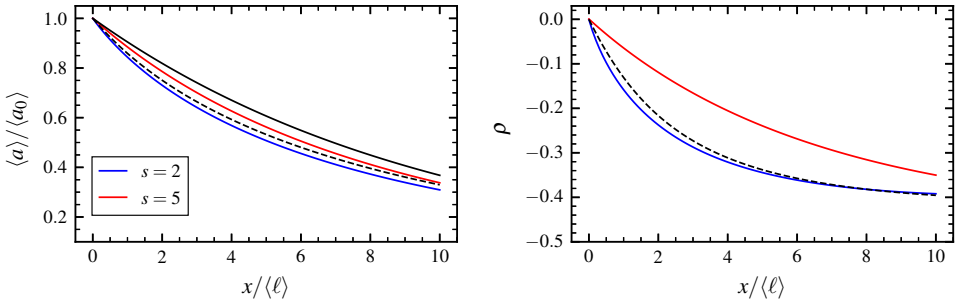

Figure 28: (left panel) Average pulse amplitude as function of radial position for a Gamma distribution of pulse velocities with different values of the shape parameter s. The full black line corresponds to the radial profile of the average amplitudes for a degenerate distribution of pulse velocities. (right panel) Radial profile of the linear correlation coefficient between pulse durations and amplitudes for a Gamma distribution of pulse velocities for different values of the shape parameter s.

In figure 29, radial profiles of the lowest order statistical moments of the process with Gamma distributed velocities for different values of the shape parameter s are presented. It is useful to notice that the lower values of the shape parameter s result in steeping of the average profile for small x same as for profile e-folding length shown in figure 30. This is expected since there is a large number of slow pulses present for s close to unity (see figure 24). There is a reduced relative fluctuation level as well as skewness and flatness moments for small x, while this quantities increase rapidly radially outwards similarly to uniform distribution of pulse velocities. The slightly increased values of this quantities at $x = 10$ compared to the case of uniform distribution of pulse velocities are observed.

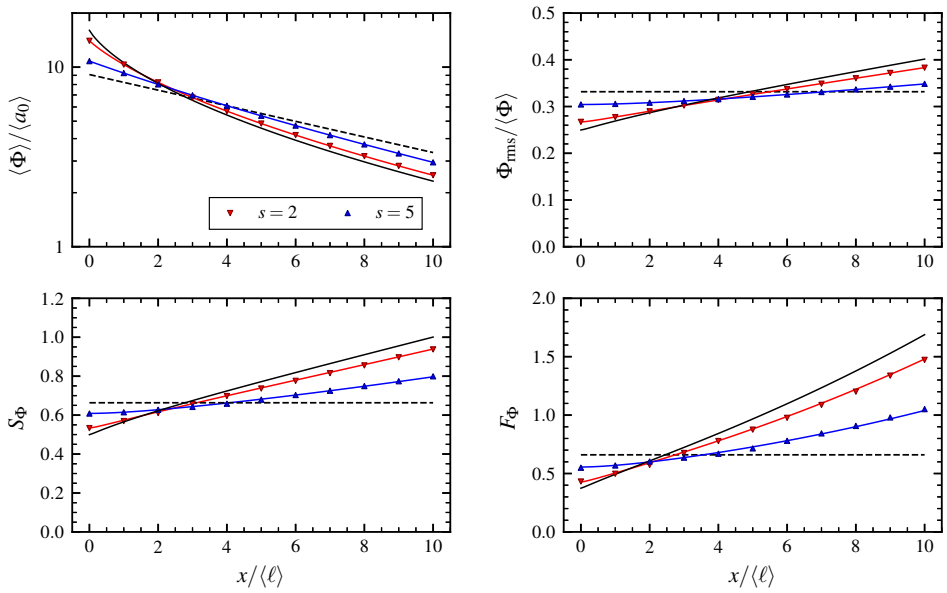

Figure 29: Radial profiles of the average value (top left), relative fluctuation level (top right), skewness (bottom left) and flatness (bottom right) for a Gamma distribution of pulse velocities with shape parameter s. Markers correspond to the simulation results while curves corresponds to numerically evaluated cumulants given by equation (2.59). The full black line indicates the radial profiles for a Gamma distribution of pulse velocities with shape parameter $s = 3/2$. The black dashed line indicates the radial profiles for a degenerate distribution of pulse velocities.

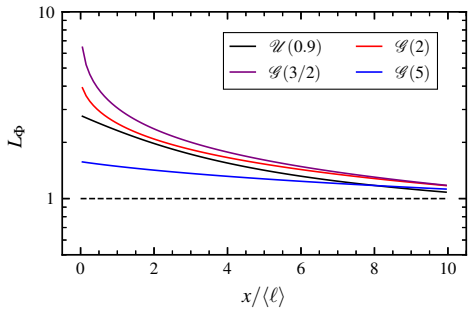

Figure 30: Comparison of the scale length profiles for a continuous uniform distribution with the width parameter $w = 0.9$ and a Gamma distribution for three different values of the shape parameter s of the pulse velocities. Here ($\mathscr{G}$) stand for a Gamma distribution and ($\mathscr{U}$) stand for a continuous uniform distribution.

The probability distribution function of the normalized process at different radial positions is presented in figure 31 for two different values of the shape parameter s. At the reference position $x = 0$, the process is Gamma distributed with shape parameter given by the shape parameter γ given by $\gamma = \tau_{\rm d}/\tau_{\rm w}$. For $s = 2$ the shape parameter is 14.03 and for $s = 5$ the shape is 10.797. Clearly, the estimated by maximum likelihood method γ parameter is consistent with theory.

The auto-correlation function and power spectral density at different radial positions for the normalized process are presented in figure 32 for various values of the shape parameter s. The time characteristics are similar to the case for a continuous uniform distribution of pulse velocities.

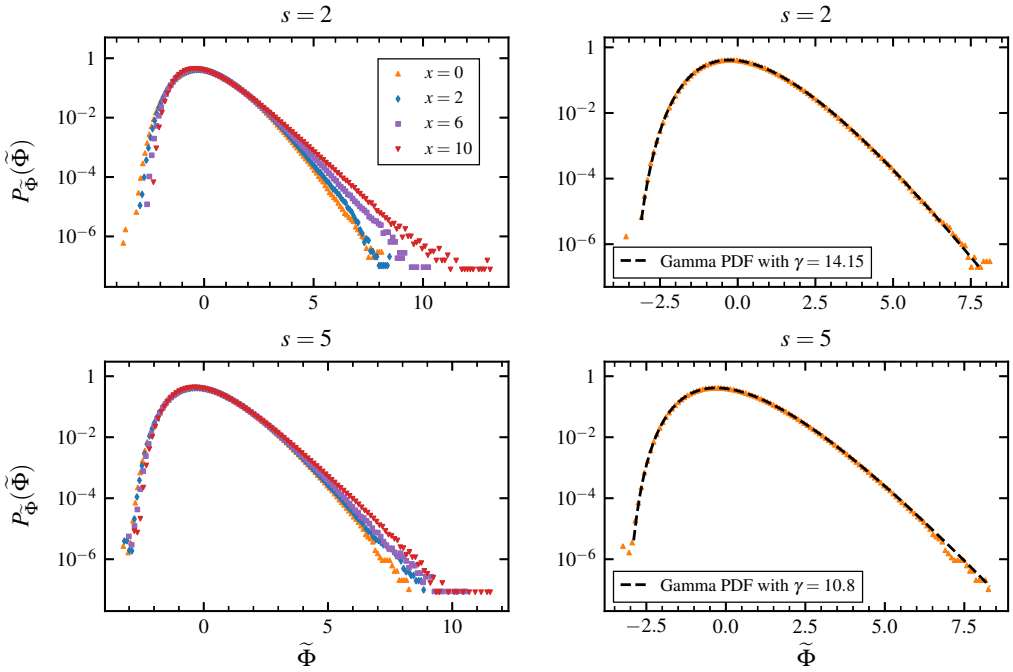

Figure 31: Probability distribution functions of the normalized process with Gamma distributed pulse velocities for different values of the shape parameter s. The black dashed line indicates a Gamma distribution with estimated shape parameter γ.

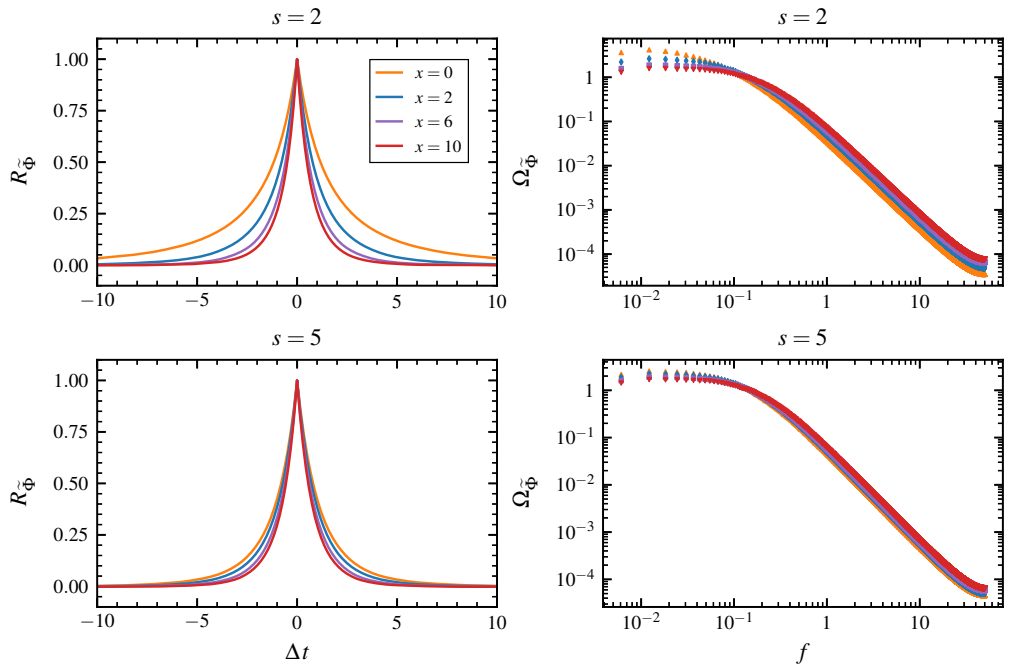

Figure 32: Auto-correlation function and power spectral density of the normalized process for different radial position with Gamma distributed pulse velocities for two different values of the shape parameter s.

4.4 Truncated exponentially distributed pulse velocities

As discussed in subsection 2.3, the marginal probability distribution of the pulse velocities should decay fast enough to zero for arbitrarily small velocities in order for the cumulant to exist. With this requirement in mind, consider a truncated exponential distribution of pulse velocities,

$$\langle v\rangle P_v(v;\langle v\rangle,\alpha) = \begin{cases} \dfrac{1}{(1-\beta)}\exp\left(-\dfrac{v-\beta\langle v\rangle}{\langle v\rangle(1-\beta)}\right), & \text{if } v \geqslant \beta\langle v\rangle, \\ 0, & \text{otherwise,} \end{cases} \tag{4.34}$$

where $\beta\langle v\rangle$ is the minimum pulse velocity.

The pulse durations given by equation (2.46) are distributed according to

$$\frac{\langle v\rangle}{\langle \ell\rangle} P_\tau(\tau;\langle v\rangle,\langle \ell\rangle,\beta) = \frac{1}{(1-\beta)}\frac{1}{\tau^2}\exp\left(\frac{\tau-\tau_{\text{ll}}\left(1-\beta\frac{\langle v\rangle}{\langle \ell\rangle}\tau\right)}{\frac{\langle v\rangle}{\langle \ell\rangle}\tau_{\text{ll}}(1-\alpha)\tau}\right), \tag{4.35}$$

for duration in the range $0 < \tau \leqslant \tau_{\max}$, where $\tau_{\max} = \tau_{\text{ll}}\langle \ell\rangle/(\beta\langle v\rangle\tau_{\text{ll}} + \langle \ell\rangle)$ is the maximum duration time. The truncated exponential velocity distribution and the corresponding duration time distribution are presented in figure 33 for various values of truncation parameter β.

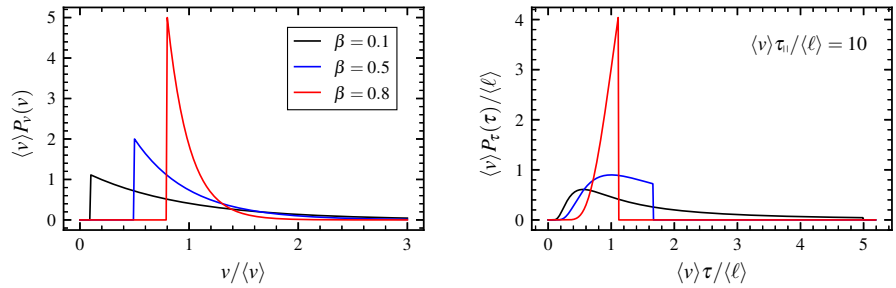

Figure 33: Marginal probability distribution function for the pulse velocities and duration times given by equations (4.34) and (4.35), respectively, for different values of truncation parameter β for a truncated exponential distribution of pulse velocities.

The average pulse duration is

$$\tau_{\text{d}} = \frac{\langle \ell\rangle}{\langle v\rangle(\beta-1)}\exp\left(\frac{1+\beta\frac{\langle v\rangle}{\langle \ell\rangle}\tau_{\text{ll}}}{\frac{\langle v\rangle}{\langle \ell\rangle}\tau_{\text{ll}}(1-\beta)}\right)\text{Ei}\left(-\frac{1+\beta\frac{\langle v\rangle}{\langle \ell\rangle}\tau_{\text{ll}}}{\frac{\langle v\rangle}{\langle \ell\rangle}\tau_{\text{ll}}(1-\beta)}\right), \tag{4.36}$$

where Ei here denotes the exponential integral function (see Appendix A). In the limit $\beta \to 1$, the average pulse duration is the same as for the case of a degenerate distribution of velocities. In the absence of linear damping, the average pulse duration takes form

$$\lim_{\langle v\rangle\tau_{\text{ll}}/\langle \ell\rangle\to\infty} \tau_{\text{d}} = \frac{\langle \ell\rangle}{\langle v\rangle(\beta-1)}\exp\left(\frac{\beta}{1-\beta}\right)\text{Ei}\left(\frac{\beta}{1-\beta}\right). \tag{4.37}$$

The average pulse duration is presented for $\langle v\rangle\tau_{\text{ll}}/\langle \ell\rangle = 10$ and $\langle v\rangle\tau_{\text{ll}}/\langle \ell\rangle \to \infty$ in figure 34 (left panel). For large $\langle v\rangle\tau_{\text{ll}}/\langle \ell\rangle$ and as β approaches zero, the pulse duration can be much longer than $\tau_{\max}$. Clearly, in the absence of linear damping, the maximum pulse duration becomes infinitely large, since the exponential integral in the equation (4.37) in the limit $\beta \to 0$ is undefined.

The distribution of pulse amplitudes at some normalized radial position is given by the product convolution between random variables a_0 and one obtained by transforming pulse velocities which are truncated exponentially distributed, $y = \exp(-x/(v\tau_{\text{ll}}))$, (see Appendix D),

$$\langle a_0\rangle P_a(a) = \frac{x/\langle \ell\rangle}{\langle v\rangle(1-\beta)\tau_{\text{ll}}\, a}\int_a^{a\exp\left(\frac{(x/\langle \ell\rangle)}{\beta\langle v\rangle\tau_{\text{ll}}}\right)} \text{d}a_0\, \ln^{-2}\left(\frac{a}{a_0}\right)\exp\left(\frac{x/\langle \ell\rangle + \beta\langle v\rangle\tau_{\text{ll}}\ln\left(\frac{a}{a_0}\right)}{\langle v\rangle\tau_{\text{ll}}(1-\beta)\ln\left(\frac{a}{a_0}\right)} - \frac{a_0}{\langle a_0\rangle}\right), \tag{4.38}$$

where amplitudes a_0 and their mean $\langle a_0 \rangle$ are specified at the reference position $x = 0$. In this case, a closed analytical expression for average amplitude is not possible to find. Therefore, the average is given by numerical evaluation of the integral over the distribution defined by equation (4.38) as illustrated in left panel of figure 35. For $\beta = 0.8$, the average amplitude profile is close to exponential with e-folding length $\langle v \rangle \tau_{\text{II}}$ which is same as for the case with constant velocities, whereas average amplitude decay much faster radially outwards for $\beta = 0.1$. The numerical estimation of amplitude distribution given by equation (4.38) normalized by numerically calculated average amplitude for $\beta = 0.1$ is presented in right panel of figure 35. There is a similar behaviour with cases considered above for large x, characterized by a strongly peaked distribution for the arbitrarily small amplitudes.

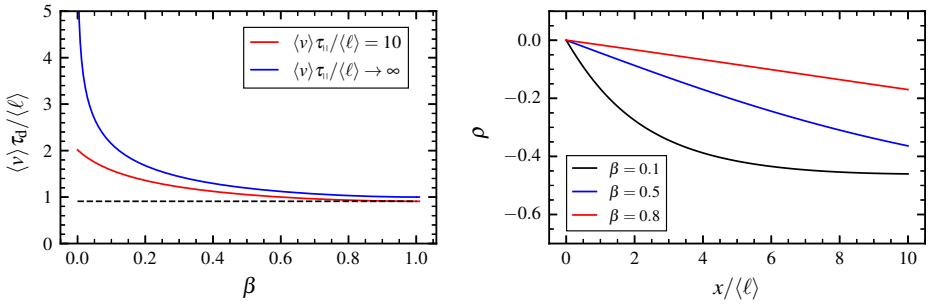

Figure 34: (left panel) Average pulse duration given by equation (4.36) as function of truncation parameter β for a truncated exponential distribution of pulse velocities. The black dashed line indicates the average pulse duration for a degenerate distribution of pulse velocities for $\langle v \rangle \tau_{\text{II}} / \langle \ell \rangle = 10$. (right panel) Radial profile of the linear correlation coefficient between pulse durations and amplitudes for an exponential distribution of pulse velocities with three different truncation parameters β.

The linear correlation between durations and amplitudes for an exponential distribution of pulse velocities for three different values of the truncation parameter β is presented in figure 34 (right panel) as function of radial position x. As expected, for a broad distribution of pulse velocities the strong correlation has been developed for large radial position.

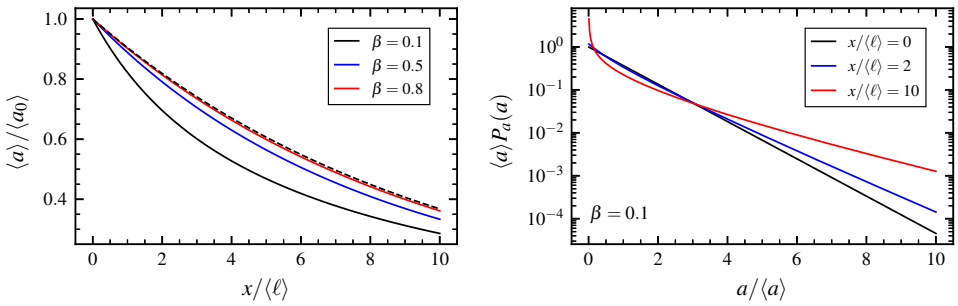

Figure 35: (left panel) Normalized average pulse amplitude as function of radial position for a truncated exponential distribution of pulse velocities with truncated parameter β. (right panel) Probability density function of the pulse amplitudes for a truncated exponential distribution of pulse velocities with truncation parameter $\beta = 0.1$ at different radial positions.

In figure 36, the radial profiles of the lowest order moments obtained both from realizations of the process and semi-analytical calculations, are presented for various values of truncation parameter β. In this case there are more slow pulses with velocities close to $v_{\min}$ compared to the uniform distribution but when comparing with Gamma distribution the arbitrarily small velocities (very close to zero) are not present. In other words the minimum velocity for exponential distribution is defined by the truncation parameter, while for Gamma distribution the velocities smaller than this are present. Consequently, the increase in intermittency with radial position for broad distribution of pulse velocities is more pronounced when this slow pulse have decayed (related to slightly larger values of relative fluctuation level, skewness and flatness). The radial variation

of profile length scale is presented in figure 37 for three different values of pulse velocities. For the case $\beta = 0.8$, the average profile is nearly exponential and there is only weak radial variation of the relative fluctuation level, skewness and flatness, this is again related to the fact that velocity distribution is narrow and very close to degenerate distribution.

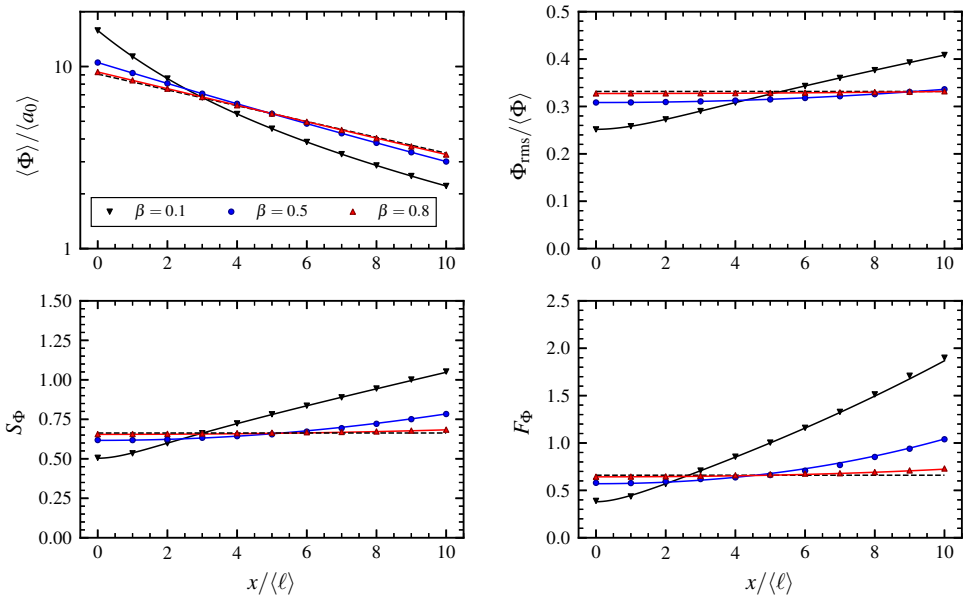

Figure 36: Radial profiles of the average value (top left), relative fluctuation level (top right), skewness (bottom left) and flatness (bottom right) for a truncated exponential distribution of pulse velocities for different values of the truncation parameter β. Markers correspond to the results obtained from realizations of the process while curves corresponds to numerically evaluated cumulants given by equation (2.59). The black dashed line indicates the radial profiles for a degenerate distribution of pulse velocities.

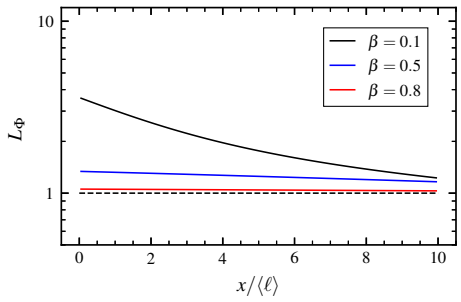

Figure 37: The scale length profiles for a exponential distribution of pulse velocities with three different values of the truncation parameter β.

The PDFs for the normalized process at different radial positions are presented in figure 38. As expected, for $\beta = 0.1$, the intermittency rapidly increases radially outwards, while for $\beta = 0.8$, the intermittency level is roughly the same for all radial positions. As β increases, the intermittency parameter γ at reference position $x = 0$ decreases as suggested by the radial profile of average pulse duration (see figure 34) when rate parameter $\tau_{\rm w}$ is fixed. The auto-correlation function as well as the power spectral density of the normalized process at different radial positions are presented in figure 39 for various values β. As was observed before, the broad distribution of pulse velocities lead to a radial change in a characteristic time of ACFs. The shape of the power spectral density is similar for all radial positions and the change only happen in an energy in the lower frequency part for broad distribution of pulse velocities (that is $\beta = 0.1$).

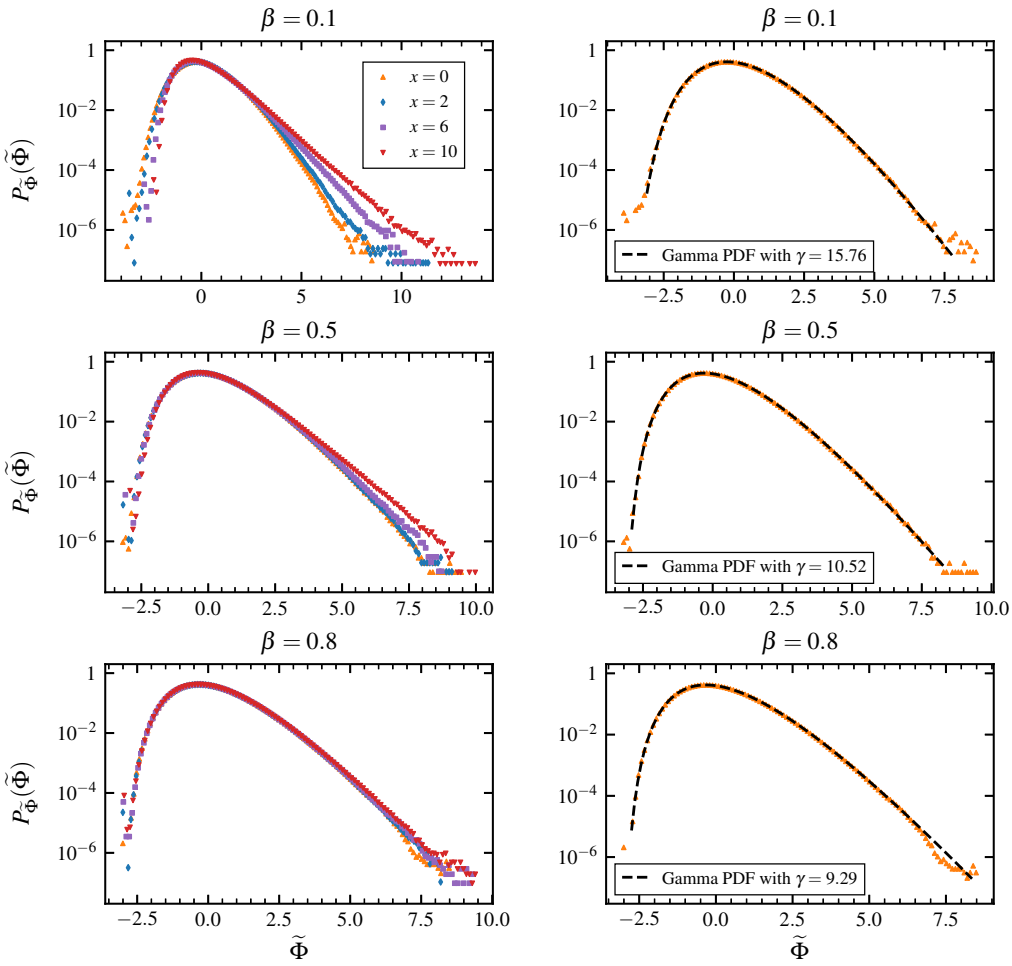

Figure 38: Probability distribution functions of the normalized process for truncated exponentially distributed pulse velocities for various values of the truncation parameter β. The black dashed line indicates a Gamma distribution with estimated shape parameter γ.

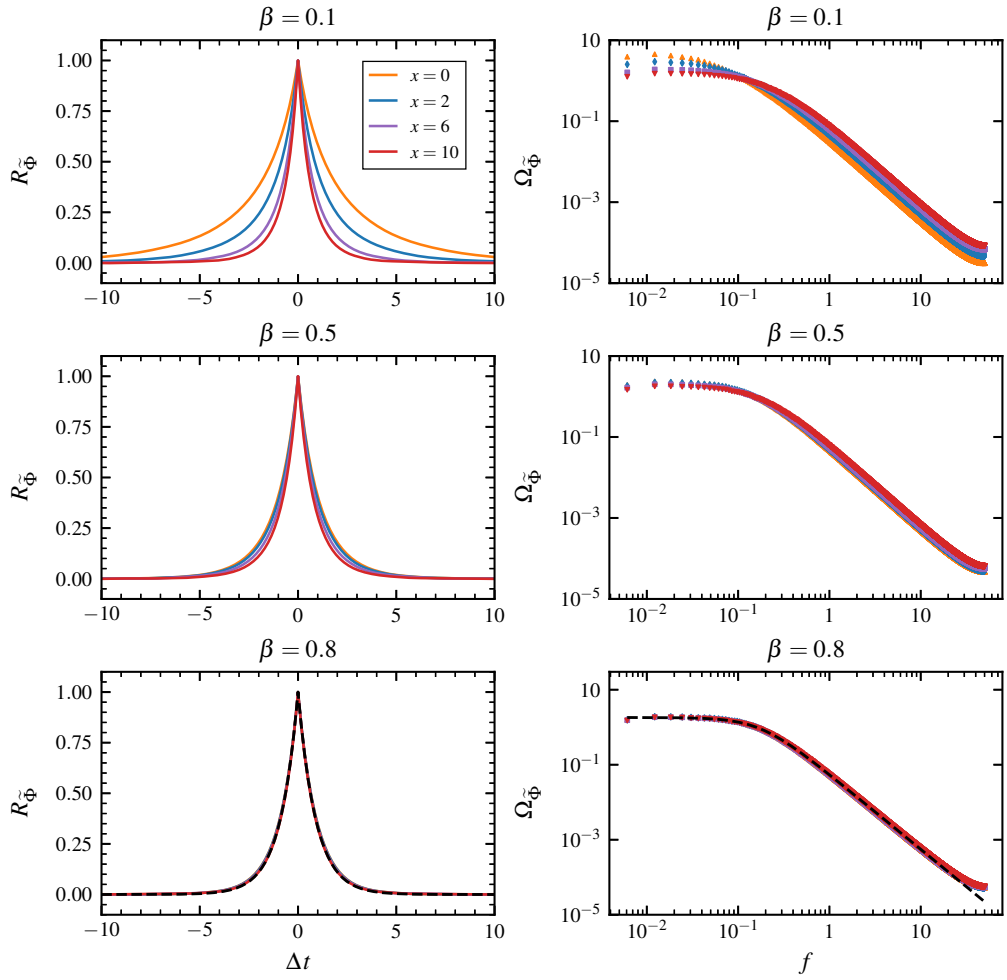

Figure 39: Auto-correlation function and power spectral density of the normalized process for different radial position with truncated exponential distribution of pulse velocities with different values of the truncation parameter β. The case $\beta = 0.8$ is compared to base the case of a degenerate distribution of pulse velocities shown with the dashed black lines.

4.5 Correlated scaling $v \sim a^\zeta$

Several regimes for blob propagation have suggested that the maximum radial blob velocity depends as a power law on blob amplitude. This motivates to consider cases where velocity is given by $v \sim a_0^\zeta$ for some scaling exponent ζ. It should be emphasized, however, that arbitrarily small amplitudes result in pulses with arbitrarily small velocities. As discussed in section 2.3, the presence of arbitrarily slow pulses will lead to the divergence of cumulants and extremely long pulse duration times. Consequently, a lower truncated exponential distribution of amplitudes is considered and given by

$$P_{a_0}(a_0; \langle a_0 \rangle, \alpha) = \begin{cases} \frac{1}{\langle a_0 \rangle (1-\alpha)} \exp\left(-\frac{a_0 - \alpha\langle a_0 \rangle}{\langle a_0 \rangle (1-\alpha)}\right), & \text{if } a \geqslant \alpha\langle a_0 \rangle, \\ 0, & \text{otherwise,} \end{cases} \tag{4.39}$$

where $\alpha\langle a_0 \rangle$ is the minimum amplitude.

Given that velocities vary as a power of amplitudes, let us define a normalizing factor v_0 that ensures the requirement for a distribution of amplitude-dependent velocities to integrate to unity, such that

$$v(a_0) = v_0 \left(\frac{a_0}{\langle a_0 \rangle}\right)^\zeta. \tag{4.40}$$

The inherent property of a mean of a normalized random variable puts a constraint on v_0, namely,

$$\langle v \rangle = \int_{\alpha\langle a_0 \rangle}^\infty \mathrm{d}a_0 \, v(a_0) P_{a_0}(a_0) = v_0 \Gamma\left(1 + \zeta, \frac{\alpha}{1-\alpha}\right)(1-\alpha)^\zeta \exp\left(\frac{\alpha}{1-\alpha}\right),$$

yielding the expression for the normalization factor v_0 as function of α and ζ,

$$v_0 = \frac{\langle v \rangle}{(1-\alpha)^\zeta} \frac{\exp\left(-\frac{\alpha}{1-\alpha}\right)}{\Gamma\left(1 + \zeta, \frac{\alpha}{1-\alpha}\right)}, \tag{4.41}$$

where Γ is an incomplete Gamma function (see Appendix A). By inserting the above expression in (4.40), the velocities are given by

$$\frac{v}{\langle v \rangle} = \frac{\exp\left(-\frac{\alpha}{1-\alpha}\right)}{\Gamma\left(1 + \zeta, \frac{\alpha}{1-\alpha}\right)} (1-\alpha)^{-\zeta} \left(\frac{a_0}{\langle a_0 \rangle}\right)^\zeta. \tag{4.42}$$

From this it follows that the pulse velocities are distributed according to

$$P_v(v; \langle v \rangle, \alpha, \zeta) = \begin{cases} \frac{(\zeta v_0)^{-1}}{(1-\alpha)} \left(\frac{v}{v_0}\right)^{\frac{1-\zeta}{\zeta}} \exp\left(-\frac{(v/v_0)^{\frac{1}{\zeta}} - \alpha}{1-\beta}\right), & \text{if } v \geqslant v_{\min}, \\ 0, & \text{otherwise,} \end{cases} \tag{4.43}$$

where $v_{\min} = v_0 \, \alpha^\zeta$ is the minimum velocity. Recalling the definition of duration times given by equation (2.46), the pulse durations are distributed according to

$$P_\tau(\tau; \langle \ell \rangle, \langle v \rangle, \alpha, \zeta) = \frac{\langle \ell \rangle (\zeta v_0)^{-1}}{(1-\alpha)\tau^2} \left(\frac{\langle \ell \rangle (\tau_{\shortparallel} - \tau)}{\tau_{\shortparallel} v_0 \tau}\right)^{\frac{1-\zeta}{\zeta}} \exp\left(-\frac{\left(\frac{\langle \ell \rangle (\tau_{\shortparallel} - \tau)}{\tau_{\shortparallel} v_0 \tau}\right)^{\frac{1}{\zeta}} - \alpha}{1-\alpha}\right), \tag{4.44}$$

for durations in the range $0 < \tau \leqslant \tau_{\max}$, where $\tau_{\max} = \tau_{\shortparallel} \langle \ell \rangle / (v_{\min} \tau_{\shortparallel} + \langle \ell \rangle)$ is the maximum duration. Distribution functions of pulse velocities given by (4.43) and durations given by (4.44) for two different values of ζ are presented in figure 44 for $\alpha = 0.1$, in figure 48 for $\alpha = 0.5$ and in figure 52 for $\alpha = 0.9$.

For the special case of $\zeta = 1$, the average pulse duration is

$$\tau_{\mathrm{d}} = \frac{\langle \ell \rangle}{\langle v \rangle (1-\alpha)} \exp\left(\frac{1 + \frac{\langle v \rangle}{\langle \ell \rangle} \tau_{\shortparallel} \alpha}{\frac{\langle v \rangle}{\langle \ell \rangle} \tau_{\shortparallel} (1-\alpha)}\right) \mathrm{E}_1\left(\frac{1 + \frac{\langle v \rangle}{\langle \ell \rangle} \tau_{\shortparallel} \alpha}{\frac{\langle v \rangle}{\langle \ell \rangle} \tau_{\shortparallel} (1-\alpha)}\right), \tag{4.45}$$

where E_1 is the exponential integral (see Appendix A). As $\alpha \to 1$, the average pulse duration is the same as for the case with degenerate distribution of pulse velocities. For other values of the

scaling exponent ζ the average pulse duration is not accessible in the closed-from. Integrating duration times numerically with respect to the distribution (4.44) gives the average pulse duration as illustrated in figure 40. As $\alpha \to 1$, it is evident that the average pulse duration is the same as for a degenerate distribution of pulse velocities.

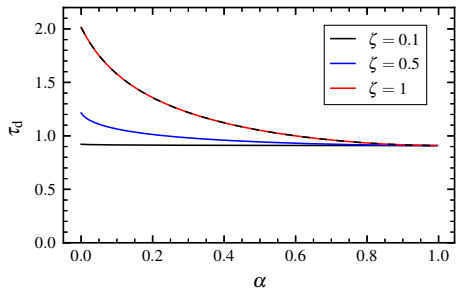

Figure 40: Calculated average pulse duration as function of truncation parameter α for $\langle v\rangle\tau_{\shortparallel}/\langle\ell\rangle = 10$ and various exponents ζ. The case $\zeta = 1$ is compared to equation (4.45) shown with the dashed black line.

Estimates of the average pulse amplitudes obtained from Monte Carlo simulations are presented in figure 41 as function of radial position. In figure 41 (left panel), the exponent is $\zeta = 0.5$ and the truncation parameter α varies. Figure 41 (right panel) shows the radial profile for the linear relation between velocities and amplitudes $\zeta = 1$ and various values of α. For $\alpha = 0.9$, the average amplitude decays approximately exponentially with radial position and with scale length $\langle v\rangle\tau_{\shortparallel}$, similar to the case for a degenerate distribution of pulse velocities.

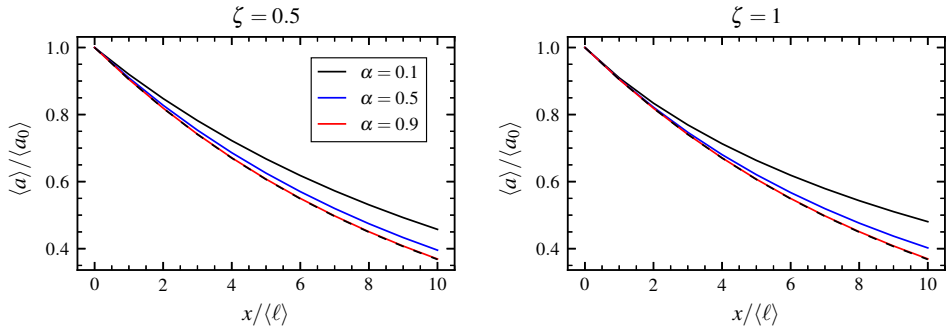

Figure 41: Estimated average pulse amplitude as function of radial position with velocities distributed according to (4.43) for various values of α and ζ. The black dashed lines indicate the average pulse amplitude for a degenerate distribution of pulse velocities.

In figure 43 the radial variation of the linear correlation coefficient between pulse amplitudes and durations for various values of truncation parameter α and two different exponents ζ is presented. Noteworthy is that there is a dependence between amplitudes and velocities at the reference position $x = 0$, and thus the radial profiles of the linear correlation coefficient of course will be different from cases considered before. For the case $\alpha = 0.9$ when distribution of pulse velocities is very narrow and thus very similar to degenerate distribution, there is a nearly perfect negative correlation at all radial positions. This is quite contradicting result, since no linear correlation should be expected. Interestingly, the linear correlation between amplitudes and durations weakens for large radial positions for broad distribution of pulse velocities. The amplitude distribution have the similar behaviour as was observed before and thus will be not presented here.

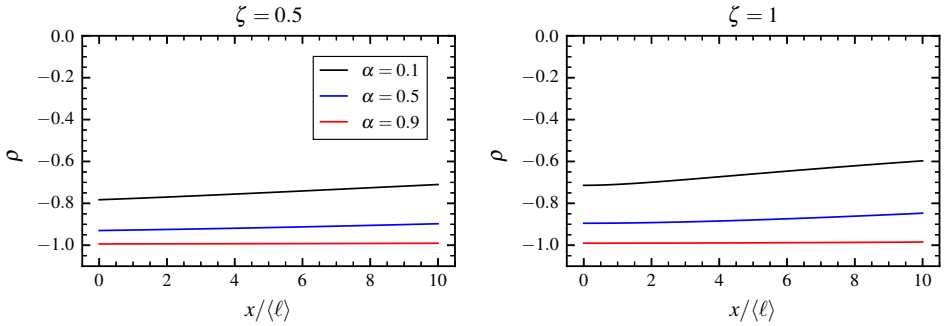

Figure 42: Radial profile of estimated linear correlation coefficient between pulse durations and amplitudes for various α and ζ.

In what follows, the radial profile of the lowest order moments, auto-correlation function and frequency power spectral density for various values of the truncation parameter α will be described separately. In figures 45 and 49, radial profiles of the lowest order statistical moments are presented for two different values of the power-law scaling coefficient ζ. The dashed black indicate the base case with a constant pulse velocity. Truncation parameter $\alpha = 0.9$ gives a narrow distribution of velocities ant thus profiles are similar to those of degenerate velocities, namely, the average profile is nearly exponential and higher order moments have only weak variation with radial position x. For this reason radial profiles corresponding to the case $\alpha = 0.9$ are not presented. The radial variation of the profile scale length is presented in figure 43 for various values of α and ζ. The change in the length scale is most prominent for the case $\zeta = 1$, while for $\zeta = 0.5$ the change is very smooth. Interestingly, the average profile in the case $\alpha = 0.8$ becomes nearly broad, in consistence that the scale length increases more rapidly throughout domain. For broad distribution of pulse amplitudes (that is $\alpha = 0.9$) and when velocities have a linear dependence with this amplitudes, the the relative fluctuation level, skewness and flatness gives the largest values compared to all the cases considered above (the intermittency of the process is very pronounced). The nuances of radial profiles for considered case will be addressed in the following subsection.

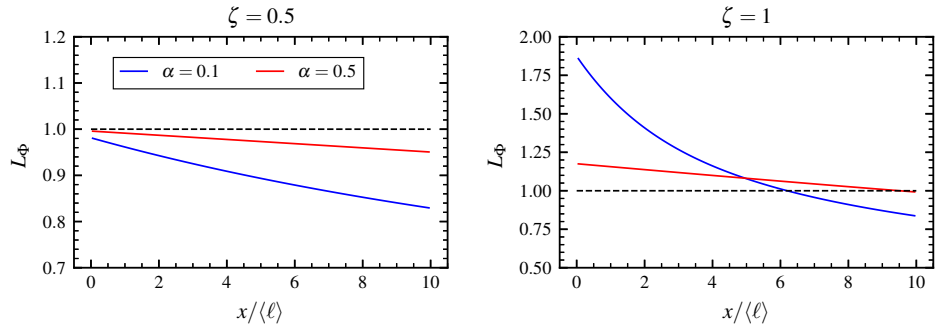

Figure 43: Radial variation of the scale length for a distribution of pulse velocities given by equation (4.43) with truncation parameter α and power-law scaling coefficients ζ.

Probability distribution function of the normalized process with amplitude dependent velocities at different radial positions are presented in figures 46, 50 and 53 for various α and ζ. The radial change of intermittency is consistent with radial profiles of the lowest order statistical moments. The fit to Gamma distribution have a good agreement to with PDFs at the reference position $x = 0$. However, the increased shape parameter γ with truncation parameter α should be addressed, but likely explanation is concerned with pulse amplitude distribution at $x = 0$ that is truncated exponential distribution. Discussion will be given in the following subsection.

The auto-correlations functions and corresponding power spectral densities are presented in figures 47 and 51. It should be noted that for the case $\zeta = 0.5$ the ACFs and PSDs have only weak radial variation, while for the case $\zeta = 1$ this change in characteristic time of ACFs and energy in lower-part frequency is clearly evident.

Case $\alpha = 0.1$

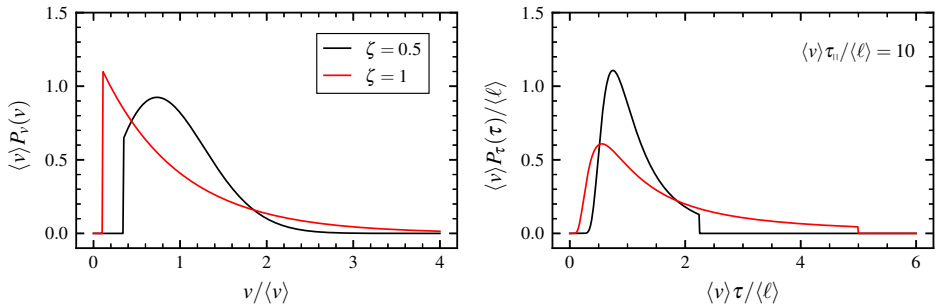

Figure 44: Marginal probability distribution function for the pulse velocities and duration times given by equations (4.43) and (4.44), respectively, with truncation parameter $\alpha = 0.1$ and two different values of ζ.

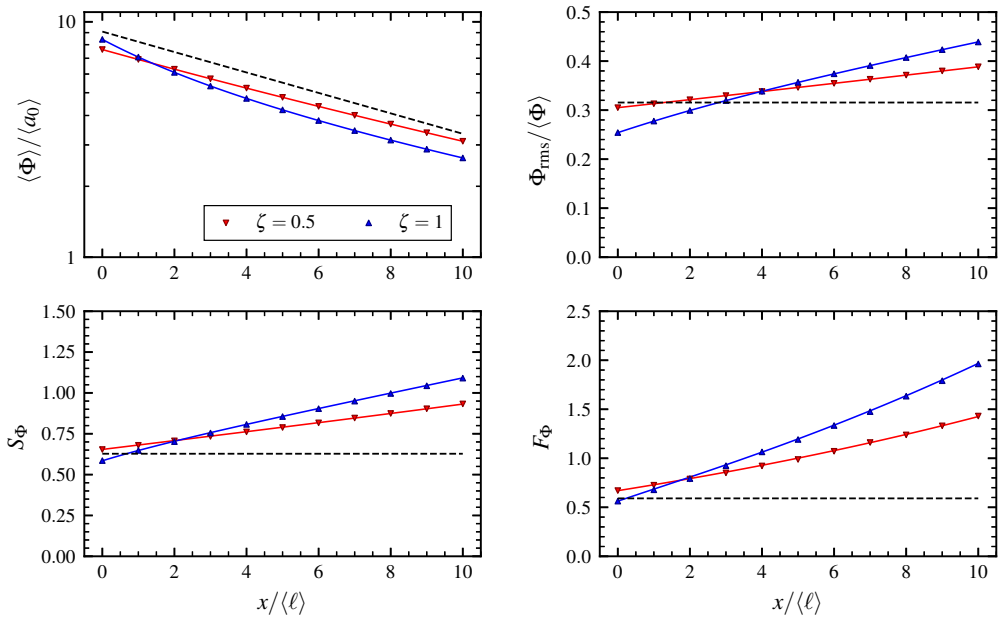

Figure 45: Radial profiles of the average value (top left), relative fluctuation level (top right), skewness (bottom left) and flatness (bottom right) for a distribution of pulse velocities given by equation (4.43) with truncation parameter $\alpha = 0.1$ and two different values of ζ. The black dashed lines indicate the radial profiles for a degenerate distribution of pulse velocities.

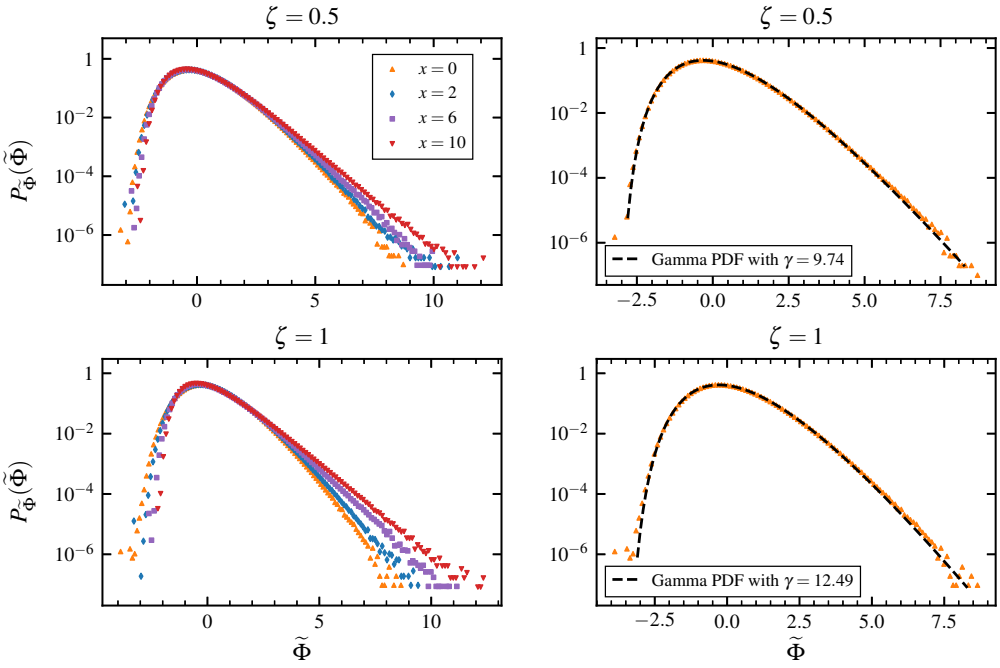

Figure 46: Probability distribution function of the normalized process with velocities distributed according equation (4.43) with truncation parameter $\alpha = 0.1$ and two different values of ζ for different radial positions. The black dashed line indicates a Gamma distribution with estimated shape parameter γ.

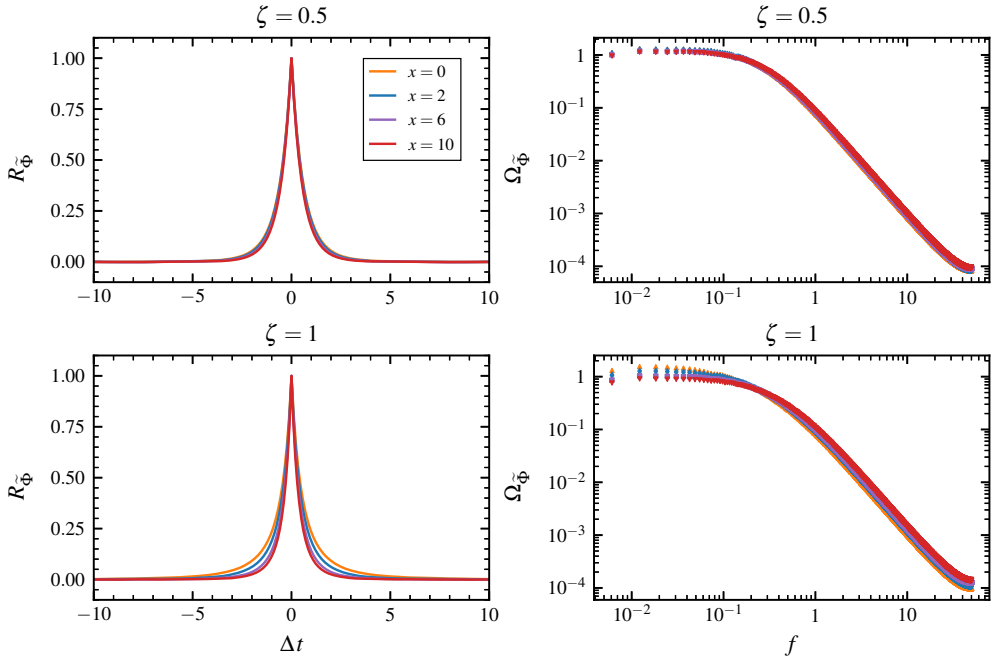

Figure 47: Auto-correlation function and power spectral density for the normalized process for different radial positions with velocities distributed according equation (4.43) with truncation parameter $\alpha = 0.1$ and two different values of ζ.

Case $\alpha = 0.5$

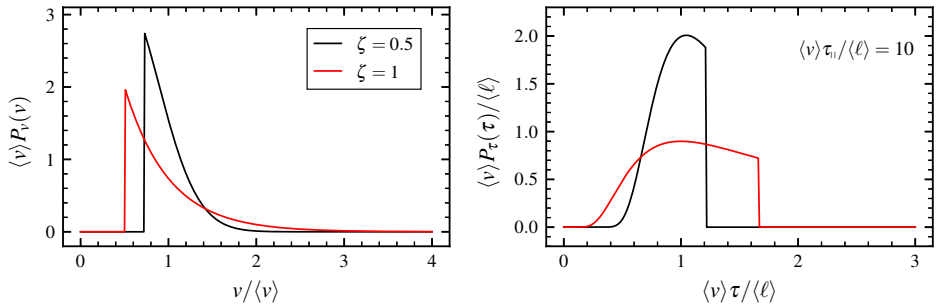

Figure 48: Marginal probability distribution function for the pulse velocities and duration times given by equations (4.43) and (4.44), respectively, with truncation parameter $\alpha = 0.5$ and two different values of ζ.

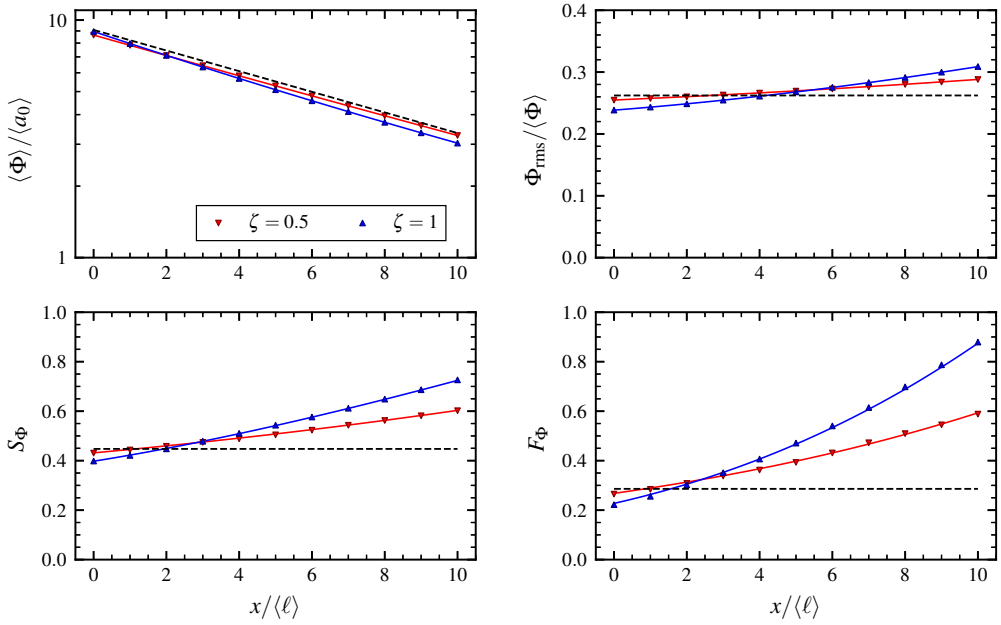

Figure 49: Radial profiles of the average value (top left), relative fluctuation level (top right), skewness (bottom left) and flatness (bottom right) for a distribution of pulse velocities given by equation (4.43) with truncation parameter $\alpha = 0.5$ and two different values of ζ. The black dashed line indicates the radial profiles for a degenerate distribution of pulse velocities.

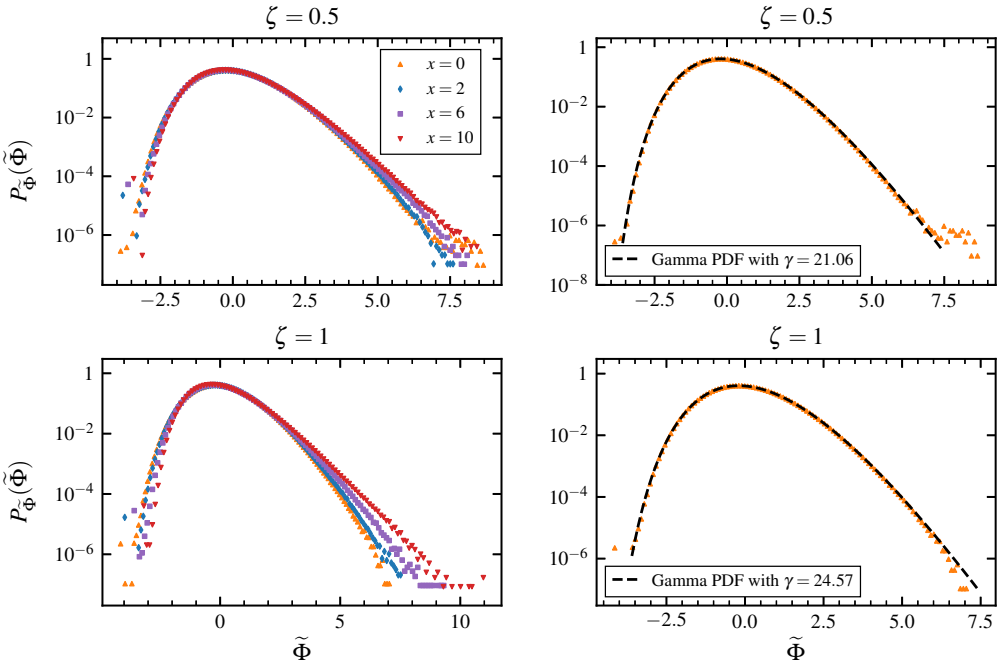

Figure 50: Probability distribution function of the normalized process with velocities distributed according equation (4.43) with truncation parameter $\alpha = 0.5$ and two different values of ζ for different radial positions. The black dashed line indicates a Gamma distribution with estimated shape parameter γ.

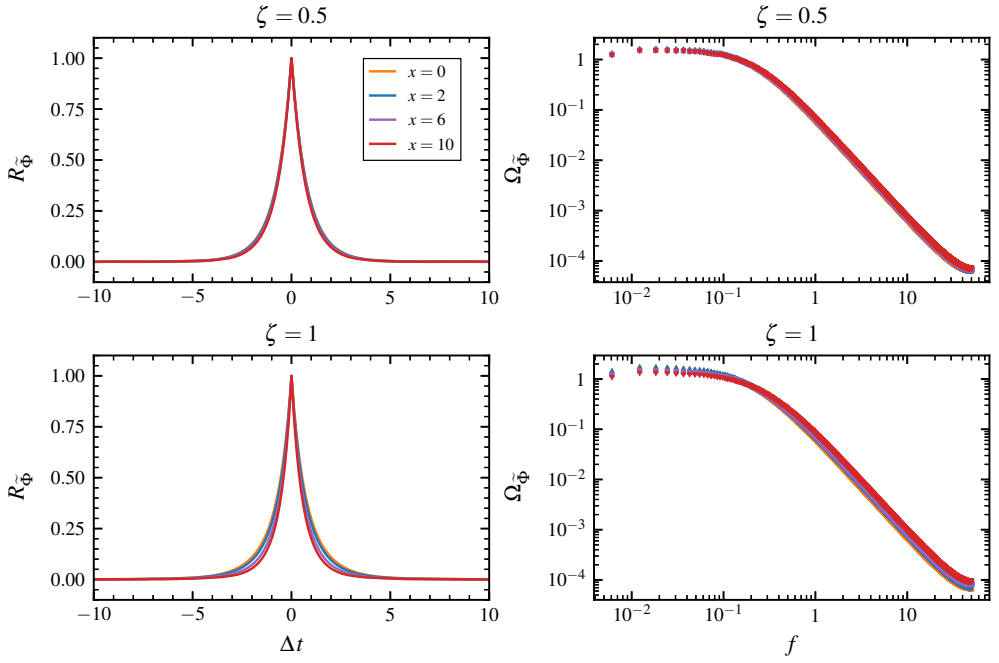

Figure 51: Auto-correlation function and power spectral density for the normalized process for different radial position with velocities distributed according equation (4.43) with truncation parameter $\alpha = 0.5$ and two different values of ζ.

Case $\alpha = 0.9$

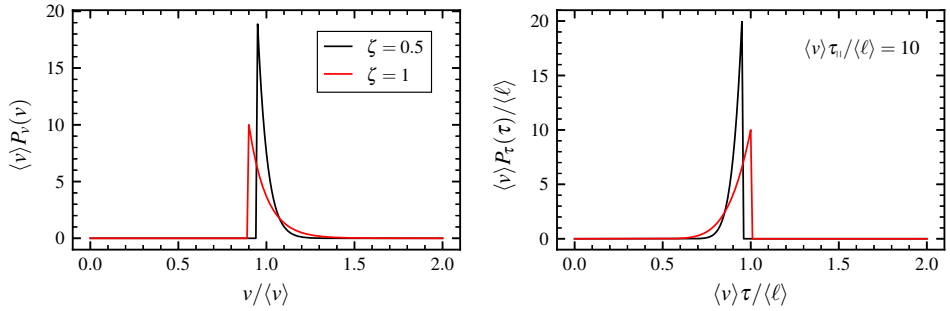

Figure 52: Marginal probability distribution function for the pulse velocities and duration times given by equations (4.43) and (4.44), respectively, with truncation parameter $\alpha = 0.9$ and two different values of ζ.

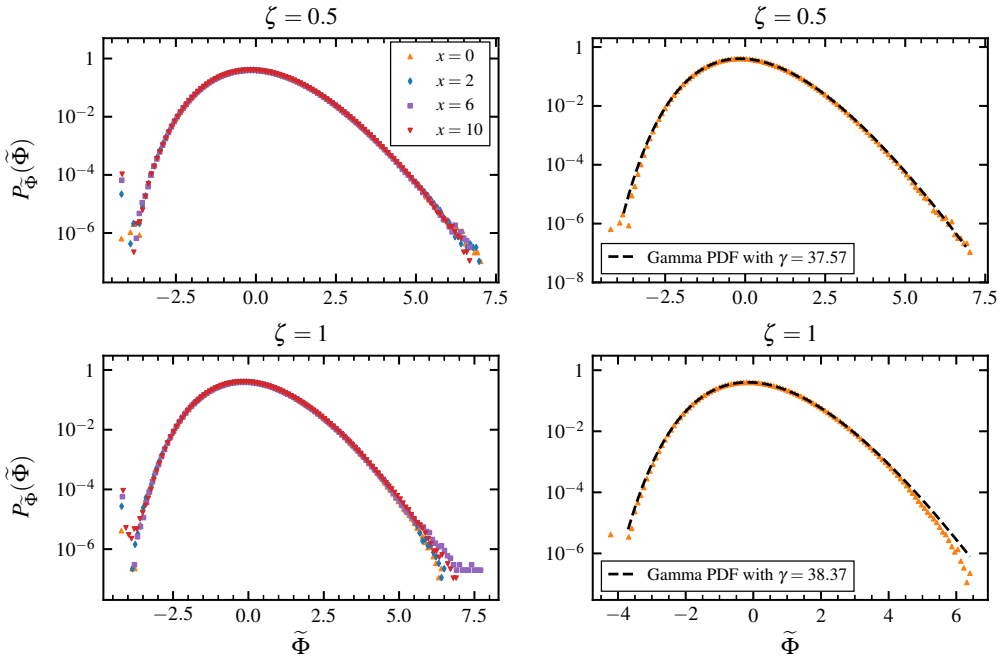

Figure 53: Probability distribution function of the normalized process with velocities distributed according equation (4.43) with truncation parameter $\alpha = 0.9$ and two different values of ζ for different radial positions. The black dashed line indicates a Gamma distribution with estimated shape parameter γ.

4.6 Discussion

In the present section, the process based on a super-position of radially propagating exponential pulses has been investigated for exponential distribution of amplitudes and different distributions of pulse velocities; discrete and continuous uniform distribution of velocities, Gamma distributed velocities and exponentially distributed velocities with truncation. For all of these, radial profiles of the average, relative fluctuation level, skewness and flatness moments of the resulting process are presented. It is evident that for a broad distribution of pulse velocities, the average profile is steep for small x and has a longer scale lengths for large x, where it is dominated by the fast pulses. Such behaviour is associated with reduced relative fluctuation level, skewness and flatness for small x, while for large x these quantities increase radially outwards.

In addition, the case with power-law relation between amplitudes and velocities is presented. As discussed in section 2, the divergence of cumulants due to arbitrarily slow pulses will not allowed the exponentially distribution of pulse amplitudes and the lower-truncated exponential distribution of amplitudes is considered instead. The pronounced effect of correlation on radial profiles of the lowest order statistical moments is evident. To examine this in more detail, consider that both pulse velocities and amplitudes are exponentially distributed with the same truncation parameter α as, for example, given by equation (4.39). It should be emphasized that this is equivalent to the case $v \sim a_0^\zeta$ with exponent parameter $\zeta = 1$, but amplitudes and velocities are uncorrelated. Figure 54 illustrates the radial profiles for the uncorrelated as well as correlated cases for two different values of the truncation parameter α and demonstrates the role of the correlation on the statistical properties of a process. The average value is smaller and, consequently, the relative fluctuation level, skewness and flatness moments are larger compared to the case with constant velocity, in contrast to the uncorrelated case, or in general to the case for a random distribution of pulse velocities. When all input parameters are specified at reference position, there is one possible explanation describing such behaviour. After single pulse arrive at reference time t_k at the reference position $x = 0$ its propagates radially and how much tail is left behind in time depends on how much pulse has been damp (recall that there is an exponential damping of the pulse amplitude with e-folding length $v\tau_{\shortparallel}$). In the case of the amplitude dependent velocities, the pulses with larger (smaller) amplitude/velocity give flatter (steeper) contributions to the profiles and are also associated with larger (smaller) relative fluctuation level, skewness and flatness moments. For a broad distribution of pulse amplitudes, the contribution of fast pulses stay longer for small x and counteracts a steeping of the average profile associated with slow pulses. For large x, the average profile has even longer scale length when compared to uncorrelated case again attributed to the competition between fast pulses and a bit slower pulses. Associated with this variation for the average profile is an increased relative fluctuation level as well as skewness and flatness moments at all radial position when compared to the uncorrelated case.

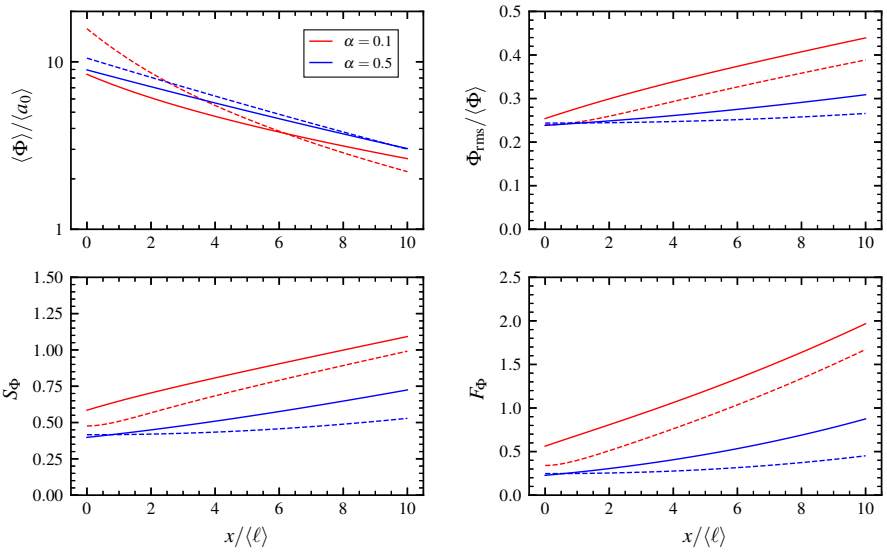

Figure 54: Comparison of the radial profiles of the lowest order statistical moments. Solid lines correspond to profiles shown in figures 45 and 49 with the power-law coefficient $\zeta = 1$. Dashed lines correspond to the profiles of the process for a truncated exponential distribution of the pulse velocities and amplitudes.

As discussed in the section 2, when end effects are neglected, the process retains its Poisson property and therefore is a FPP process generalized to the the case of a random distribution of pulse durations. Such process is characterized by the rate parameter τ_{w}, the pulse durations and amplitudes, where the last are given by

$$\tau = \frac{\tau_{\shortparallel}\ell}{v\tau_{\shortparallel} + \ell}, \quad a(x) = a_0 \exp\left(-\frac{x}{v\tau_{\shortparallel}}\right).$$

The rate parameter τ_{w} and durations τ but amplitudes a are independent of the radial position x. This identify that the are two mechanism by which the statistic of the process can change radially; the pulse amplitudes will be modified by a broad distribution of pulse velocities, and the exponential distribution specified at the reference position $x = 0$ will be altered at other positive radial positions; a random velocity distribution will lead to build up linear correlation between pulse durations and amplitudes.

It was addressed that the amplitude distribution at $x \neq 0$ is implausible to find in closed form for a continuous distribution of pulse velocities. However, its integral form can be found by product convolution of amplitudes with specified at the reference position $x = 0$ and transformed velocities, where transformation is given by exponent in amplitude equation. Further, the numerical estimates indicate that the probability distribution functions can be well approximated by the Gamma-Pareto distributions type as illustrated in figures 55 and 56. Here the PDFs are normalized by average amplitude for corresponding radial position, to emphasize the radial change of shape. The estimations of shape parameter for Gamma and Pareto distributions has been performed by least squares method. For $x > 0$, the amplitude distribution transit from exponential distribution to approximately a Gamma distribution with shape parameter smaller than unity. Moreover, the shape parameter will further decrease to zero with increasing radial position. For very large x amplitudes follow a $a^{-\alpha}$ power law i.e. Pareto distribution. This findings can be interpreted as follows: the process at large radial positions will be dominated by the fast pulses which have large amplitudes due to their short radial transit times. At the same time, the slow pulse amplitude attenuation leads to a higher probability for small pulse amplitudes. Such a change of shape in the amplitude distribution leads to changes in statistical moments, even if the average amplitude is kept constant.

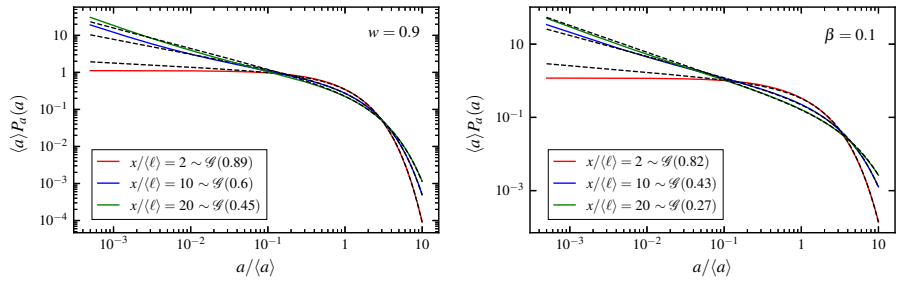

Figure 55: Numerically evaluated probability distribution of the pulse amplitudes for a continuous uniform distribution of pulse velocities with with width parameter $w = 0.9$ (left panel) and for an exponential distribution of pulse velocities with truncation parameter $\beta = 0.1$ at different radial positions presented in log-log plot. The black dashed lines indicate a Gamma ($\mathscr{G}$) distribution with estimated shape parameter α. The estimated shape parameters are presented in the inset.

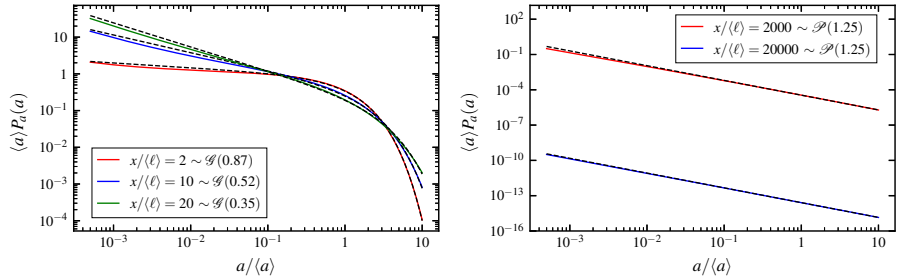

Figure 56: Numerically evaluated probability density function of the pulse amplitudes for a Gamma distribution of pulse velocities with shape parameter $s = 2$ at different radial positions. The black dashed lines indicate a Gamma ($\mathscr{G}$) or Pareto ($\mathscr{P}$) distributions with estimated shape parameter α, respectively. The estimated shape parameters are presented in the inset.

To illustrate this effect, consider a super-position of uncorrelated pulses with a Gamma amplitude distribution with shape parameter α,

$$\langle a\rangle P_a(a;\langle a\rangle,s) = \frac{\alpha}{\Gamma(\alpha)}\left(\frac{\alpha a}{\langle a\rangle}\right)^{\alpha-1}\exp\left(-\frac{\alpha a}{\langle a\rangle}\right), \quad a>0. \tag{4.46}$$

Neglecting correlations between pulse amplitudes and durations, the first four moments of the FPP are given by

$$\langle\Phi\rangle = \gamma\langle a\rangle, \tag{4.47a}$$

$$\frac{\Phi_{\rm rms}}{\langle\Phi\rangle} = \frac{1}{\gamma^{1/2}}\left(\frac{\alpha+1}{2\alpha}\right)^{1/2}, \tag{4.47b}$$

$$S_\Phi = \frac{2^{3/2}}{3\gamma^{1/2}}\frac{\alpha+2}{[\alpha(\alpha+1)]^{1/2}}, \tag{4.47c}$$

$$F_\Phi = \frac{1}{\gamma}\frac{(\alpha+2)(\alpha+3)}{\alpha(\alpha+1)}. \tag{4.47d}$$

This shows that both the degree of pulse overlap, determined by γ, and the shape parameter s of the amplitude distribution determines the degree of intermittency. For small α, the intermittency of the process is much stronger than for an exponential amplitude distribution, corresponding for $\alpha = 1$.

As another relevant case, consider a super-position of uncorrelated pulses with a truncated Pareto amplitude distribution with shape parameter α. The distribution and its moments are given by

$$P_a(a;\alpha,\beta,\langle a\rangle) = \beta a^{-\alpha}, \quad a_\downarrow \leqslant a \leqslant a_\uparrow, \tag{4.48a}$$

$$\langle a^n\rangle = \beta\, a_\downarrow^{n+1-\alpha}\frac{1-\Delta^{\alpha-n-1}}{\alpha-n-1}, \quad \alpha\neq 1,\, n+1, \tag{4.48b}$$

where the parameters with appropriate normalization are given by

$$a_\downarrow = \langle a \rangle \frac{(\alpha-2)}{(\alpha-1)} \frac{(1-\Delta^{\alpha-1})}{(1-\Delta^{\alpha-2})},$$
$$a_\uparrow = a_\downarrow \Delta^{-1},$$
$$\beta = \frac{\alpha-1}{1-\Delta^{\alpha-1}} a_\downarrow^{\alpha-1}.$$

Here $\Delta = a_\downarrow/a_\uparrow$ is the width parameter of the distribution, where $a_\downarrow$ is the minimum pulse amplitude, $a_\uparrow$ is the maximum pulse amplitude and n is the order of raw moments. The advantage of introducing the truncated Pareto distribution rather than standard Pareto distribution, is that all its moments will always exist. It is noteworthy that for the values $\alpha = 1$ and $\alpha = n+1$, moments given by (4.48b) do not hold directly but can be found by making use of well-defined limits

$$\lim_{\alpha\to 1} \frac{1-\Delta^{\alpha-1}}{\alpha-1} = \lim_{\alpha\to n+1} \frac{1-\Delta^{\alpha-n-1}}{\alpha-n-1} = \ln \Delta^{-1}. \tag{4.50}$$

The lowest order moments of the FPP are given by

$$\langle \Phi \rangle = \gamma \langle a \rangle, \tag{4.51a}$$
$$\frac{\Phi_{\rm rms}}{\langle \Phi \rangle} = \frac{1}{\gamma^{1/2}} \frac{\alpha-2}{1-\Delta^{\alpha-2}} \left[\frac{(1-\Delta^{\alpha-1})(1-\Delta^{\alpha-3})}{2(\alpha-1)(\alpha-3)} \right]^{1/2}, \tag{4.51b}$$
$$S_\Phi = \frac{2^{3/2}}{3\gamma^{1/2}} \frac{(\alpha-3)(1-\Delta^{\alpha-4})}{(\alpha-4)(1-\Delta^{\alpha-3})} \left[\frac{(\alpha-3)(1-\Delta^{\alpha-1})}{(\alpha-1)(1-\Delta^{\alpha-3})} \right]^{1/2}, \tag{4.51c}$$
$$F_\Phi = \frac{1}{\gamma} \frac{(1-\Delta^{\alpha-1})(1-\Delta^{\alpha-5})}{(\alpha-1)(\alpha-5)} \left[\frac{\alpha-3}{1-\Delta^{\alpha-3}} \right]^2. \tag{4.51d}$$

As expected, both pulse overlap and the amplitude shape parameter determine intermittency level for the process.

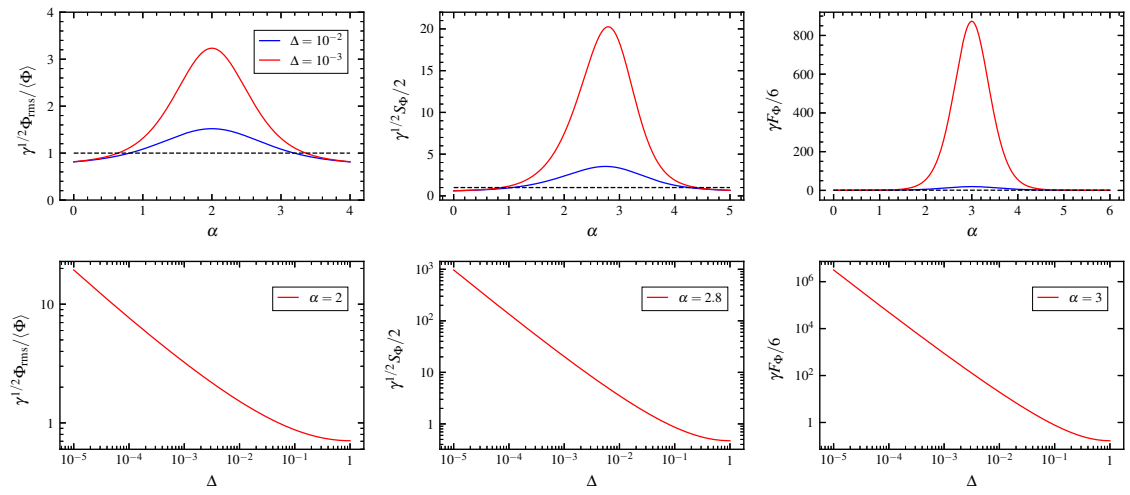

Figure 57: (top row) Statistical moments of the FPP as function of the shape parameter α for a truncated Pareto distribution of amplitudes with width parameter $\Delta = \{10^{-2}, 10^{-3}\}$. Black dashed lines give statistical moments for an exponential amplitude distribution. (bottom row) Statistical moments as function of the width parameter Δ for a truncated Pareto distribution of amplitudes with shape parameter α that gives sharp peak in the top row.

It is clear from figure 57 that for a broad distribution of amplitudes, the shape parameter in the approximate range $1 < \alpha < n+1$, where n is a highest order of the corresponding statistical moment (for example skewness gives $n = 3$), leads to a stronger intermittency of the process in comparison to an exponential amplitude distribution.

An additional mechanism that contributes to the radial variation of statistical properties of the process is the build up of correlation between amplitudes and durations as x increases. The

reason for this is an exponential decay of the pulse amplitudes in the presence of linear damping and that durations and amplitudes get correlated by a velocity distribution. In particular, for a non-degenerate distribution of velocities, pulses with larger (smaller) velocities will have larger (smaller) amplitudes and duration times. In order to illustrate this, the linear correlation coefficient between pulse durations and amplitudes was presented for considered velocity distributions as a function of the radial position x. It reveals strongly negative correlation for a broad distribution of pulse velocities at large radial positions which will further strengthen the intermittency level of the process. Based, on all mentioned above, it is anticipated that a broad distribution of pulse velocities leads to a non-exponential profiles and a change in the pulse amplitude statistics and their correlation with pulse durations.

The probability distribution function for the normalized process is presented for a random distribution of pulse velocities. For exponentially distributed pulse amplitudes independent of pulse sizes and velocities, the distribution $P_{\tilde{\Phi}}$ is a Gamma distribution and radially outwards becomes strongly skewed and flattened with an exponential tail towards large fluctuations. For lower-truncated exponential distribution of pulse amplitudes it is found that as the truncation parameter α increases, the distribution of the process at the reference position is more symmetric and Gaussian-like (characterized by low intermittency level) likely ascribed to changes in amplitude distribution. In the case of amplitudes distributed according to (4.39), the closed-form expression of a distribution of the process (plausibly) can not be found, as it was in the case of exponentially distributed amplitudes (that is a Gamma-distributed process). It also worth to note that the PDF of the process can be well approximated by Gamma distribution as illustrated in figures 46, 50 and 53. For the purpose of illustration, consider the FPP process with truncated exponential distribution of amplitudes. The lowest order statistical moments are given by

$$\langle a^n \rangle = [\langle a \rangle (1-\alpha)]^n \exp\left(\frac{\alpha \langle a \rangle}{\langle a \rangle (1-\alpha)}\right) \Gamma\left(n+1, \frac{\alpha \langle a \rangle}{\langle a \rangle (1-\alpha)}\right), \tag{4.52}$$

where Γ here is an incomplete Gamma function (see Appendix A). This gives the relative fluctuation level as well as skewness and flatness moments but mean value, $\langle \Phi \rangle = \gamma \langle a \rangle$, dependent on the parameter α, as shown in figure 58.

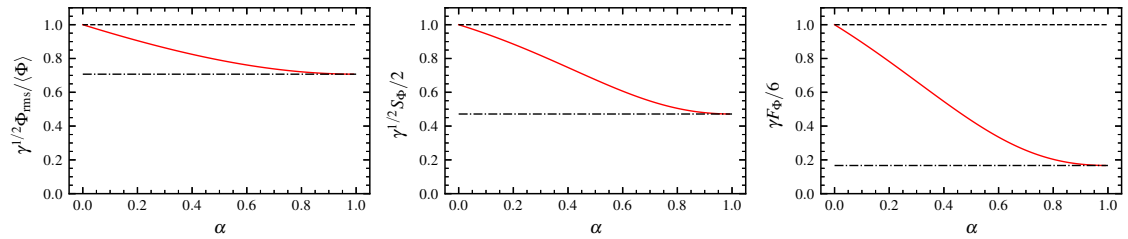

Figure 58: Statistical moments as function of parameter α for a truncated exponential distribution of amplitudes. Black dashed lines give statistical moments for an exponential amplitude distribution.

For $\alpha = 0$, this is equivalent to the exponential distribution validated by dashed black line. However, as α increase, there is a significant fall in relative fluctuation level, skewness and flatness. As $\alpha \to 1$, this is the same as for degenerate distribution of amplitudes. In order to validate this asymptotic limit, uniform distribution of pulse amplitudes can be considered, where the first four moments of such FPP process are given by

$$\frac{\Phi_{\rm rms}}{\langle \Phi \rangle} = \frac{1}{\gamma^{1/2}} \left(\frac{w^2+3}{6}\right)^{1/2}, \quad S_\Phi = \frac{6^{3/2}}{3\gamma^{1/2}} \frac{w^2+1}{(w^2+3)^{3/2}}, \quad F_\Phi = \frac{36}{20\gamma} \frac{w^4+10w^2+5}{(w^2+3)^2}. \tag{4.53}$$

In the limit $w \to 0$, that is the case for constant amplitude, this gives $\Phi_{\rm rms}/\langle \Phi \rangle = 1/(2\gamma)^{1/2}$, $S_\Phi = 2^{3/2}/(3\gamma^{1/2})$ and $F_\Phi = 1/\gamma$ which is consistent with limiting case shown by dashed and dotted lines.

The auto-correlation function and power spectral density for the normalized process are also presented for a random distribution of pulse velocities. In general, the auto-correlation function is a two-sided decaying exponential function and the power spectral density has a Lorentzian shape and falls as f^{-2}, which is follows from assuming an one-sided exponential pulses. A broad distribution of pulse velocities leads to a significant change in an e-folding time of an auto-correlation function and a decrease of the energy in the low-frequency part of the spectrum radially outwards.

5 Time-dependent pulse velocities

The model with time-independent velocities diverges for negative radial positions $x < 0$ if velocities are allowed to be arbitrarily small. The reason for this divergence is that at negative distances the amplitudes of the pulses with velocity v grows as $\exp[-x/(\tau_{\shortparallel} v)]$, therefore slow moving pulses can become arbitrarily large. This is not physical, since it is expected that large amplitude pulses will have large radial velocities. For this reason it is necessary to formulate a model in which pulses move slower as the amplitude decreases for positive radial positions, and they move faster as their amplitude increases for negative radial positions. With this motivation, consider velocities that are given by a power law dependence on instantaneous amplitude,

$$V_k(t) = v_0 \left(\frac{A_k(t)}{\langle a_0 \rangle} \right)^{\zeta}, \tag{5.1}$$

where one should recall definition of instantaneous pulse amplitude (2.30),

$$A_k(t) = a_{k,0} \exp\left(-\frac{t - t_k}{\tau_{\shortparallel}} \right).$$

Importantly, here v_0 is a constant and $a_{k,0}$ are initial pulse amplitudes specified at reference position $x = 0$.

Stagnation of pulses

The radial position of a pulse is given by

$$X_k(t) = \int_{t_k}^{t} \mathrm{d}t' V_k(t') = \frac{v_0 \tau_{\shortparallel} a_{k,0}^{\zeta}}{\zeta \langle a_0 \rangle^{\zeta}} \left[1 - \exp\left(-\frac{\zeta (t - t_k)}{\tau_{\shortparallel}} \right) \right].$$

As $t \to \infty$ the pulse position approaches

$$X_{k,\max} = \frac{v_0 \tau_{\shortparallel} a_{k,0}^{\zeta}}{\zeta \langle a_0 \rangle^{\zeta}}. \tag{5.2}$$

The time it takes for pulse k to reach the radial position x is $T_k(x)$

$$T_k(x) = t_k - \frac{\tau_{\shortparallel}}{\zeta} \ln\left(1 - \frac{\zeta \langle a_0 \rangle^{\zeta} x}{v_0 \tau_{\shortparallel} a_{k,0}^{\zeta}} \right). \tag{5.3}$$

For large radial positions x, the argument in the logarithm becomes negative. The reason is that the pulses have decayed before reaching such position. Under this consideration, the expected number of pulses arriving at the radial position x can be written as

$$\langle K \rangle(x) = \frac{T}{\tau_{\mathrm{w}}(0)} \left\langle \Theta\left(\frac{v_0 \tau_{\shortparallel} a_{k,0}^{\zeta}}{\zeta \langle a_0 \rangle^{\zeta}} - x \right) \right\rangle, \tag{5.4}$$

where Θ is a Heaviside step function. Here Heaviside function emphasize that for some radial position x, pulse with initial velocity $\sim a_0^{\zeta}$ will stagnate and will not contribute to the moments of the process. When pulses are assumed to be uncorrelated in the stationary limit $T \to \infty$, the arrival times at the radial position $x > 0$ will also follow a Poisson process with an increased waiting time

$$\frac{\tau_{\mathrm{w}}(0)}{\tau_{\mathrm{w}}(x)} = \left\langle \Theta\left(\frac{v \tau_{\shortparallel} a_{k,0}^{\zeta}}{\zeta \langle a_0 \rangle^{\zeta}} - x \right) \right\rangle, \tag{5.5}$$

In particular, assuming exponentially distributed pulse amplitudes and degenerate pulse velocities, the expression takes the form

$$\tau_{\mathrm{w}}(x) = \tau_{\mathrm{w}}(0) \exp\left[\left(\frac{\zeta x}{v_0 \tau_{\shortparallel}} \right)^{\frac{1}{\zeta}} \right]. \tag{5.6}$$

For $\zeta = 1$, there is an exponential growth of the average waiting time, with a characteristic length given by the product $v_0 \tau_{\shortparallel}$. Consequently, the loss of pulses due to stagnation will result in an increasing waiting time.

5.1 Exponential pulse amplitude distribution

As was discussed in section 2, the model for time-independent velocities is mathematically ill-defined for the negative radial positions if arbitrarily small velocities are present. However, the divergence of the model can be regularized by considering that the velocities are given by (5.1). Therefore, in contrast to the time-independent case $v \sim a_0^{\zeta}$, a requirement of a truncated exponential distribution of initial pulse amplitudes can be relaxed. Given that pulse arrives at $x = 0$ at reference time $t = t_k$, the exponential factor in (5.1) is equal to unity, so that

$$V(t = t_k) = v_0 \left(\frac{a_0}{\langle a_0 \rangle} \right)^{\zeta}, \tag{5.7}$$

where constraint on v_0 can be determined by

$$\langle V_0 \rangle = \int_0^{\infty} \mathrm{d}a_0 \, V(t = t_k) P_{a_0}(a_0), \tag{5.8}$$

here $\langle V_0 \rangle$ emphasize the average pulse velocity at the reference position $x = 0$. Therefore, velocities with appropriate normalization are readily obtained as

$$\frac{V(t)}{\langle V_0 \rangle} = \frac{1}{\Gamma(1+\zeta)} \left(\frac{A_k(t)}{\langle a_0 \rangle} \right)^{\zeta}. \tag{5.9}$$

It is straightforward to deduce that velocity distribution at the reference position is similar to one given in equation 4.43 but the support is not restricted i.e. $\alpha \to 0$.

The average waiting time τ_w given by equation (5.6) is presented in figure 59 as function of radial position for two different values of power-law scaling coefficients ζ. For $\zeta = 1$, the waiting time increase by factor 2.7 and provide that the large number of pulses have stagnated. While for the case $\zeta = 0.5$ the waiting time have only weak variation with radial position in considered range, provide that most of the pulses have yet not been stagnated. In order to quantify this effect, the radial position where pulses on average will be stagnated can be found and is given by integrating equation (5.2) over amplitude distribution,

$$\langle X_{\max} \rangle = \frac{\langle V_0 \rangle \tau_{\shortparallel}}{\zeta}. \tag{5.10}$$

It is to be noted that the position where pulse on average will stagnate increase with parallel transit time and decrease with power-law scaling coefficient.

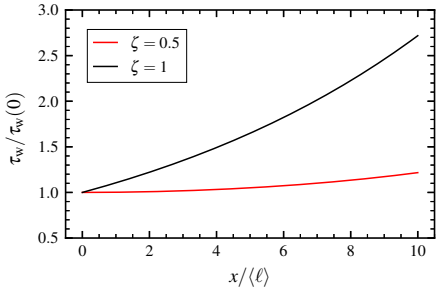

Figure 59: Radial profile of the average waiting time for the time-dependent pulse velocities which are degenerate distributed for various ζ.

The radial profiles of the average value, relative fluctuation level, skewness and flatness moments are presented in figure 60 for realizations of the process (markers) with two different values of power-law scaling coefficient ζ. For comparison the profiles for the case when velocities depends on initial amplitude with truncation parameter $\alpha = 0.1$ are shown by solid curves on the same figure (the profile are equivalent to one presented in figure 45). The choice of $\alpha = 0.1$ is motivated by the fact that its gives a broad distribution of amplitudes. By expecting figure 60 it can be noted that the average profiles for time-dependent velocities decay slower, and, consequently, the higher order moments increase slower. At first glance this findings might look quite contradicting, since it is

expected that the number of pulses contributing to the moments decrease largely for $\zeta = 1$. One reason is that on average pulse will stagnate at $x = 10$ for $\zeta = 1$ and at $x = 20$ for $\zeta = 0.5$. Thus, it is evident that profiles are likely to dependent on several mechanisms at the same time. This aspect will be addressed later in discussion.

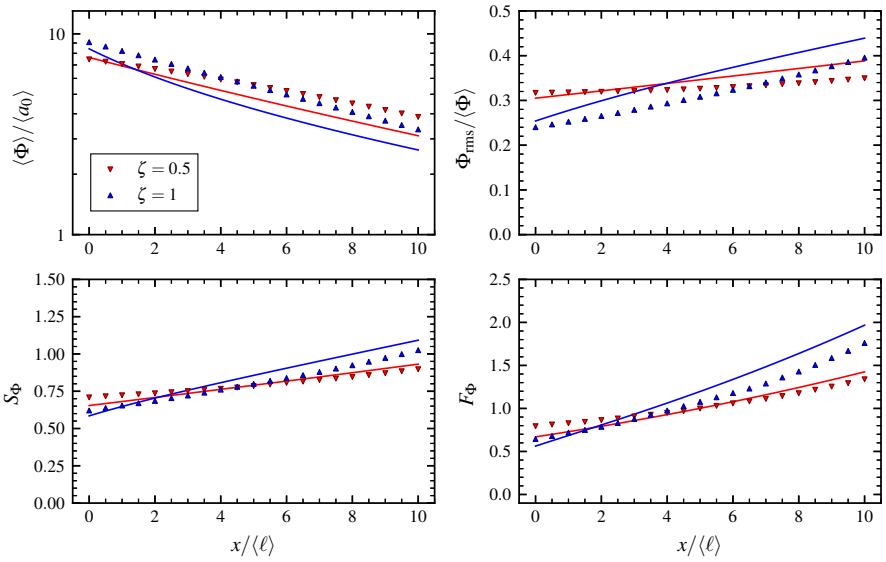

Figure 60: Radial profiles of the average value (top left), relative fluctuation level (top right), skewness (bottom left) and flatness (bottom right) with pulse velocities dependent on the instantaneous amplitude for two different values of the power-law coefficient ζ. Curves correspond to the radial profiles of the pulse velocities given by power-law of the initial amplitude.

The probability distribution function of the normalized process at different radial positions is presented in figure 61 for two different values of power-law scaling coefficient ζ. The shape parameter γ has been estimated by fitting a Gamma distribution to the realizations at the reference position $x = 0$ via maximum likelihood method. It is evident that the PDF of the realizations of the process with time-dependent velocities can be well approximated by a Gamma distribution. The slightly elevated tail of the $P_{\tilde{\Phi}}$ for the case $\zeta = 1$ is observed. Nevertheless, radially outwards the distribution function becomes strongly skewed and has nearly exponential tail towards large fluctuation amplitudes. The same change in the shape of the PDF radially outwards has been identified in previous section and is consistent with the radial profile of the lowest order statistical moments presented in figure 60.

The normalized auto-correlation function and corresponding power spectrum are shown in figure 62 for the different radial positions x. The most striking feature is evident for auto-correlation function for the case $\zeta = 0.5$, where the e-folding time scale and energy in low-frequency part of the spectrum increase slightly radially outwards. Thus this results might indicate weak long range correlations for large x. Radially constant e-folding time scale for the case $\zeta = 1$ scale is observed.

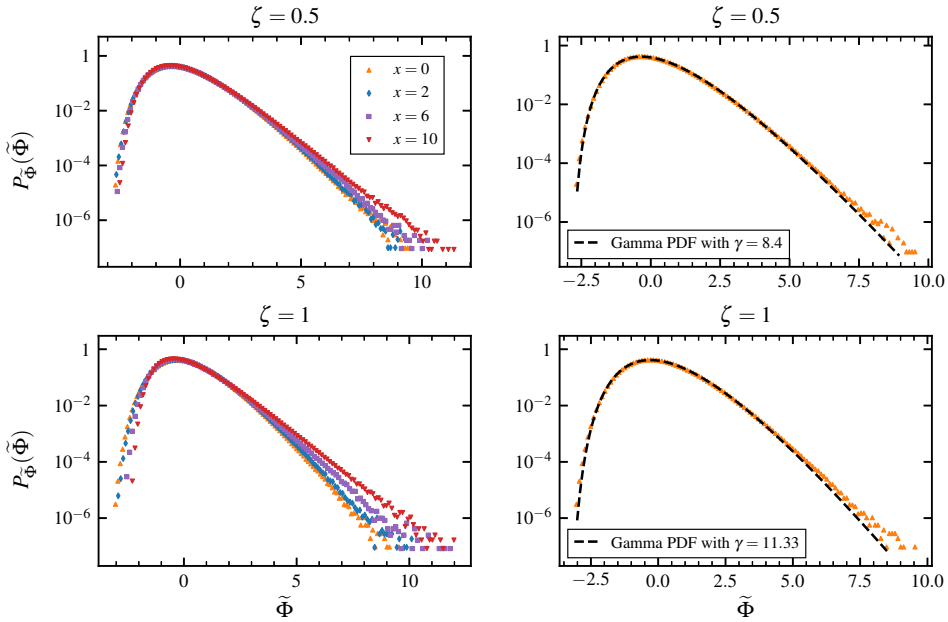

Figure 61: Probability distribution function of the normalized process for degenerate distribution of pulse velocities for various ζ. The black dashed line indicates a Gamma distribution with estimated shape parameter γ.

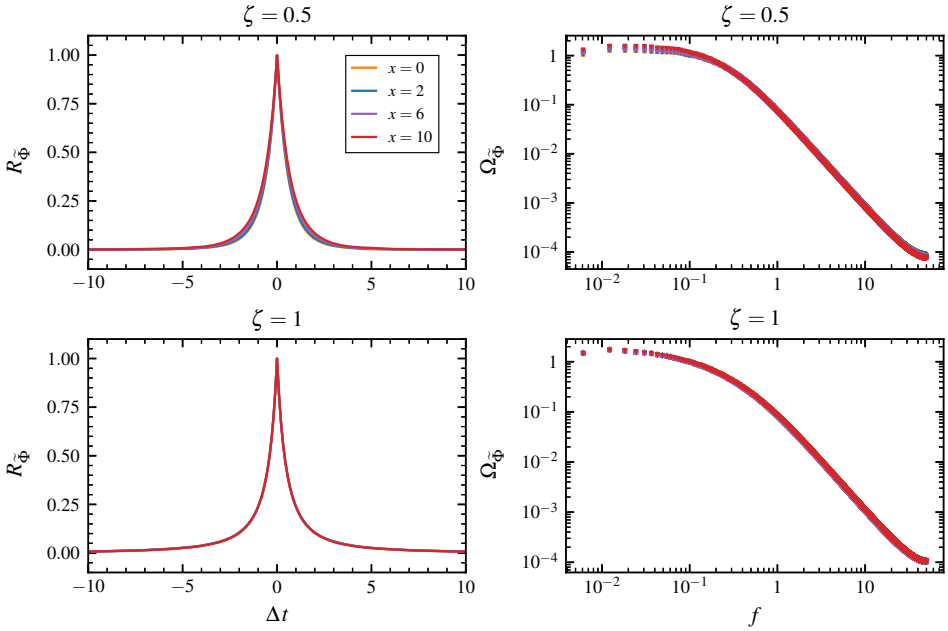

Figure 62: Auto-correlation and power spectral density functions of the normalized process at different radial positions with an exponential amplitude distribution for different values of the power-law coefficient ζ.

5.2 Truncated exponential distribution of initial pulse amplitudes

In order to gain some insight into the effect of pulse velocities depending on its instantaneous amplitude, consider the case for truncated exponentially distributed amplitudes. Noteworthy is that at reference position $x = 0$ the statistical properties of the pulses are equivalent to the correlated scaling case with time-independent velocities. The radial profile of the average waiting time is given by integrating equation (5.5) over considered amplitude distribution

$$\tau_{\mathrm{w}} = \tau_{\mathrm{w}}(0) \exp\left[\frac{\left(\frac{\zeta x}{v_0 \tau_{\mathrm{ii}}}\right)^{\frac{1}{\zeta}} - \alpha}{(1-\alpha)}\right], \quad \text{if } \alpha \leqslant \left(\frac{\zeta x}{v\tau_{\mathrm{ii}}}\right)^{\frac{1}{\zeta}}, \tag{5.11}$$

otherwise the waiting time $\tau_{\mathrm{w}}(0)$ is the same. The average waiting time is shown in figure 63 as function of radial position for two different values of the power-law scaling coefficients $\zeta = 0.5$ (left panel) and $\zeta = 1$ (right panel). Interestingly, when the minimum initial amplitude is defined, the process retain the constant pulse rate τ_w for $x > 0$, and eventually will increase to the same value as for exponential distribution of pulse amplitudes at $x = 10$.

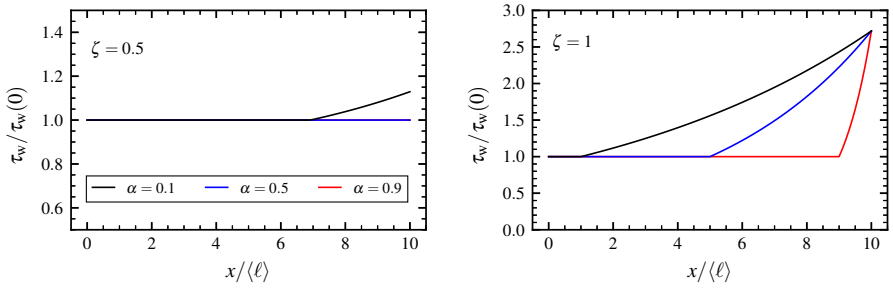

Figure 63: Radial profile of the average waiting time for the time-dependent pulse velocities which are degenerate distributed for various ζ.

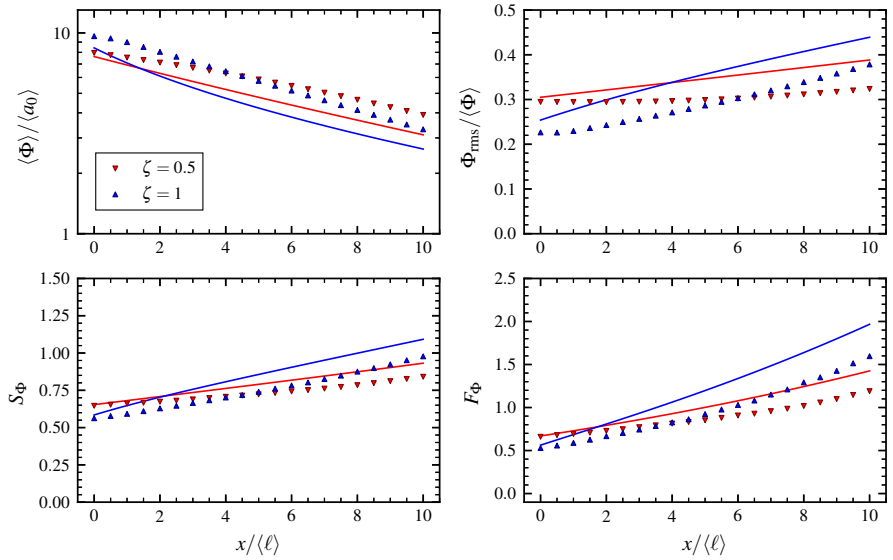

Figure 64: Radial profiles of the average value (top left), relative fluctuation level (top right), skewness (bottom left) and flatness (bottom right) with pulse velocities dependent on the instantaneous amplitude for two different values of the power-law coefficient ζ. Curves correspond to the radial profiles of the pulse velocities given by power-law of the initial amplitude.

In figure 64 the radial profiles obtained from realizations of the process of the average value, relative fluctuation level, skewness and flatness moments are presented for two different values of power-law scaling coefficient ζ. The solid curves indicate case with time-independent velocities.

Visually, the observed profiles are qualitatively similar to those given in previous subsection, but the relative fluctuation level, skewness and flatness moments have slightly smaller values (the intermittency is a bit weaker).

The probability distribution function of the normalized process at different radial positions is presented in figure 65 for two different values of power-law scaling coefficient ζ. The parameter γ has been estimated by fitting a Gamma distribution to the realizations of the process at the reference position $x = 0$.

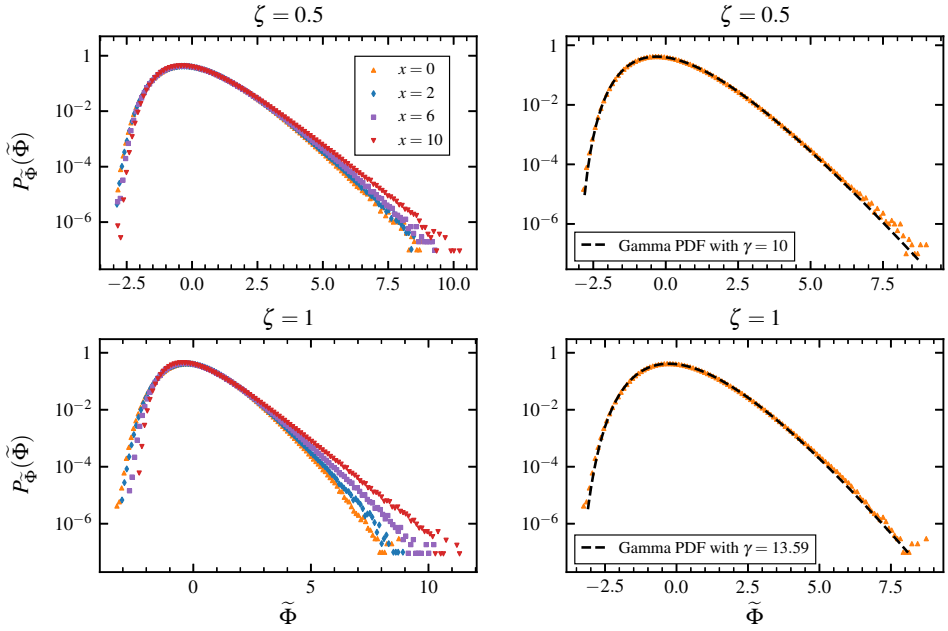

Figure 65: Probability distribution function of the normalized process for truncated exponential amplitude distribution for various ζ. The black dashed line indicates a Gamma distribution with estimated shape parameter γ.

The normalized auto-correlation function and corresponding power spectrum are shown in figure 66 for the different radial positions x. Evidently, the time characteristics of the process are equivalent to the case presented in previous subsection.

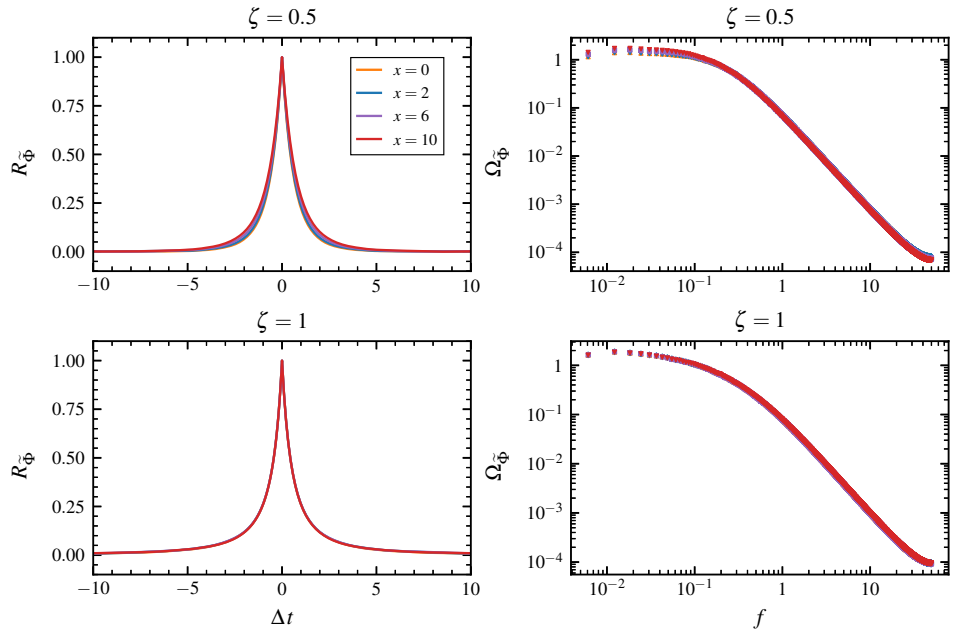

Figure 66: Auto-correlation and power spectral density functions of the normalized process at different radial positions with truncated exponential amplitude distribution for $\alpha = 0.1$ and different values of the power-law scaling coefficient ζ.

5.3 Discussion

The model concerned in present section is accounted for a pulse velocity modification resulting from the reduction of amplitude in the presence of linear damping. That is the case in which the radial velocity of a pulse depends on the instantaneous amplitude, instead of just initial amplitude. The important feature of this case attributed to pulse stagnation and increased relative fluctuation level of the process due to the decrease of the number of pulses contributing to the moments and increase of the average waiting time. However it wasn't identify directly in case study given above and thus required further analysis. In general, it is seen that the the scale length of the average profile have only weak variation. Interestingly, it seems that scale length is longer for small x, which is the opposite of what one have seen in section 4. However this findings is still can be supported by the argument given in discussion of section 4. The pulses associated with larger (smaller) amplitude/velocity give flatter (stepper) contributions to the profile and are also associated with larger (smaller) relative fluctuation level, skewness and flatness moments. Whereas in case considered here due to change in velocity distribution, the contribution of fast pulses stay (even longer) for small x, but slow pulse contribution will be more pronounced for large x. The change in velocity distribution can be illustrated, in the simplest case when amplitudes are exponentially distributed at reference position and velocities have linear dependence with instantaneous amplitudes (that is $\zeta = 1$). By neglecting the evolution of pulse parameters, it is possible to estimate the velocities at a fixed radial position x. By taking into account the time it takes pulse to reach the radial position position x, the velocities at this radial position are given by

$$V(x) = v_0\left(\frac{a_0}{\langle a_0\rangle}\right) - \frac{x}{\tau_{\shortparallel}}. \tag{5.12}$$

Clearly, the velocity distribution is an exponential distribution shifted by factor $-x/\tau_{\shortparallel}$.

For the cases presented here, the probability density function of the normalized process can be well approximated by a Gamma distribution at reference position $x = 0$. Radially outwards distribution becomes strongly skewed and have heavy tail towards large amplitude fluctuations. This is correspond to what have been found in previous section on time-independent velocities.

The auto-correlation function function and corresponding power spectral density were presented in both cases. While the shape of ACFs and PSDs are consistent with assumption of one-sided

exponential pulse function (double expontial decay of ACF and Lorentzian shape of PSD), the time scale correlation change is remarkably different from what have been observed for time-independent case. Clearly, there is some mechanism presented which counteracts the substantial e-folding time decay for the case $\zeta = 1$, and actually increase it for the case $\zeta = 0.5$. The possible explanation attributed to weak long range correlations for the case $\zeta = 0.5$ may be connected to power-law distributed pulse durations. It was demonstrated in the framework of a filtered Poisson process with one-sided exponential pulse function how can a self-similar scaling of the $1/f^{\beta}$ type emerge from Pareto-distributed durations times [45]. This argument has a right to exist, since the change in velocity distribution will clearly affect the duration times distribution.

6 Conclusion and outlook

In this thesis, the statistical properties of a stochastic process based on a super-position of radially propagating uncorrelated pulses have been investigated. Particular focus was placed on one-sided exponential pulses and the implications of the distribution of pulse velocities, as well as their correlation with amplitudes. Since analytic expressions of relevant statistics of the process associated with the model described in the present work can be obtained only in simplified cases, the model has been numerically implemented. Results obtained from the realizations of the process confirm the analytical and semi-analytical predictions given by the model. This allows claiming the validity of the presented results. Moreover, the model has no time-dependent input parameters, thus reducing over-fitting and improving interpretative capabilities. The time-dependence of pulse velocities results from the amplitude reduction due to parallel transit time and is thus not involved directly. The radial profiles of the lowest order statistical moments and important statistical averages such as average duration time, average amplitude, and linear correlation coefficient were presented. Moreover, the amplitude distribution, as well as distribution of normalized process, the auto-correlation function and corresponding power spectral density at different radial positions, were presented. The results show that a broad distribution of pulse velocities is sufficient to provide radial variation of relevant statistics of the process. It was found that there is two mechanisms that can change the statistics of the process radially. A change in the pulse amplitude statistics (distribution and average value) and amplitudes correlation with pulse durations both arise from considering a broad distribution of pulse velocities. Moreover, it is evident that the properties of the pulses such as the correlation between amplitudes (both initial and instantaneous) and velocities play an important role in determining radial profiles, so that approaches based on mean pulse properties can miss important effects. The model also capable to describe the phenomena of pulse stagnation, which is observed in numerical simulation and imaging data.

In section 2, a stochastic model based on a super-position of pulses moving radially outwards in a magnetized plasma has been presented. This accounted for random joint probability distribution of pulse velocities, sizes and amplitudes. General results for the cumulants and requirement on their existence, lowest order statistical moments and correlation functions for time-independent velocities have been presented and closely follow manuscript [36].

In section 3, the numerical implementation of a stochastic model has been presented. The requirement on sampling time and duration of time series have been provided.

Section 4 focused on the statistical properties of a stochastic process describing the radial motion of one-sided exponential pulses with exponentially distributed amplitudes, fixed sizes and a random distribution of velocities. A particular case motivated by numerical simulations when pulse velocity scales with amplitude have been considered. For the cases of a discrete uniform distribution of pulse, velocities closed-form expressions of statistical averages, radial average profile, distributions of amplitudes and process itself, as well as auto-correlation function and corresponding power spectrum were derived and presented. For a continuous distribution of pulse velocities, if possible the semi-analytical (special functions are involved) expressions of the statistical averages of the process were provided. In section 5, two simplest cases of time-dependent velocities have been presented.

In conclusion, it should be emphasised, that the results are consistent compared to measurement data from experiments on the TCV and Alcator C-Mod devices [7, 32]. In the former, the profiles are steeper close to the separatrix, and tend to flatten at a certain distance from the separatrix and close to the first wall in the far SOL, especially for the large line-averaged core plasma density $\bar{n}_e$ when profiles become broad. Moreover, it was found that large $\bar{n}_e$ result in significantly larger radial velocities. This is consistent with presented results for a broad distribution of filament (pulse) velocities, result in a similar behaviour. Moreover, model is able to reproduce the characteristic PDFs of plasma fluctuations and their radial variations.

6.1 Future work and prospects

Based on results found in this thesis, a number of ideas for future work can be proposed:

- The model can be further generalized so it can include distribution of parallel transit times, and its implication can be studied for a random distribution of pulse velocities.
- Put some thought into possibility to define the velocity distribution, such that it can give a closed form expression for amplitude distribution when initial amplitudes specified to be

exponentially distributed. It will provide a strong argument when claim the universality of amplitude distribution behaviour.

- More thorough investigation of the effect of correlation between pulse velocities and amplitudes. Test for robustness concerning changes in the amplitude distributions can be performed first. The two-sided exponential pulse function should be also considered in this investigation. A better understanding about the role of correlation will compliment the analysis of time-dependent velocities.
- Case with time-dependent velocities should be analyzed further to see the role of pulse stagnation on statistical moments of the process. Most obvious approach is either increase the length of radial domain or the strength of the parallel transit time.
- Consider the amplitude (instantaneous) dependent velocities with a random statistical distribution. The simplest case is to consider discrete uniform distribution of pulse velocities. Some work have already been done on this topic, but more thoughts should be given to correctly define statistical averages of the model parameters at the reference position.

A Useful Functions, Integrals and Sums

Series expansion for exponential function

$$e^{\lambda} = 1 + \lambda + \frac{\lambda^2}{2!} + \frac{\lambda^3}{3!} \ldots = \sum_{k=0}^{\infty} \frac{\lambda^k}{k!} \tag{A.1}$$

Useful sum concerning derivation of the auto-correlation function

$$\sum_{k=0}^{\infty} k(k-1)p(k) = \sum_{k=2}^{\infty} k(k-1)\frac{\lambda^k e^{-\lambda}}{k!} = \lambda^2 e^{-\lambda} \sum_{k=2}^{\infty} \frac{\lambda^{k-2}}{(k-2)!} = \lambda^2 \tag{A.2}$$

Some special mathematical functions [46], these were used repeatedly throughout this thesis.

- The Gamma function defined by

$$\Gamma(z) = \int_0^{\infty} \mathrm{d}t \, \exp(-t)t^{z-1} \tag{A.3}$$

- The upper incomplete Gamma function defined by

$$\Gamma(a, z) = \int_z^{\infty} \mathrm{d}t \, \exp(-t)t^{a-1} \tag{A.4}$$

- The Exponential integral $E_1(z)$ is defined by

$$\mathrm{E}_1(z) = \int_z^{\infty} e^{-t}/t \, \mathrm{d}t, \tag{A.5}$$

  for $z \neq 0$. For $x > 0$,

$$\mathrm{Ei}(-x) = -\int_x^{\infty} e^{-t}/t \, \mathrm{d}t = -E_1(x). \tag{A.6}$$

  $\mathrm{Ei}(x)$ is undefined when $x = 0$, or when x is not real.

- The Exponential integral is generalized to, for $n = 0, 1, \ldots, x > 0$

$$\mathrm{E}_n(z) = \int_1^{\infty} e^{-zt}/t^n \, \mathrm{d}t \tag{A.7}$$

  where n is the order of the integral.

- The modified Bessel function of the first kind $I_v(x)$ is a particular solution of the second-order differential equation

$$x^2 y''(x) + xy'(x) - (x^2 + v^2)y(x) = 0,$$

  and it can be expressed by the infinite series

$$\mathrm{I}_v(x) = \sum_{n=0}^{\infty} \frac{1}{n!\Gamma(v + n + 1)} \left(\frac{x}{2}\right)^{2n+v}.$$

  While the modified Bessel function of the second kind $K_v(x)$ is defined by

$$\mathrm{K}_v(x) = \frac{\pi(\mathrm{I}_{-v}(x) - \mathrm{I}_v(x))}{2\sin(\pi v)}, \tag{A.8}$$

  where the right-hand side of the identity of (A.8) is the limiting value in case v is an integer. The integral form is given

$$\mathrm{K}_v(x) = \frac{1}{2}\left(\frac{x}{2}\right)^v \int_0^{\infty} \mathrm{d}t \, \frac{e^{-t-(x^2/4t)}}{t^{v+1}} \tag{A.9}$$

B Advection and Characteristics

In the advection-dissipation model, the equation in question was

$$\partial_t \phi_k(x,t) + v_k(t)\partial_x \phi_k(x,t) = -\frac{1}{\tau_{\text{II}}}\phi_k(x,t)$$

This equation is a first order linear PDE and can be solved using the method of characteristics. The initial data is given by

$$\phi_k(x,t_k) = a_k\ \varphi\left(\frac{x}{\ell_k}\right).$$

Let $\gamma(s) = (x(s), t(s))$ be a parameterized curve, where each point on the curve has velocity equal to the scalar value of the vector field $\mathbf{f}(x,t) = (a(x,t), b(x,t))$. This gives

$$\begin{aligned}\frac{d\gamma}{d\mathbf{s}} &= \mathbf{f}(\gamma(s)),\\ \frac{dx}{ds} &= a,\\ \frac{dt}{ds} &= b.\end{aligned}$$

These are called the characteristic base curves. Let $\phi_k(x,t)$ be a solution of the advection-dissipation model equation and define

$$\phi_k(s) = \phi_k(\gamma(s)) = \phi_k(x(s), t(s)).$$

Then

$$\begin{aligned}\frac{d\phi_k(s)}{ds} &= \partial_x\phi_k\frac{dx}{ds} + \partial_t\phi_k\frac{dt}{dx}\\ &= a\partial_x\phi_k + b\partial_t\phi_k\end{aligned}$$

By letting $b = 1$ and $a = v_k(t)$ this can be used to solve the advection-dissipation equation. However, this is not enough, the initial data also has to be satisfied. This can be done by introducing a second curve parameterized by τ in which the initial data is imposed. This gives

$$\phi_k(x(\tau), t(\tau)) = a_k\ \varphi\left(\frac{x}{\ell_k}\right),$$

and thus

$$(x(\tau), t(\tau)) = (\tau, t_k),$$

must hold, for it to satisfy the initial data. In order to get a solution from this, it is necessary to invert the system from being described in terms of s and τ to a system of x and t. This is only possible if the Jacobian of the coordinate change in non-zero on the entire line where the initial data is imposed.

Using this procedure, the problem can be reduced to solving a set of coupled ODEs, rather than a PDE. Choosing parameterized curves

$$\begin{aligned}t &= t(s,\tau),\\ x &= x(s,\tau),\\ \phi_k &= \phi_k(s,\tau).\end{aligned}$$

the characteristic base curves are given as

$$\begin{aligned}\frac{\mathrm{d}t}{\mathrm{d}s} &= 1, \quad t(0,\tau) = t_k,\\ \frac{\mathrm{d}x}{\mathrm{d}s} &= v_k(t), \quad x(0,\tau) = \tau,\\ \frac{\mathrm{d}\phi_k}{\mathrm{d}s} &= -\frac{\phi_k}{\tau_{\text{II}}}, \quad \phi_k(0,\tau) = a_k\ \varphi\left(\frac{\tau}{\ell_k}\right).\end{aligned}$$

Then

$$\begin{aligned}&\partial_\tau t = 0, \quad \partial_\tau x = 1 \quad \text{at} \quad (0,\tau) \Rightarrow \\ &\Delta(0,\tau) = \left(v_k \partial_\tau t - \partial_\tau x\right)\big|_{(0,\tau)} = -1 \neq 0,\end{aligned}$$

Thus, the Jacobian $\Delta \neq 0$ along the entire initial curve, and the solution is valid. Solving for the variable t gives:

$$\frac{\mathrm{d}t}{\mathrm{d}s} = 1 \Rightarrow t = s + t_0(\tau),\ t(0,\tau) = t_k \Rightarrow t_0 = t_k \Rightarrow t = s + t_k.$$

Observing that $t = s + t_k$, the equation for x can be solved by

$$\frac{\mathrm{d}x}{\mathrm{d}s} = v_k(t) \Rightarrow x(s,\tau) = x_0(\tau) + \int_0^s ds'\, v_k(s' + t_k)$$

Combining with the initial data

$$\begin{aligned}&x(0,\tau) = \tau \Rightarrow x_0(\tau) = \tau, \\ &x(s,\tau) = \tau + \int_0^s ds'\, v_k(s' + t_k).\end{aligned}$$

By a change of variable $\sigma = s + t_k$, this can be rewritten into

$$x(s,\tau) = \tau + \int_{t_k}^{s+t_k} d\sigma\, v_k(\sigma)$$

And the final equation in the system has the solution

$$\phi_k(s,\tau) = \phi_{k,0}(\tau) \exp\left(-\frac{s}{\tau_{\text{II}}}\right),$$

which, by imposing the initial data, has the unique solution

$$\phi_k(s,\tau) = a_k\, \varphi\left(\frac{\tau}{\ell_k}\right) \exp\left(-\frac{s}{\tau_{\text{II}}}\right).$$

Since the conditions for the inverse function theorem holds, the equations

$$\begin{aligned}t &= s + t_k, \\ x &= \tau + \int_{t_k}^{s+t_k} d\sigma\, v_k(\sigma),\end{aligned}$$

can be inverted to yield

$$\begin{aligned}s(x,t) &= t - t_k, \\ \tau(x,t) &= x - \int_{t_k}^{t} dt'\, v_k(t') = x - X_k(t).\end{aligned}$$

Consequently, the solution to the initial value problem is

$$\phi_k(x,t) = a_k \exp\left(-\frac{t - t_k}{\tau_{\text{II}}}\right) \varphi\left(\frac{x - X_k(t)}{\ell_k}\right).$$

C Random variable transformation

When the probability distribution $f(x)$ of random variable X is known, it may be desirable to find the distribution of new random variable $g(X)$, where function g must be a one-to-one transformation (refers as Borel function in literature).

Let X has probability distribution $f_X(x)$ and function $g : \mathbb{R} \to \mathbb{R}$ is monotone. Then the probability distribution of random variable $Y = g(X)$ is given by

$$f_Y(y) = f_X(g^{-1}(y)) \left|(g^{-1}(y))'\right|. \tag{C.1}$$

Scalar multiplication

Let X be a continuous random variable with PDF $f_X(x)$. Let $Y = \theta X$ with $\theta > 0$. Then

$$f_Y(y) = \frac{1}{\theta} f_x\Big(\frac{y}{\theta}\Big). \tag{C.2}$$

Power transformation

Let X be a continuous random variable with PDF $f_X(x)$. Let $Y = X^{1/n}$. Then if $n > 0$,

$$f_Y(y) = n\, y^{n-1} f_X(y^n), \quad y > 0, \tag{C.3}$$

while, if $n < 0$,

$$f_Y(y) = -n\, y^{n-1} f_X(y^n). \tag{C.4}$$

In the special case $Y = 1/X = X^{-1}$, it gives inverse X distribution

$$f_Y(y) = \frac{1}{y^2} f_X\left(\frac{1}{y}\right). \tag{C.5}$$

Exponentiation

Let X be a continuous random variable with PDF $f_X(x)$. Let $Y = \exp(X)$. Then, for $y > 0$,

$$f_Y(y) = \frac{1}{y} f_X(\ln y). \tag{C.6}$$

D On the product of random variables

When the pulse ϕ_k arrive at position ξ, its amplitude becomes

$$a_{\xi k} = a_k \exp\left(-\frac{\xi}{\tau_{\shortparallel} v_k}\right)$$

where the marginal probability distributions of amplitudes a_k and velocities v_k are specified at reference position $\xi = 0$. In general, when the velocities are randomly distributed, the distribution of pulse amplitudes $a_{\xi k}$ at $\xi \neq 0$ will be different from one specified at the reference position.

Let X and Y be two independent random variables whose respective PDFs, $f(x)$ and $g(y)$, are defined on $\mathbb{R}^+$. Consider a random variable Z constructed by a multiplication of these two variables. It is then shown that the PDF of Z, $h(z)$, is obtained as the Mellin convolution of $f(x)$ and $g(y)$

$$h(z) = f(x) \mathbin{\hat{*}} g(y),$$

with the operator $\hat{*}$ denoting Mellin convolution. Note that if f and g are PDFs, then h is also a PDF defined on $\mathbb{R}^+$. And the integral representation

$$h(z) = \int_0^\infty \frac{\mathrm{d}y}{y} f\left(\frac{z}{y}\right) g(y) \tag{D.1}$$

$$= \int_0^\infty \frac{\mathrm{d}x}{x} g\left(\frac{z}{x}\right) f(x) \tag{D.2}$$

since Mellin convolution is an associative and commutative operation [47]. In what follows, the particular cases of the broad distribution of pulse velocities will be examined.

Uniformly distributed velocities:

Consider the marginal velocity distribution given by (4.22), then the reciprocal random variable $U = 1/V$ is distributed according to

$$p_u(u) = \frac{1}{2s\langle v\rangle} u^{-2}, \quad v_{\max}^{-1} \leqslant u \leqslant v_{\min}^{-1}. \tag{D.3}$$

Consider the transformation $Y = \exp\left(-\frac{\xi}{\tau_{\shortparallel}} U\right)$, the PDF of random variable Y becomes

$$f_y(y) = \frac{\xi}{2s\langle v\rangle \tau_{\shortparallel}} \frac{1}{y \ln^2 y}, \tag{D.4}$$

which is non-zero for $y_{\min} \leqslant y \leqslant y_{\max}$, where $y_{\min/\max} = \exp\left[-\xi/(v_{\min/\max}\tau_{\shortparallel})\right]$.

It follows that the PDF of product random variable $Z = XY$, precisely the Mellin convolution of $f_x(x)$ and $f_y(y)$, is given by

$$f_z(z) = \frac{\xi}{2s\tau_{\shortparallel}} z^{-1} \int_{z/y_{\max}}^{z/y_{\min}} \mathrm{d}x\, e^{-x} \ln^{-2}, \left(\frac{z}{x}\right), \quad z > 0 \tag{D.5}$$

where the limits of integration of x is determined from the relation

$$y = \frac{z}{x} \quad x \geqslant 0, \quad y_{\min} \leqslant y \leqslant y_{\max}.$$

Gamma distributed velocities:

The inverse Gamma distribution is defined as

$$p_u(u) = \frac{u^{-1}}{\Gamma(k)} \left(\frac{k}{u}\right)^k \exp\left(-\frac{k}{u}\right), \quad u > 0. \tag{D.6}$$

The transformed variable Y has distribution

$$f_y(y) = \frac{y^{-1}}{\Gamma(k)} \left(\frac{\xi k}{\tau_{\shortparallel}}\right)^k \left(-\frac{1}{\ln y}\right)^{1+k} \exp\left(\frac{\xi k}{\tau_{\shortparallel} \ln y}\right), \tag{D.7}$$

which is non-zero for $0 < y < 1$. It follows that the PDF of product random variable $Z = XY$, the Mellin convolution of $f_x(x)$ and $f_y(y)$, is given by

$$f_z(z) = \frac{1}{\Gamma(k)} \left(\frac{\xi k}{\tau_{\text{II}}}\right)^k \int_z^\infty \mathrm{d}x \left(-\frac{1}{\ln(z/x)}\right)^{1+k} \exp\left(\frac{\xi k}{\tau_{\text{II}} \ln(z/x)} - x\right), \quad z > 0 \tag{D.8}$$

where the limits of integration of x is determined from the relation

$$y = \frac{z}{x} \quad x \geqslant 0, \quad 0 \leqslant y \leqslant 1.$$

Truncated exponentially distributed velocities:

Consider that the random variable V is distributed according (4.34), then its reciprocal $U = 1/V$ distributed according

$$p_u(u) = \frac{1}{(1-\alpha)} \frac{1}{u^2} \exp\left(-\frac{u^{-1} - \alpha}{1-\alpha}\right), \quad 0 < u \leqslant \frac{1}{\alpha}, \tag{D.9}$$

and zero otherwise. The transformed variable Y has distribution given by

$$f_y(y) = \frac{1}{(1-\alpha)} \frac{1}{y \ln^2 y} \exp\left(\frac{\ln^{-1} y + \alpha}{1-\alpha}\right), \quad \exp\left(-\frac{1}{\alpha}\right) \leqslant y < 1 \tag{D.10}$$

It follows that the PDF of product random variable $Z = XY$, is the Mellin convolution of $f_x(x)$ and $f_y(y)$, is given by

$$f_z(z) = \frac{1}{(1-\alpha)} \int_z^{z/y_{\min}} \mathrm{d}x \frac{1}{\ln^2(z/x)} \exp\left(\frac{\ln^{-1}(z/x) + \alpha}{1-\alpha}\right), \quad z > 0, \tag{D.11}$$

where the limits of integration of x is determined from the relation

$$y = \frac{z}{x} \quad x \geqslant 0, \quad y_{\min} \leqslant y \leqslant 1.$$

E Source code

The following Python code is used to generate synthetic process. Code for evaluating the statistics does not provided here, as this is all done using standard and straight forward python libraries and methods.

```
import numpy as np

class Filament:
    """
    pulseshape : string
        1-exp: one-sided exponential pulse
    alpha: float
        power-law coeficient define the dependence on instantenoius amplitude
    """

    def __init__(self, t_reference:float, amplitude:float, size:float, v:float,
    filament_shape='1-exp', alpha=0.0) -> None:

        self.t_ref = t_reference
        self.amplitude = amplitude
        self.size = size
        self.v = v
        self.filament_shape = filament_shape
        self.drainage = 10.
        self.alpha = alpha
        self.time_dependent_v = True if alpha > 0.0 else False
        self.optimizations = True
        # Option to enable optimizations.
        # Avoids duplicate computations when computing matrices
        # with identical rows or columns.
        self.optimizations = True

    def discretize_filament(self, t:np.ndarray, x:np.ndarray) -> np.ndarray:
    # Computes the entire discretized filament in its contribution domain
        if self.optimizations:
            arr = self.__drain(t) * self.__filament_arrival(t)
            return self.amplitude * self.__shape(x, t) * np.tile(arr, (t.shape[1],
    1)).T
        else:
            return (self.amplitude * self.__drain(t) * self.__shape(x, t) * self.
    __filament_arrival(t))

    def __drain(self, t: np.ndarray) -> np.ndarray:
    # Computes the dampening of the filaments amplitude
        if self.optimizations:
            return np.exp(-(t[:,0] - self.t_ref)/self.drainage).T
        else:
            return np.exp(-(t - self.t_ref)/self.drainage)

    def __filament_position(self, t:np.ndarray) -> np.ndarray:
    # Calculates the positions of the filament for the discretized times
        if self.optimizations:
            if self.time_dependent_v is False:
                return self.v*(t[:,0] - self.t_ref)
            else:
            else:
                return self.v*self.drainage/self.alpha*self.amplitude**self.alpha*\
                    (1 - np.exp(self.alpha/self.drainage*(self.t_ref - t[:,0])))
        else:
            if self.time_dependent_v is False:
                return self.v*(t - self.t_ref)
            else:
                return self.v*self.drainage/self.alpha*self.amplitude**self.alpha*\
                    (1 - np.exp(self.alpha/self.drainage*(self.t_ref - t)))

    def __shape(self, x: np.ndarray, t: np.ndarray) -> np.ndarray:
        if self.filament_shape == '1-exp':
        # Creates the shape. The Heaviside function is here to make sure
        # that the filament has no contibution in regions it has not yet reached.
            if self.optimizations:
                fil_pos = x - np.tile(self.__filament_position(t), (t.shape[1], 1))
    .T
```

```
                return np.exp(fil_pos/self.size) * np.heaviside( -fil_pos , 1)
            else:
                return np.exp((x - self.__filament_position(t)) / self.size) * np.
    heaviside(-(x - self.__filament_position(t)), 1)

    def __filament_arrival(self, t: np.ndarray) -> np.ndarray:
        if self.optimizations:
            return np.heaviside(t[:,0] - self.t_ref, 1)
        else:
            return np.heaviside(t - self.t_ref, 1)
```

```
import numpy as np
from scipy.special import gamma, gammaincc
from tqdm import tqdm
from .filament import Filament

class generate_synthetic_signal:
    """
    Parameters
    ----------
    Tend : float
        Time length of signal.
    Pavl: Pavl = [Pa, Pl, Pv]
          Pa = [average:float, 'dist':string]
          Pl = [average:float, 'dist':string]
          Pv = [average:float, s:float, 'dist':string]
        All features of joint distribution.
    dt : float
        Time-step size.
    dx : float
        Distance between two consecutive locations.
    drainage: float
        Parallel transient time by default 10.
    """
    def __init__(self, Tend:float, inverse_t_w:float, Pavl:list, dt:float=1e-1, dx:
    float=1e-1, drainage=10., alpha=0.0) -> None:

        self.T=Tend
        self.dx=dx
        self.dt=dt
        self.inverse_t_w=inverse_t_w
        self.drainage=drainage
        self.K=int(self.T*inverse_t_w)
        self.Pa=Pavl[0]
        self.Pl=Pavl[1]
        self.Pv=Pavl[2]
        self.alpha=alpha
        self.time_dependent_v = True if alpha > 0.0 else False

        self.__filaments =[]


    def rv_discrete(
        self,
        dist: str,
        s: float=0.5,
        ):
            if dist == 'deg':
                return np.ones(self.K)
            elif dist == '2v':
                return np.random.choice([1-s, 1+s], size=self.K, p=[0.5,0.5])
            elif dist == 'exp':
                return np.random.exponential(size=self.K, scale=1.0)
            elif dist == 'unif':
                return np.random.uniform(low=1-s, high=1+s, size=self.K)
            elif dist == 'gamma':
                return np.random.gamma(s,1/s,size=self.K)
            elif dist == 'truncated_exp':
                return np.random.exponential(size=self.K, scale=(1-s)) + s

    def sample_filaments(self):
        __t_arrival = np.random.uniform(low=0, high=self.T, size=self.K)

        __amplitudes = self.rv_discrete(dist=self.Pa[1], s=self.Pa[0])
```

```
63          __sizes = self.rv_discrete(dist=self.Pl)
64
65          distlist_V = ['deg', '2v', 'unif', 'exp',  'truncated_exp', 'gamma', '
    correlated_scaling']
66          assert(self.Pv[1] in distlist_V), 'Invalid distribution function of the
    velocities'
67
68          if self.Pv[1]=='correlated_scaling':
69              __velocities = 1/(gamma(1+self.Pv[0])*gammaincc(1+self.Pv[0], self.Pa
    [0]/(1-self.Pa[0])))*np.exp(-self.Pa[0]/(1-self.Pa[0]))*(1-self.Pa[0])**(-self.
    Pv[0])*(__amplitudes)**self.Pv[0]
70          else:
71              __velocities = self.rv_discrete(dist=self.Pv[1], s=self.Pv[0])
72          for k in range(self.K):
73              self.__filaments.append(
74                  Filament(__t_arrival[k], __amplitudes[k], __sizes[k], __velocities[
    k], filament_shape='1-exp', alpha=self.alpha)
75              )
76          return
77
78      def superposing_filaments(self, error:float):
79
80          self.sample_filaments()
81
82          x = np.arange(0, int(10/self.dx)+1)*self.dx
83          t = np.arange(0, int(self.T/self.dt)+1)*self.dt
84
85          __x, __t = np.meshgrid(x, t)
86
87          Phi = np.zeros((t.size, x.size))
88
89          for f in  tqdm(self.__filaments):
90          # Starting index of contribution of current filament
91              start = int(f.t_ref/self.dt)
92          # Ending index of contribution of current filament.
93          # Based upon when largest contribution of filament
94          # is below the 'error'-variables threshold
95              if self.time_dependent_v is False:
96                  stop = start + int((-np.log(error) + x.size)/(self.dt*f.v))
97              else:
98                  stop = start + int((-f.drainage * np.log(error/f.amplitude)) / self
    .dt)
99          # Adding values of the filament in it's region of contribution
100             Phi[start:stop, :] += f.discretize_filament(
101                     t=__t[start:stop, :],
102                     x=__x[start:stop, :]
103                     )
104         return Phi
```

References

[1] S. I. Braginskii. Transport processes in a plasma. *Reviews of Plasma Physics*, 1:205, January 1965.

[2] A. A. Galeev and R. Z. Sagdeev. Neoclassical theory of diffusion. In *Advances in Plasma Physics*, volume 6, pages 311–420. 1976.

[3] R. J. Bickerton, A. Taroni, M. L. Watkins, J. Wesson, and D. C. Robinson. Comparison between experiment and theory [and discussion]. *Philosophical Transactions of the Royal Society of London. Series A, Mathematical and Physical Sciences*, 322(1563):173–188, 1987. URL: http://www.jstor.org/stable/37749.

[4] J. W. Connor, G. F. Counsell, S. K. Erents, S. J. Fielding, B. LaBombard, and K. Morel. Comparison of theoretical models for scrape-off layer widths with data from COMPASS-D, JET and Alcator C-Mod. *Nuclear Fusion*, 39(2):169–188, 1999.

[5] J. W. Connor and O. P. Pogutse. On the relationship between mixing length and strong turbulence estimates for transport due to drift turbulence. *Plasma Physics and Controlled Fusion*, 43(2):155–175, February 2001. doi:10.1088/0741-3335/43/2/306.

[6] P. C. Stangeby. Modeling plasma contact with the main vessel walls of a divertor tokamak. *Physics of Plasmas*, 9(8):3489, 2002.

[7] O. E. Garcia, J. Horacek, R. A. Pitts, A. H. Nielsen, W. Fundamenski, V. Naulin, and J. Juul Rasmussen. Fluctuations and transport in the TCV scrape-off layer. *Nuclear Fusion*, 47(7):667–676, 2007.

[8] B. LaBombard, R. L. Boivin, M. Greenwald, J. Hughes, B. Lipschultz, D. Mossessian, C. S. Pitcher, J. L. Terry, S. J. Zweben, and Alcator Group. Particle transport in the scrape-off layer and its relationship to discharge density limit in Alcator C-mod. *Physics of Plasmas*, 8(5):2107, 2001. doi:10.1063/1.1352596.

[9] N. Ben Ayed, A. Kirk, B. Dudson, S. Tallents, R.G.L. Vann, and H. R. Wilson. Inter-ELM filaments and turbulent transport in the mega-amp spherical tokamak. *Plasma Physics and Controlled Fusion*, 51(3):035016, 2009. doi:10.1088/0741-3335/51/3/035016.

[10] M. Greenwald, J.L. Terry, S.M. Wolfe, S. Ejima, M.G. Bell, S.M. Kaye, and G.H. Neilson. A new look at density limits in tokamaks. *Nuclear Fusion*, 28(12):2199–2207, 1988. doi:10.1088/0029-5515/28/12/009.

[11] F. Militello, P. Tamain, W. Fundamenski, A. Kirk, V. Naulin, and A. H. Nielsen. Experimental and numerical characterization of the turbulence in the scrape-off layer of MAST. *Plasma Physics and Controlled Fusion*, 55(2):025005, 2013.

[12] B. LaBombard, R. L. Boivin, M. Greenwald, J. Hughes, B. Lipschultz, D. Mossessian, C. S. Pitcher, J. L. Terry, and S. J. Zweben. Particle transport in the scrape-off layer and its relationship to discharge density limit in Alcator C-Mod. *Physics of Plasmas*, 8(5 II):2107–2117, 2001.

[13] Sergei I. Krasheninnikov. On scrape off layer plasma transport. *Physics Letters A*, 283:368–370, 2001. doi:10.1016/S0375-9601(01)00252-3.

[14] O.E. Garcia, N.H. Bian, V. Naulin, A.H. Nielsen, and J. Juul Rasmussen. Mechanism and scaling for convection of isolated structures in nonuniformly magnetized plasmas. *Physics of Plasmas*, 12(9):090701, 2005. doi:10.1063/1.2044487.

[15] N. Bian, Sadruddin Benkadda, J.-V Paulsen, and Odd Erik Garcia. Blobs and front propagation in the scrape-off layer of magnetic confinement devices. *Physics of Plasmas*, 10:671–676, 2003. doi:10.1063/1.1541021.

[16] R.J. Maqueda, D.P. Stotler, and S.J. Zweben. Intermittency in the scrape-off layer of the national spherical torus experiment during h-mode confinement. *Journal of Nuclear Materials*, 415:S459–S462, 2011. doi:https://doi.org/10.1016/j.jnucmat.2010.11.002.

[17] S.I. Krasheninnikov, D. A. D'Ippolito, and J. R. Myra. Recent theoretical progress in understanding coherent structures in edge and SOL turbulence. *Journal of Plasma Physics*, 74(5):679–717, 2008. doi:10.1017/S0022377807006940.

[18] D. A. Russell J. R. Myra and D. A. D'Ippolito. Collisionality and magnetic geometry effects on tokamak edge turbulent transport. i. a two-region model with application to blobs. *Journal of Plasma Physics*, 13(11):112502, 2006. doi:10.1063/1.2364858.

[19] R. Kube and O. E. Garcia. Velocity scaling for filament motion in scrape-off layer plasmas. *Physics of Plasmas*, 18(10):102314, 2011. doi:10.1063/1.3647553.

[20] D.A. D'Ippoloto, J.R. Myra, and Zweben S.J. Convective transport by intermittent blob-filaments: Comparison of theory and experiment. *Physics of Plasmas*, 18(6):060501, 2011. doi:10.1063/1.3594609.

[21] R. Kube, O.E. Garcia, B. LaBombard, J.L. Terry, and S.J. Zweben. Blob sizes and velocities in the Alcator C-Mod scrape-off layer. *Journal of Nuclear Materials*, 438:S505–S508, 2013.

[22] O.E. Garcia, N. Bian, and W. Fundamenski. Radial interchange motions of plasma filaments. *Physics of Plasmas*, 13:082309–082309, 08 2006. doi:10.1063/1.2336422.

[23] J.R. Angus and S.I. Krasheninnikov. Inviscid evolution of large amplitude filaments in a uniform gravity field. *Physics of Plasmas*, 21(11):112504, 2014. doi:10.1063/1.4901237.

[24] J. T. Omotani, F. Militello, L. Easy, and N. R. Walkden. The effects of shape and amplitude on the velocity of scrape-off layer filaments. *Plasma Phys. Control. Fusion*, 58(1):014030, 2016. doi:10.1088/0741-3335/58/1/014030.

[25] C. Theiler, I. Furno, P. Ricci, A. Fasoli, B. Labit, S. H. Muller, and G. Plyushchev. Cross-field motion of plasma blobs in an open magnetic field line configuration. *Phys. Rev. Lett.*, 103:065001, 2009. doi:10.1103/PhysRevLett.103.065001.

[26] A. Theodorsen, O. E. Garcia, J. Horacek, R. Kube, and R. A. Pitts. Scrape-off layer turbulence in TCV: Evidence in support of stochastic modelling. *Plasma Physics and Controlled Fusion*, 58(4):044006, 2016.

[27] Ghassan Antar, Glenn Counsell, Yang Yu, Brian Labombard, and Pascal Devynck. Universality of intermittent convective transport in the scrape-off layer of magnetically confined devices. *Physics of Plasmas*, 10, 2003. doi:10.1063/1.1536166.

[28] A. Theodorsen, O. E. Garcia, R. Kube, B. LaBombard, and J. L. Terry. Relationship between frequency power spectra and intermittent, large-amplitude bursts in the Alcator C-Mod scrape-off layer. *Nuclear Fusion*, 57(11):114004, 2017.

[29] O. E. Garcia, R. Kube, A. Theodorsen, J. G. Bak, S. H. Hong, H. S. Kim, the KSTAR Project Team, and R. A. Pitts. SOL width and intermittent fluctuations in KSTAR. *Nuclear Materials and Energy*, 12:36–43, 2017.

[30] R. Kube, O. E. Garcia, A. Theodorsen, D. Brunner, A. Q. Kuang, B. LaBombard, and J. L. Terry. Intermittent electron density and temperature fluctuations and associated fluxes in the alcator c-mod scrape-off layer. *Plasma Physics and Controlled Fusion*, 60(6):065002, 2018. doi:10.1088/1361-6587/aab726.

[31] G. Y. Antar, P. Devynck, X. Garbet, and S. C. Luckhardt. Turbulence intermittency and burst properties in tokamak scrape-off layer. *Physics of Plasmas*, 8(5):1612–1624, May 2001. doi:10.1063/1.1363663.

[32] R. Kube, A. Theodorsen, O. E. Garcia, B. LaBombard, and J. L. Terry. Fluctuation statistics in the scrape-off layer of Alcator C-Mod. *Plasma Physics and Controlled Fusion*, 58(5):054001, 2016. doi:10.1088/0741-3335/58/5/054001.

[33] O. E. Garcia, R. Kube, A. Theodorsen, B. LaBombard, and J. L. Terry. Intermittent fluctuations in the Alcator C-Mod scrape-off layer for ohmic and high confinement mode plasmas. *Physics of Plasmas*, 25(5):056103, 2018. doi:10.1063/1.5018709.

[34] O. E. Garcia, J. Horacek, and R. A. Pitts. Intermittent fluctuations in the TCV scrape-off layer. *Nuclear Fusion*, 55(6):062002, 2015. doi:10.1088/0029-5515/55/6/062002.

[35] O. E. Garcia, R. A. Pitts, J. Horacek, J. Madsen, V. Naulin, A. H. Nielsen, and J. Juul Rasmussen. Collisionality dependent transport in TCV SOL plasmas. *Plasma Physics and Controlled Fusion*, 49(12B):B47–B57, 2007. doi:10.1088/0741-3335/49/12B/S03.

[36] J.M. Losada, O. E. Garcia, and A. Theodorsen. Stochastic modelling of blob-like plasma structures: I time-independent velocities. 2022. To be published.

[37] John Rice. On generalized shot noise. *Adv. Appl. Prob.*, 9:553–565, 1977.

[38] O. E. Garcia. Stochastic Modeling of Intermittent Scrape-Off Layer Plasma Fluctuations. *Phys. Rev. Lett.*, 108(26):265001, 2012. doi:10.1103/PhysRevLett.108.265001.

[39] O. E. Garcia, R. Kube, A. Theodorsen, and H. L. Pécseli. Stochastic modelling of intermittent fluctuations in the scrape-off layer: Correlations, distributions, level crossings, and moment estimation. *Physics of Plasmas*, 23(5):1–14, 2016.

[40] F. Militello and J.T. Omotani. Scrape off layer profiles interpreted with filament dynamics. *Nuclear Fusion*, 56(10):104004, 2016. doi:10.1088/0029-5515/56/10/104004.

[41] F. Militello and J. T. Omotani. On the relation between non-exponential scrape off layer profiles and the dynamics of filaments. *Plasma Physics and Controlled Fusion*, 58(12):125004, 2016. doi:10.1088/0741-3335/58/12/125004.

[42] N. Campbell. The study of discontinuous phenomena. *Proc. Cambr. Phil. Soc.*, 15:117–136, 1909.

[43] R. Kube and O. E. Garcia. Convergence of statistical moments of particle density time series in scrape-off layer plasmas. *Physics of Plasmas*, 22:012502, 2015. doi:10.1063/1.4905513.

[44] P. Moschopoulos. The distribution of the sum of independent gamma random variables. *Annals of the Institute of Statistical Mathematics*, 37:541–544, 12 1985. doi:10.1007/BF02481123.

[45] M. A. Korzeniowska. Long-range correlations from a super-position of uncorrelated. *NFS RPK meeting 2022*.

[46] *NIST Digital Library of Mathematical Functions*. http://dlmf.nist.gov/, Release 1.1.5 of 2022-03-15. F. W. J. Olver, A. B. Olde Daalhuis, D. W. Lozier, B. I. Schneider, R. F. Boisvert, C. W. Clark, B. R. Miller, B. V. Saunders, H. S. Cohl, and M. A. McClain, eds. URL: http://dlmf.nist.gov/.

[47] Melvin Dale Springer. *The Algebra of Random Variables*. Wiley series in probability and mathematical statistics. John Wiley & Sons, 1979.